Polyglycerol-based, Chemically Defined Artificial Stem Cell Scaffold Engineering for iPSCs' 3D Culture

Inaugural-Dissertation

to obtain the academic degree

Doctor rerum naturalium (Dr. rer. nat.)

Submitted to the Department of Biology, Chemistry, and Pharmacy

of Freie Universität Berlin

by

Wanjun Liang

From Rizhao, China

Berlin, November 2019

This Ph.D thesis was carried out under the supervision of Prof. Dr. Nan Ma and Prof. Dr. Rainer Haag from October 2015 until August 2019 at the Institute of Chemistry and Biochemistry of the Freie Universität Berlin. The four years of studies have been supported by China Scholarship Council (CSC).

1st Reviewer: Prof. Dr. Nan Ma, Freie Universität Berlin
2nd. Reviewer: Prof. Dr. Rainer Haag, Freie Universität Berlin

Day of defense: 19.12.2019

Acknowledgements

I really want to express my heartfelt appreciate to my doctoral supervisor Prof. Dr. Rainer Haag for giving me the opportunity to be a member of the outstanding Haag research group. During the four years PhD learning life, he extended to me so much academic and scientific support. He always treated the work with chariness and responsibility. His great erudition and dedication showed in the guiding of my projects express me deeply and will always inspire me to become a person like him in the future.

I would like to express my sincere gratitude to my supervisor Prof. Dr. Nan Ma for guiding me in all the aspects of research and taking part in subsequent defense procedure. She discussed many things with me and she gave me a lot of guidance in cell biology. I also really thank Dr. Wenzhong Li for giving me and discussing with me interesting project ideas.

I would like to express thanks to all the cooperation partners I have been working with during my PhD study. I particularly would like to say thanks to Dr. Wenzhong Li, Dr. Leixiao Yu, Dr. Luis Jose Luis Cuellar-Camacho, Suqiong Zhou, Felix Reisbeck, Anja Stöshel, Marleen Selent, Prof. Dr. Mohsen Adeli, and Dr. Olaf Wagner for discussing my projects, and making corrections for the manuscripts and supplying lots of materials and characterization data. I thank Dr. Carlo Fasting for the HPLC measurements. I thank Prof. Anke Schindler for SEM test. I thank Dr. Pamela Winchester for proofreading and polishing my manuscripts and this thesis. Also, I thank Dr. Wiebke Fischer for helping me always. Without their help, I could not do well in my PhD studies.

I especially acknowledge Dr. Mathias Dimde, Felix Reisbeck, Dr. Wei, Dr. Pradip Dey, Dr. Manoj Kumar Muthyala, and Dr. Sumati Bhatia for their help on many occasions and friendship.

I thank my labmates and office mates, Dr. Fatemeh Zabihi, Vahid Ahmadi Soureshjani, Mohammad Suman Chowdhury, Paria Pouyan, Ann-Cathrin Schmitt, Boonya Thongrom, Hanna, Mingjun, Suqiong, Yuanwei, Yan, Yi, Dr. Shenyi, Dr. Lingyan, Dr. Zhenzhui, Dr. Changzhu, Dr. Chunhong, Dr. Chong, Qingcai, Dr. Yinan, Zhaoxu, Fang, Zewang, Yong, and Chuangxiong for all lab discussions and fun activities. It's your company that makes the everyday life not tedious and research work interesting.

I would like to thank all the present and past group members of Haag group for their support and providing me a nice working environment. I acknowledge all the research facilities in the

Institute of Chemistry and Biochemistry, Free University Berlin and would like to thank Dr. Andreas Schäfer, Dr. Andreas Springer, and their colleagues for NMR and mass measurements.

I gratefully acknowledge financial support from the China Scholarship Council for the funding for four years and the SFB 765 of the German Science Foundation (DFG). Without that, my dream of doing PhD in Germany would have never been possible. Also special thanks to Beate Rogler and my German language teacher Miss Nina and English teacher Prof. Peter.

I acknowledge all my family members for their support and confidence on me. Four years is not a short time. Sometimes, I can't help feeling homesick. It's the encouragement and faith from them that help me overcome the difficulty again and again in a foreign land life. I feel lucky to have my parents' affections and blessings with me, which helps me to get all the success in my life. I also acknowledge my sisters' support and encouragement for gaining this degree and taking care of my responsibilities towards my family. Finally, I would also give my thanks to Xinxin for keeping faith in me, also her courage, love, and support.

If I forgot some of you, please forgive me.

Contents

Chapter 1 Introduction ……..……...1

1.1 Stem cells ……...…….……1

1.1.1 Embryonic stem (ES) cells and their disadvantages …….……..…….2

1.1.2 Induced pluripotent stem cell (iPSCs) ……...…….……..…3

1.1.3 The application of iPSCs ……...…….……..…7

1.1.4 Major challenges in iPSCs application …….……10

1.1.5 Current approaches for iPSCs culture ……...…….……11

1.1.5.1 Two-dimensional culture techniques ……..……11

1.1.5.2 Three-dimensional culture techniques ……..……..…13

1.2 Extracellular niche or matrices devises for iPSCs' 3D culture ……..…15

1.2.1 Niche and microenvironments of iPSCs ……...…….……17

1.2.2 Materials used for scaffold or niche in iPSCs' 3D culture …….……...19

1.2.1.1 Naturally derived and hybrid materials ……..……20

1.2.1.2 Synthetic polymers ……...…….…….……22

1.2.1.3 Advantage and challenges of synthetic polymers as scaffold materials ……24

1.2.2 Strategies for gelation ……....25

1.2.2.1 Covalent crosslinking gelation ……..25

1.2.2.2 Noncovalent crosslinking gelation …….……27

1.2.3 Material design considerations for engineering the 3D cell microenvironment….27

1.2.3.1 Substrate stiffness ……..28

1.2.3.2 Substrate degradation …….…...……29

1.2.3.3 Surface receptors and biological cues ……...……30

Chapter 2 Scientific Goals…….…….……31

Chapter 3 Chemically Defined Stem Cell Microniche Engineering for iPSCs' 3D Culture and Expansion…….....34

3.1 Results and Discussion…….……...……34

3.1.1 Establishment of the chemically defined, artificial 3D microniche engineering…..34

3.1.2 Overall assess to the performance of the artificial 3D microniche system……..…38

3.2 Conclusion……42

3.3 Materials preparation and related experiment operation……43

3.3.1 Synthesis procedures of materials……43

3.3.2 Surfactant preparation ……49

3.3.3 Cell culture……51

3.3.4 Microniche engineering……52

3.3.5 Cell viability assay……54

3.3.6 Proliferation assay ……54

3.3.7 Immunofluorescent staining……54

3.3.8 RT-qPCR reaction……55

3.3.9 ALP staining……55

3.3.10 AFM tests ……56

3.3.11 Rheology tests……57

3.3.12 Gelation efficiency to precursor ratios……58

3.3.13 SEM test ……59

3.3.14 Morphology property of the microniche……59

3.3.15 Degradability characterization of the microniche particles ……60

3.3.16 iPSCs' response to microniche stiffness……62

3.3.17 Optimal seeding density for iPSCs microniche culturing ……63

Chapter 4 Advanced controlled-releasable iPSCs' 3D artificial niches based on dendritic polyglycerol and poly(N-isopropylacrylamide)-co-polyethylene glycol polymers via physical-chemical-co-gelation strategy……65

4.1 Results and Discussion ……65

4.1.1 Establishment of control-releasable 3D Hydrogel based artificial Niche microenvironment by ECM mimicking ……65

4.1.2 Precursors synthesis and the fabrication of novel hydrogel scaffold niche……68

4.1.3 Stiffness characterization of the hydrogel niche formed with various precursors' ratios and concentrations……70

4.1.4 iPSCs' response to the precursors ratios of materials for establishing a 3D niche environment……72

4.1.5 iPSCs' viability response to the stiffness and precursor content of the 3D

niche environments……75
4.1.6 iPSCs' viability and expansion efficiency response to cell seeding density….79
4.1.7 Overall performance of dPG-pNIPAAm-co-PEG 3D niche culture system in supporting iPSCs' proliferation……81
4.1.8 Control release and cells' harvest……83
4.1.9 Cell quality characterization……..85
4.2 Conclusion……87
4.3 Materials preparation and related experiment operation……88
4.3.1 Synthesis procedures of materials……88
Chapter 5 Summary & Conclusion……92
Chapter 6 Zusammenfassung……94
Chapter 7 Outlook……96
Chapter 8 References……97
Chapter 9 Appendix……106

List of Abbreviations

iPSCs	induced pluripotent stem cell
DF	degree of the functionalization
ECM	the extracellular matrix
dPG	dendritic polyglycerol
dPGS	the sulfate of the dendritic polyglycerol
CCK-8	cell counting kit-8
HA	hyaluronic acid
MMP	matrix metalloproteinases
ALP	alkaline phosphatase
PDMS	poly (dimethylsiloxane)
c[RGDfK]	cyclic Arg(Pmc)-GlyAsp(OtBu)-D-Phe-Lys(Boc)
PEG	Poly ethylene glycol
PEG-DA	Poly ethylene glycol diacrylate
PEG-DGE	Poly ethylene glycol diglycidylether
PSS	poly(4-styrenesulfonic acid)
BCN	Bicycle [6.1.0]non-4-yn-9-ylmethyl (4-nitrophenyl) carbonate
PCL	polycaprolactone
SPAAC	strain promoted azide alkyne cycloaddition
2D	Two dimensional
3D	Three dimensional
SEM	Scanning electron microscopy
EB	Embryoid bodies

Chapter 1 Introduction

1.1 Stem Cells

It has been classically described that pluripotency, as a cell's ability to be differentiated into three germ layers including endoderm, mesoderm and ectoderm – is crucial in the long term of germinal development. This intrinsic property could lead to organ and tissue regeneration in animals or humans if it is properly controlled.[1] What is a stem cell? Stem cell are pluripotent cells that can differentiate into other types of cells. Of course, they have the ability to produce more of the same type of stem cells by ways of their self-renewal. Stem cell research originated in the 1960s by Canadian scientists, Ernest A McCulloch, and Till and James E.[2-3] Now, stem cell biology has become popular. Actually, our human body is full of potential, as shown in **Figure 1-1A**. In our body, the cells always follow a similar course like life's paths. All the stem cells in an early embryo have the potential to develop into other kinds of cells than can make up the body. All of these versatile cells are defined as pluripotent stem cells.[4] At an early stage, there are lots of pluripotent cells inside the embryo. Soon all of these cells start to develop along different pathways in our body. For example, as shown in **Figure 1-1B**, some of these cells will become neurons, muscle cells, or bone cells.

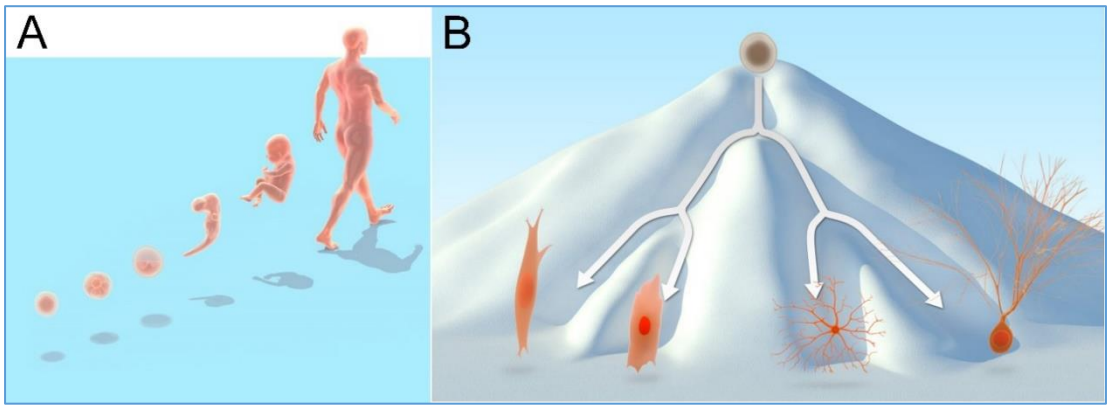

Figure 1-1. (A) Your body is full of potential. (B) The researcher named Conrad Hal Waddington compared the development of the human body to a landscape of peaks and valleys. Imagine the stem cell as a ball perched on the mountaintop. As it specializes, it rolls down the slope, following the

course of a certain valley. Cells do not normally climb back to the top and become stem cells again, and they do not cross the ridges into neighboring valleys and become another type of cell.[4] Copyright 2012 The Nobel Assembly at Karolinska Institute.

In a word, stem cells are undifferentiated cells, which have both of self-renewal capacity and differentiation ability. The stem cells (hSCs), which usually include embryonic stem cells (ESCs),[5] and induced pluripotent stem cells (iPSCs),[6] show great promise in supplying sources for regenerative therapies and modelling diseases.[7-9] Therefore, these pluripotent cells can be widely used in the fields of organ repair and renewal, a source of artificial organs and tissues, new drug development, tools for gene therapy, gene function study, toxicology, pharmacological research, and the research on cancer.

1.1.1 Embryonic stem (ES) cells and their disadvantages

ESC cells are cells that are derived from the mammalian blastocysts' inner cell mass. Because they can differentiate into all of the three germ layers cells,[10-13] they present an excellent source for regenerative medicine, the pharmaceutical industry, and early human development research. For example, it has been reported that ESCs derived from a blastocyst can be cultured *ex vivo* and be differentiated into heart cells, as shown in **Figure 1-2**.[14] Besides, it was reported by the Yoshiki Sasai group that polarized cortical tissues could be self-organized formated from ESCs under proper control.[15] In addition, human ES are very useful in researching the disease mechanisms, screening the safety of drugs, and treating patients with various diseases such as spinal cord injury, Parkinson disease, and diabetes.[16]

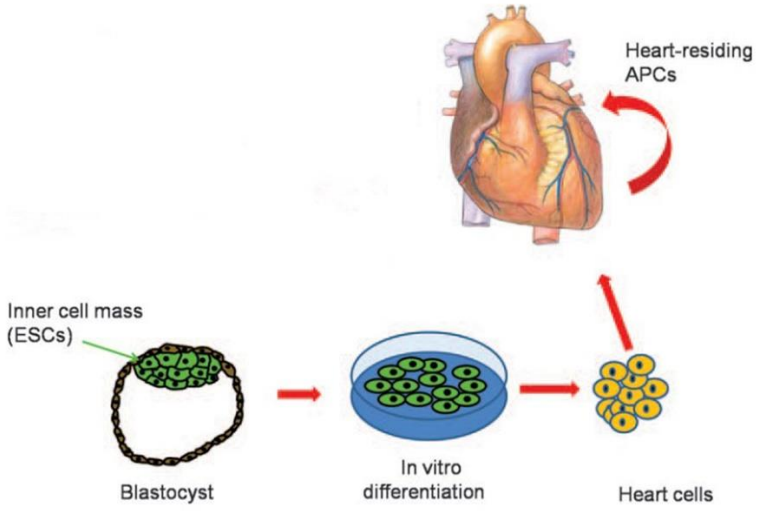

Figure 1-2. Potential sources of the stem progenitor cells for cardiac repair. The ESCs derived from inner cell mass of a blastocyst can be manipulated to differentiate into heart cells.[14] Copyright 2008, Mary Ann Liebert, Inc.

As mentioned above, embryonic stem cells are very useful in many research fields. However, there are still some disadvantages for these cells used in clinical application. For example, embryonic stem cells are obtained from embryo and the destruction of preimplantation embryos may cause ethical and moral disputes. Besides, that would also cause problems of tissue rejection following the transplantation in patients.[13] One issue is the process by which embryonic stem cells are harvested. Because, obtaining ESC cells inevitably resulting in destruction of the embryo at the blastocyst stage to extract the inner cell mass. This step, in the view of many pro-life groups, is a destruction of life. So, to evade this problem, new stem cell sources in regenerative medicine are urgently needed. One approach to circumvent these issues is to generate pluripotent stem cells directly from the patients' own cells.[4, 13]

1.1.2 Induced pluripotent stem cell

The 2012' nobel prizes in physiology and medicine was awarded to Shinya Yamanaka and John B. Gurdon for their contributions in finding cells' true potential. They discovered that have shown that, under certain situations, some cells can go into

reverse, which reveals a shocking view about how cells and organisms develop.[4]

In 2006, Yamanaka and his research group demonstrated that they produced pluripotent stem cells (iPSC) for the first time from mouse embryonic of adult fibroblasts by adding four essential factors, including Oct3/4, Klf4, c-Myc, and Sox2, under the cell culture conditions of ES.[13] (**Figure 1-3)** Besides, as reported by Boyer's group and Loh's group, the factors of Sox2, Oct3/4, especially Nanog have special function and work as key transcription factors in maintaining their pluripotency.[17-18] Yamanaka group found that, among these three factors, Oct3/4 and Sox2 are essential in the induction of the iPSC cells, while Nanog is dispensable for the generation of that cells. Beyond these, they also found that c-Myc and Klf4 work as key factors in the generation of the iPSC cells, and they could not be replaced by any other factors.[13] Therefore, they called these four transcription factors as "Yamanaka factors".

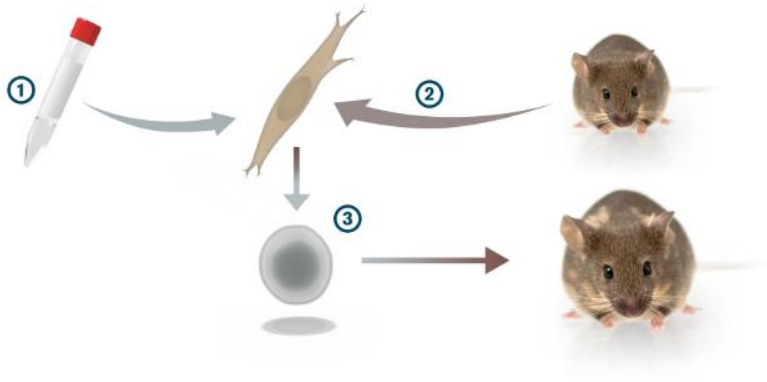

Figure 1-3. Shinya Yamanaka group studied genes that are important for the function of the stem cell. When they inserted four of these genes（1）into fibroblast cells got from mouse skin（2）, these fibroblasts were reprogrammed and became pluripotent stem cells（3）, which could develop into all of the different cell types in a mouse. These cells were named by them induced pluripotent stem cells (iPS cells).[4] Copyright 2012, The Nobel Assembly at Karolinska Institute.

In 2017, Shinya Yamanaka and his working group successfully generated iPSC cells from the skin cells of human.[4] (**Figure 1-4)** They demonstrated that the generation of the human iPSC cells from the human fibroblasts could be achieved by

adding the same factors: Sox2, Oct3/4, Klf4, and c-Myc. They also found that the obtained hiPSC cells were similar to human embryonic stem (ES) cells in a lot of characteristics such as telomerase activity, morphology, gene expression proliferation, and surface antigens.[6] The possibility of reprogramming the differentiated cells into pluripotent cells is really useful for the generation of patient- or disease-specific stem cells, which will be widely used in the understanding the mechanisms of certain disease.

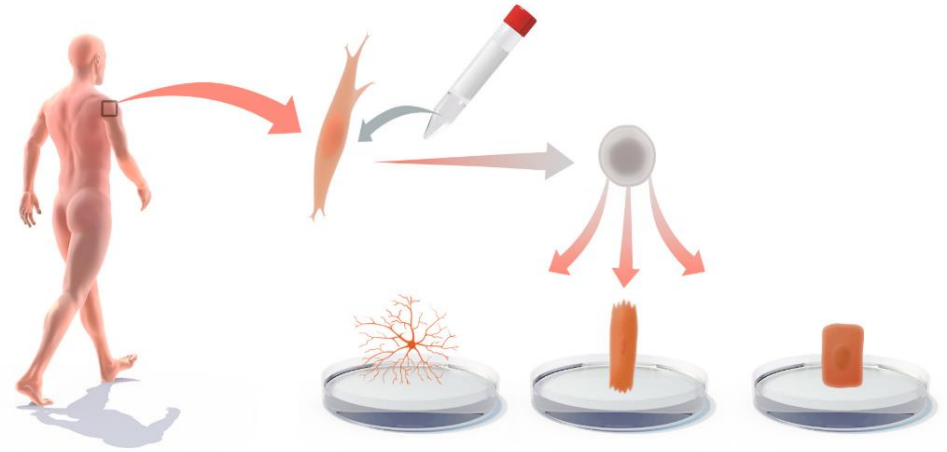

Figure 1-4. iPSC can be generated *in vitro* from cells taken from the patient as a simple skin sample. Then, from this, scientists can differentiate iPSCs into liver cells, nerve cells, and heart cells and use them to find the cause of the patient's disease or test the effect of pharmaceuticals.[4] Copyright 2012 The Nobel Assembly at Karolinska Institute.

Following Yamanaka and his research group' description, iPSC cells have provided a useful tool for pharmaceutical screening, disease modelling, therapeutic regeneration as well as precision medicine [1] Since the discovery of these cells, many approaches and methods have been attempted to improve the original protocol of how to culture these cells. For example, the Lutolf group has reported a 3D environment system that can promote iPSC's generation. In their work, an artificial niche environment can be established and adjusted by modulating their composition, degradability, as well as their stiffness.[19] Moreover, a full systematic analysis of how to reprogram somatic cells in an engineered 3D environment was investigated. The 3D environment boosts reprogramming can impose the physical cell confinement through accelerating the

mesenchymal-to-epithelial transition. During this process, the 3D environmental signals can act synergistically with the reprogramming factors in increasing somatic plasticity of the cells. Beyond these, they also investigated the affect of the biophysical cues in 3D environment in influencing renewal and differentiation of stem cell. Lutolf group also reported an approach for iPSC reprogramming as shown in **Figure 1-5**. To find an optimal synthetic 3D mircroenvironment to promote pluripotency for iPSC generation, they chose a kind of enzymatically crosslinked, PEG-based hydrogel to mimic the composition of the matrix and modulated their mechanical properties by varying content of the polymers. To mimic the ECMS' biochemical cues, they further functionalized the matrix metalloproteinase (MMP) degradable PEG networks with s special kind of the adhesion peptide argininеglycine-aspartate-serine-proline. A mouse model system was employed by expressing Yamanaka factors to assess how to achieve the pluripotency in the artificial 3D environment. They also did the reprogramming test by adding doxycycline. Then, the Oct4–GFP+ iPSC colonies appeared in 3D gels was quantified over several days. The study of immune-fluorescence staining test demonstrated that 3D-iPSCs generated in that system could express the main pluripotency markers such as Oct4, Sox2, as well as Nanog. These research have provided a first proof of principle for the stem cell 3D reprogramming. Beyond that, their work also paves the way for the future investigations about the study of synthetic 'reprogramming niche establishment', which shows great promise in achieving a better understanding of the cues and factors that can regulate cell fate and affect their further applications in clinical therapy.

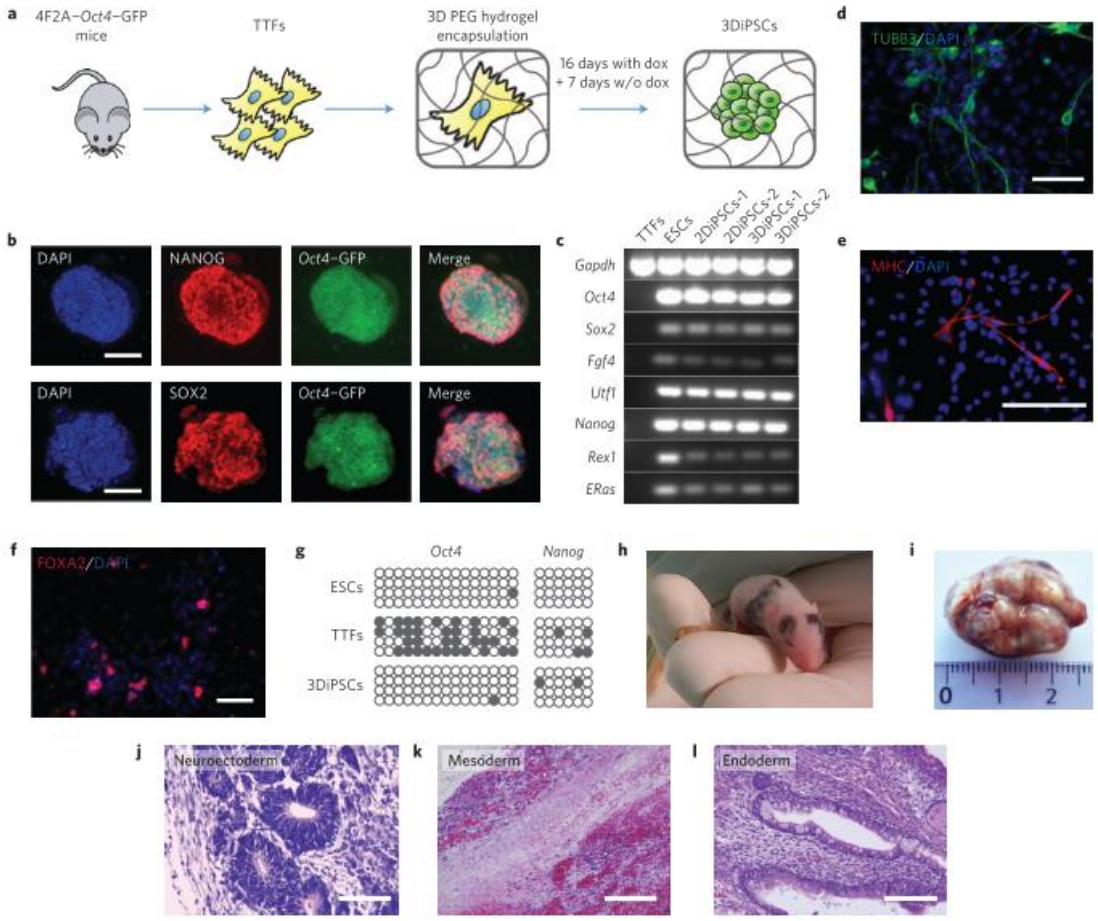

Figure 1-5. Generation of 3D iPSCs in chemically defined 3D microenvironments. (a), Schematic representation of the one-step 3D reprogramming protocol for miPSCs. (b), The immunocytochemistry analysis of the pluripotency markers. (c), The RT–PCR analysis of pluripotency marker genes in two clones of 3DiPSCs compared with 2D-iPSCs. (d-f), The immunostaining showing differentiation of 3D-iPSCs into neuroectodermal, mesodermal and endodermal cell types. (g), The methylation analysis of Oct4 and Nanog promoters in 3D-iPSCs, ESCs and tail-tip fibroblasts. (h), The chimaeric mouse generated with 3D-iPSCs. (i – l), 3D-iPSCs are able to differentiate *in vivo* into neuroectoderm, mesoderm and endoderm. Scale bars, 50 μm (b, d – f, k, l) or 25 μm (j), dox, doxycycline.[19] Copyright www. 2016 Nature.

1.1.3 Applications of iPSCs

The discovery of the iPSCs has opened up unprecedented opportunities in many research fields such as pharmaceutical industry, clinic therapy and laboratories.[13.20-21] After a decade of constraints, the induced pluripotent stem cells biology is now a

flourishing research area, following the achievement of the human iPSCs. These cells have the capacities of indefinite in vitro expansion and meanwhile they can be redirected to many cell lines, supplying abundant prospects in certain biomedical applications. Since iPSCs cells can be generated from the patients' own cells as shown in **Figure 1-6**,[9] transplantation therapies based on these patient-specific cells lines could circumvent the challenge immunological rejection.[4]

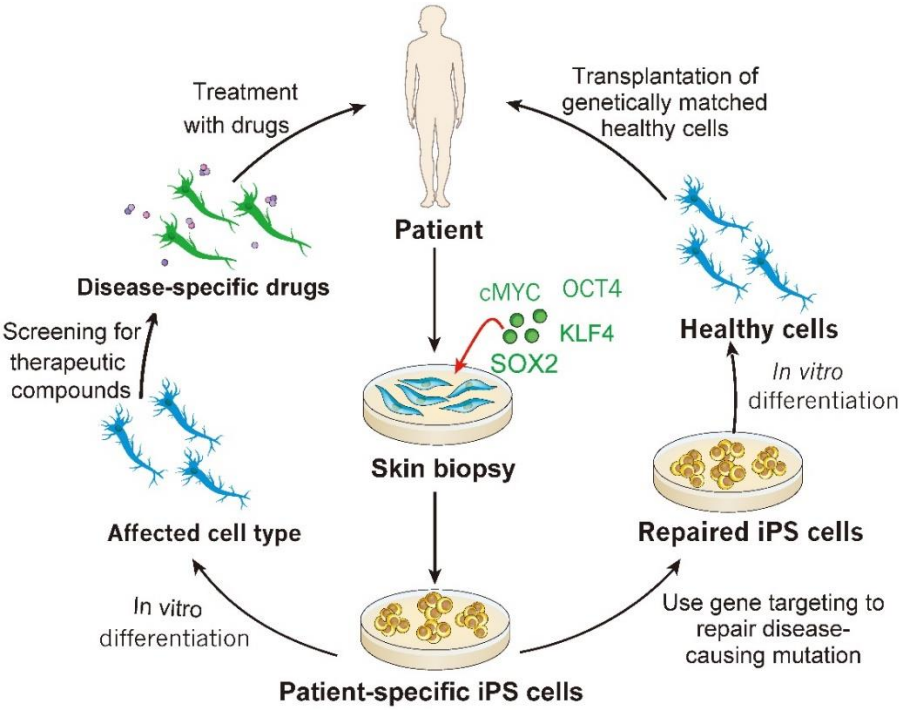

Figure 1-6. The medical applications of iPSC cells. Copyright 2012 Nature.[9]

Compared to controversial embryonic stem cells, of which the derivation might cause destruction to the preimplantation embryos, iPSC cells avoid the prominent ethical problems.[4, 22] Besides, these cells can be in an autologous fashion and grow into a large amount of cells after expansion in expansion *in vitro*, is very important for complex tissue formation. Actually, some of them have already been used in conjunction with scaffolds to generate different tissues.[23-25] They therefore are promising in many applications, such as tissue engineering and organ replacement, especially in the application of using lab grown tissues to replace or renew injured, aged, or diseased tissue in patient,[15, 26-28] cell replacement therapies,[29-35] compound

screening and drug candidate selection,[36-38] and disease modeling.[39] Besides of their crucial roles in clinical studies and research, iPSCs could also be very useful in investigating the molecular mechanism of numerous diseases. There are lots of diseases that have been modeled by applying iPSCs to better understand the etiology. Beyond that, iPSCs also play important roles in the production of patient-specific cells without immune rejection.[40]

For example, human pluripotent stem cells (hPSCs) can be used in the cell replacement therapy for cardiovascular disease.[29, 41] Converting the mouse fibroblasts into cardiomyocytes is usually a promising strategy. Briefly, there are several approaches can generate and support differentiated cell types(cardiomyocytes). One approach to generate cardiomyocytes is to establish iPSCs and then to differentiate them into particular cell lineages (cardiomyocytes). Another alternative approach to generate differentiated cardiomyocytes is to create partially reprogrammed cells (iPSCs) that can differentiate these cells to the desired cell type. The advantage of this method over the approach by establishing iPSCs is speed. Besides, there is also a direct reprogramming method, in which the cells can be directly differentiated to the desired cardiomyocytes cells without reprogrammed cell stage.[29, 41] Overall, the human pluripotent stem cells (hPSCs) indeed play crucial roles in the cell replacement therapy for cardiovascular disease.

Combined with the iPSC cells, the patient-specific cardiomyocytes can paly keys roles in applications about drug discovery and testing, as well as disease modeling. The approach that uses hPSCs to generate cardiomyocytes shows much more promise in potential applications than that with source of adult heart-derived cardiac progenitor cells.[29] Another popular stem cell therapy focus on human neurodegenerative disorders. During that research, the neurons used in transplantation could be generated by iPSC cells. Thus, the brain can produce new neurons from the patient's own cells and raise hope for the stem cell therapy in human neurodegenerative disorders.[31] For example, these stem cell therapies were well used in stroke, Parkinson's disease,

amyotrophic lateral sclerosis, and Huntington's disease.

In 2012, Nishimura's group reported a new approach to generate the rejuvenated antigen-specific T cells by pluripotency reprogramming.[32] As we know, T cells are very important in supplying systemic immunity that against pathogens. In particular, cytotoxic T lymphocyte is one of the major components of immunity that response to viral infections.[42] So, immunotherapy with T cells is a promising therapeutic strategy in treatment of cancer and viral infection. However, there is challenge of exhaustion of antigen-specific T cells in these diseases. To overcome the challenge, they reprogrammed antigen-specific $CD8^+$ T cells from patient to pluripotency. After that, the T cell-derived iPSCs were further differentiated into $CD8^+$ T cells. This rejuvenated cells not only have antigen-specific killing activity but also exhibit a specific T cell receptor. Similarly, the human tumor antigen-specific T cells can also be regenerated from mature $CD8^+$ T cell derived iPSC cells.[33] All of these approaches have broad applications in adoptive immunotherapy.

In addition, iPSC cells have also been reported as sources for dental pulp stem cells in regenerative medicine.[43] After being bio-printed in 3D environment, iPSC cells and hepatocyte-like cells differentiated from them can be used in the generation of mini-livers.[44] The approach of bio-printed iPSCs will play crucial roles in producing patient specific organs or tissues.

1.1.4 Major challenges in iPSCs' application

However, it should be noted that, during each of these applications, a large amount of cells with prolonged self-renewal ability and high pluripotency are needed. In general, by most current cell therapy protocols and those under development, the numbers of iPSCs-derived cells needed for the effective therapy fall in the range of thousands or millions to billions for per patient. For instance, myocardial infarction results in the damage or ablation of at least 10^9 myocytes.[45] Furthermore, approximately 1.3×10^9 beta cells or $\sim10^5$ surviving dopaminergic neurons are required separately for insulin

independence in Parkinson patients and the patients with other diseases.[46]. To get a large amount of iPSCs-derived cells, the number of the iPSCs must also be guaranteed. Therefore, large numbers of iPSCs cells are needed in various applications. So, these therapeutic uses of the iPSC cells necessitate their efficient expansion in large scale under well-defined conditions.

Besides the large amount of the iPSC cells, their quality is also very important and being the guarantee of their expression potency. As the iPSC cells can differentiate into other cells, during the culture process, there are various epigenetic changes that may lead to their self-renewing potential decreases and finally lead to the loss of pluripotency. So, all the iPSC cells that used for differentiating into downstream products for further application should keep high self-renewing ability and well pluripotency. For example, the use of iPSC cells in disease modeling is based on the fact that these cells can self-renew and differentiate into other types of cell lines. These advantages can benefit them to be further used to study different disease models.[40] Therefore, development of strategies to efficiently remove the induction factor of impurities and to supply a safety matrix without animal-derived materials will be essential for iPSC cells' reprogramming culture and expansion. So, approach for the culture and expansion of reliable iPSC lines are already emerging. Currently, numerous approaches are being investigated to get reliable iPSC cell culture. Because of the source of variability and xenogeneic contamination, all of the poorly defined materials that may pose risks not only in pathogen but also in immunogenic transfer and severely limit their further use of iPSCs for therapeutic applications should be avoided.

1.1.5 Current approaches for iPSCs culture

1.1.5.1 Two-dimensional culture technique

Since the beginning of iPSCs' generation, numerous methods and strategies have been explored to get a better culture protocol to supply high quality cells, of which, most are based on the traditional 2D culture system. For a long time in the beginning, conventional 2D cultures play a crucial role in fundamental researches, for example,

these approaches have provided crucial insights into many biophysical and biochemical mechanisms that responsible for iPSCs' grow and culture, including cell spreading, adhesion, proliferation as well as differentiation. Nevertheless, it is impossible for 2D cultures system to fully capture a native cell microenvironment' chemical and physical properties.

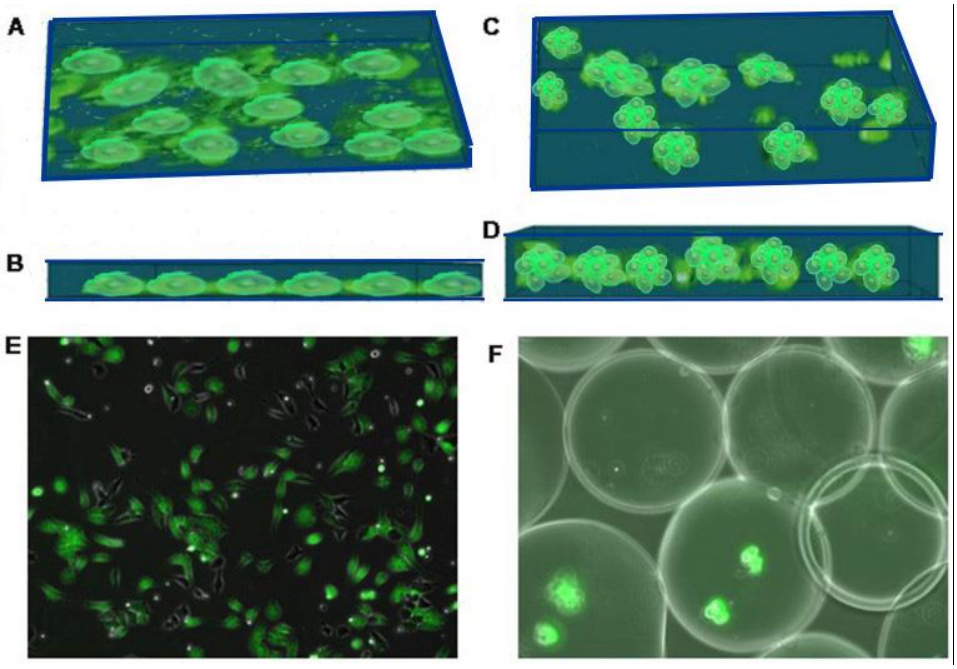

Figure 1-7. Morphological differences of the cells in 2D and 3D cultures. Cell in 2D cultures do not fully capture the physical and chemical properties of the native microenvironment. miPSCs in 2D culture and in 3D microenvironment. Copyright 2011, Mary Ann Liebert, Inc.[47]

More and more research have suggested that the cells cultured on 2D environment differ greatly from those grown in vivo.[48] Currently, mainstream 2D iPSCs cultures are using laminin or matrigel as a substrate for the cells to attach on when the cells are planted on the culture dish. However, suffering from the inherent heterogeneity, limited scalability and poor reproducibility, there is bottleneck for the 2D culture system to provide a well-proportioned environment and produce cells with high-quality for downstream applications, especially for clinical applications.[46, 49] Moreover, the

laminin or matrigel generated by mouse embryonic fibroblasts (MEFs) will also limit reproducibility and/or scalability of the cells, meanwhile pose risk for pathogen and immunogenic transfer.[10, 50, 51]

1.1.5.2 Three-dimensional culture technique

Generally, key biology signals both from their substrate and from one another are essential to promote cell survival and rapid proliferation.[52] But in 2D cultures, biology signals are difficult to distribute uniformly. The nutrients and oxygen in the monolayers are uniform, which is mat the cases for cell masses, i.e. tumors. While in 3D tumor spheroids, the environment is much more representative of that in vivo tumors, in which, compared to the outer layer, the inner cells face a natural gradient have less access to nutrients and oxygen. To solve these problems and improve the culture protocol, several preliminary attempts have been made to modify cultures systems from 2D to 3D (Figure 1-7).

3D culture is a method to embed cells in a three dimensional matrix and allow cells to interact with their surrounding extracellular framework. This kind of 3D models show great promise in the applications of studying the disease mechanisms and discovering the drug therapeutics. With these cultures, small molecule drugs can be screened to understand the disease pathways and these can be very useful for predicting the efficiency and the toxicity of drug treatment. Most important of all, cells cultured in 3D environments usually behave differently than in 2D cultures.[53] Therefore, more and more 3D cultures are studied.

In the past several years, many approaches and methods have been tried for large-scale culture iPSCs, attempting supply excellent cell sources for regenerative medicine. Most of these approaches rely on the combined use of multiple growth components and multicellular association, with all of these to achieve optimal conditions that can support cell grow fast and expansion with high efficiency.[54] Among all of these methods, scaffold culture is one of the most important cultures. On scaffold cultures, especially in a static 3D suspension culture,[46, 55] such as cell aggregates,[10, 56] cells on

microcarriers[57, 58] have been used widely, because these cultures can enable large-scale production of iPSC cells with high efficiency. But, for these culture systems, significant challenges are still inevitable. It is difficult to control culture outcome. Substantial cell agglomeration can in some cases lead to differentiation or death and poor viability. Even if in 3D dynamic suspension culture, cell damage is also inevitable due to the system's physical shear force.

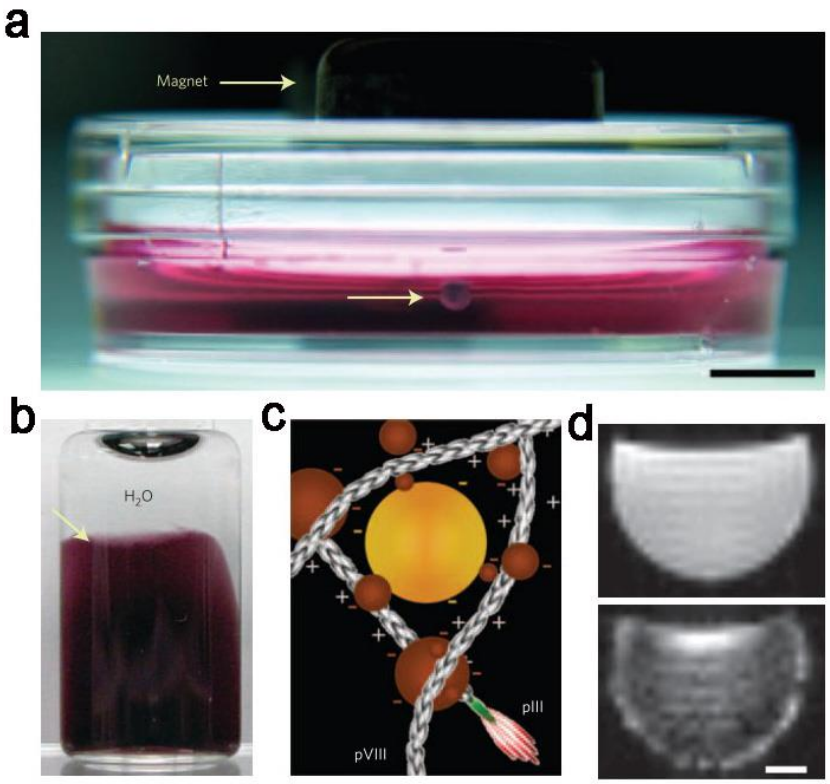

Figure 1-8. Magnetic iron oxide-containing hydrogels for hiPS culture. a, Human glioblastoma cells treated with magnetic iron oxide (MIO)-containing hydrogel held at the air–medium interface by magnet. Scale bar, 5 mm. b, MIO-containing hydrogel in water. c, Scheme of electrostatic interactions of MIO and gold nanoparticles with phage (pIII and pVIII indicate surface capsid proteins). d, MRI image of purified hydrogel in solution: MIO-free hydrogel control and MIO-containing hydrogel (bottom panel). Scale bar, 2 mm. Copyright 2010, reproduced with permission from Nature.[59]

Facing these challenges, Glauco Souza, a chief scientific officer from n3D Biocience in Houston, has proposed a promising spin - off iPSCs 3D cell culture system as shown in **Figure 1-8**.[59] In their system, cells are decorated with a NanoShuttle that

is made of magnetic nanoparticles. In the magnetic field, the NanoShuttle will bring the cells together while levitating them, which is more like the body's environment than conventional cell cultures. Though the approach applied here gives an interesting sight for 3D environment establishment, there is still the challenge that the magnetic particles may cause adverse consequences for the cells containing them, which is more or less unavoidable.

Lei has reported another kind 3D culture system for the efficient expansion of hPSC.[60] They built a completely defined 3D environment conditions by employing a kind of thermoresponsive hydrogel. The construction of their system was based on free of any animal-derived factors, but with only recombinant biology factors. According to their culture method, 3D system can supply expansion of the multiple iPSCs lines under optimal parameters and a good protocol. What's more, it can supply a high expansion efficiency. Obviously, it means that the 3D cell culture matrices used here could well represent their geometry, chemistry, and signaling environment of the ECM. However, the only fly in the ointment is that, if this system used in 3D iPSC culture, the way of releasing cells from the designed matrices by enzymatically degradation will inevitably be harmful to the proliferated cells. Besides, too hydrophobic environment (PNIPAAm materials) will usually lead to have a strong preference for a defined medium, not even stable in pure PBS solution.

Although all of these traditional methods for 3D scaffold or 3D suspension-based cultures have shown some very useful characters, any of them has shown to be obviously insufficient for the certain challenges in culturing cells for biology applications. Better artificial 3D cell culture matrices should be by coordinately feasible apply of advanced materials,[19,61,62] new fabricating approaches, processing methods,[63- 64] and biology cues.[65-67] Ideally, this artificial environment should be capable of better representing all the geometry, chemistry signals of the natural extracellular matrix's environment.

1.2 Extracellular niche or matrices devises for iPSCs' 3D culture

Notably, *in vivo*, the stem cells usually reside in an specialized microenvironment, called niche, which not only serves as a structure for cell's survival and support but also offers many physical and biochemical cues that can work together to regulate cell fate through a complex crosstalk.[48, 68, 69] At the same time, cells can also sense and respond all of the signals around in their environment, which can control the cell fate. So, it would be of great benefit for cell culture and expansion to construct an artificial microniche model, which can recapitulate the key interactions among the niche components in a controlled setting. Therefore 3D microenvironment engineering is particularly important in establishing a robust production system for iPSCs' 3D culture.[46, 48, 68, 70]

In 3D microenvironment engineering, the interactions between cells and their environment must be clear, especially for the crosstalk. Crosstalk between the cells and the niche around them is mostly mediated by soluble growth factors. The outside instructions can be conveyed to the inside cells through a special signal transduction network and the growth factor receptors on the cell membrane. Therefore, these network and receptors are crucial in leading to biological cellular responses and functionalities.[71] The ECM can regulate cell fate by working as a mediator of mechanical constraints applied to cells, as well as affecting the cells via its architecture properties.[72] Most of the fundamental characteristics and behaviors of stem cells are usually determined and controlled by the matrix-binding. In turn, with their overall functionalities, the complex cell–matrix feedback loop, are also contributed by cells.[73] While designing new synthetic biomaterials for artificial extracellular establishment, the functions of native ECM must be considered in mimicking their properties.[74, 82]

To tailor a microenvironment for iPSC 3D cultures, artificial microniches need to be designed with various biocompatible materials[75-78] and be engineered by a coordinated controlling over physical properties and biochemical activity to influence all of the specific interactions (cell-matrix, cell-cell) in a cellular system,[48, 68] including certain patterns of biomechanical and biochemical properties. Meanwhile, all of these

microniches need to be assembled in ways that terrific maneuverability and feasibility.

1.2.1 Niche and microenvironments of iPSCs

Most approaches for iPSCs culture are focused two main goals: to preserve pluripotency, or provide certain cues for specific differentiation.[79] However, both of the maintaining pluripotency or stimulating differentiation are depend on the signals from their local niche environment.[80] The niche is usually defined by extracellular matrices and the soluble molecules which were created by cells. The niche or microenvironment plays particular roles for stem cell regulation especially in stem cell 3D culture. Stem cells are usually quiescent in the niche without stimuli. But, after given a stimuli, they will switch to a proliferative phenotype soon. Therefore, the fate of the iPSCs are deeply related with their interactions with the niche. Recently, more and more studies have focused on regulating stem cell by supplying them with a special engineered microenvironment, especially for 3D culture. During any establishment of the artificial niche engineering, integrations of biophysical or biochemical cues such as, cell-cell contacts, biomolecules cues, cell-matrix interaction, and certain mechanical properties are needed.

There are many basic strategies in regulating the fate of iPSCs by altering their microenvironmental cues. Firstly, the adhesion interactions between iPSCs and the surrounding environment are important, because there are usually specific iPSCs receptors need to present and lead to adhesion for maintaining their colony status. [79] Those molecules for cell adhesion are usually proteins that located on the surface of the cells. As reported, among these proteins, cadherins, selectins, integrins, and immunoglobulins are usually involved in the interaction,[81] but, undifferentiated ESCs only express E-cadherin,[82, 83] which suggests that E-cadherin is very important in maintaining the ESCs' pluripotent state. Several ECM proteins like laminin, fibronectin, and collagen have been reported to be crucial both in maintaining cells' self-renewal capacity and differentiation ability. Recently, more and more adhesion molecules have been tested and used in the establishment of 3D microniche culture systems. For

example, specific peptide sequence like RGD, especially circular RGD, has been used for cell adhesion in many systems.

Besides that, biochemical cues are also important factors that can influence iPSCs' maintenance, performing as signaling molecules in directing cell communications in the microniche. The partial pressure of oxygen and mechanical forces have also shown to be a important factor to modulate cell fate during embryonic development in drosophila.[84] Obviously, proteins of ECM are also important for structure, orientation maintenance of the microniche, because they can provide instructive signals by providing ligand interaction with the integrins expressed by cells.[85] Meanwhile, the parameters such as stiffness, shape, and elasticity that usually direct stem cell keep maintenance or differentiation.[86-89] Additionally, stem cell niches can maintain self-renewal and the long-term quiescence by altering the characteristics of the environment, such as hypoxia and metabolic regulation as shown in **Figure 1-9**. [90-94] Therefore, taken together, the general consensus is that all of these factors should be considered and used to regulate self-renewal and cell fate directly by a coordinated control of the microniche construct for iPSCs cells culture.[95]

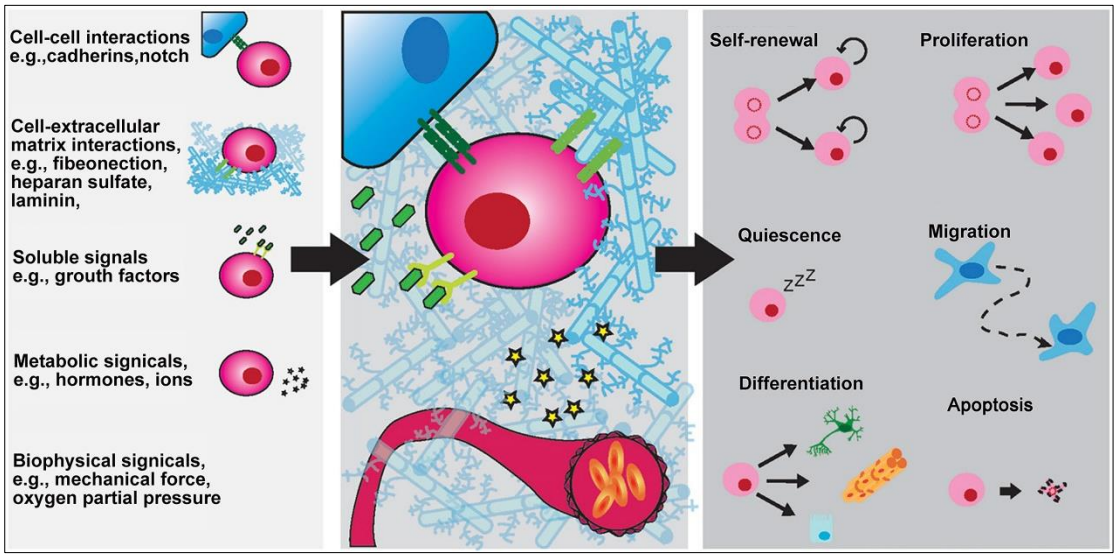

Figure 1-9. The schematic representation of the stem cell niche and underlying regulatory mechanisms. There are lots of factors (left) present in the stem cell niche that can work in tightly regulating the stem cells behavior and fate choice. In fact, *in vivo*, stem cells reside in anatomically

defined location - the stem cell niche (center). The niche is a multi-faceted entity (right), such as self-renewal, proliferation, migration and differentiation.[94] Copyright 2016, reproduced with permission from STEM CELL Translational Medicine.

1.2.2 Materials used for scaffold or niche in iPSCs 3D culture

Biomaterials play more and more prominent roles in the application of tissue engineering and in the application of the pluripotent stem cell regenerative medicine.[96] With the development of the biomaterial science, the biocompatibility of these materials has been evolved and the biomaterials become more sophisticated. Since then, the understanding of cell–material interactions has also grown according to the integration of biological signals and the properties of the materials that are dropped into a cell scaffold or 3D environment. This should usually be taken into consideration as well. Many strategies have been established for the stem cell scaffolds and 3D environments.[97]

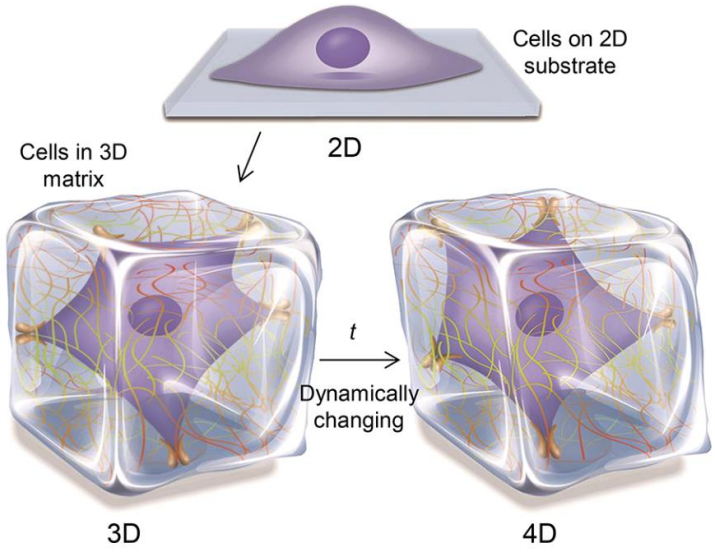

Figure 1-10. Natural biomaterials present a crucial subset for use as tissue engineering templates due to their bioactivity, biocompatibility, tunable degradation and mechanical kinetics and their intrinsic structural resemblance of native tissue ECM. Copyright 2017 from ACS.[101]

Research on iPSCs' 3D cultures has been aimed to investigate the possible strategies that allow for the cells to maintain their self-renewal and proliferation

abilities without any change of the phenotype. However, novel biocompatible materials used to establish the 3D environments play a great role in influencing cells. Thus, to use of hydrogels scaffolds to provide native microenvironment' geometrical similarities is currently an area of extensive research.[79] More and more biocompatible materials are chosen as sources for materials for 3D environment or cell niche research.

Biocompatible materials, especially hydrogels, which are characterized by diverse physical properties, high water content, and good biocompatibility, are kind of 3D networks that can be easily fabricated practically into any shape, size, or form.[62, 63, 67, 98, 99] By applying approach of coordinated controlling all of their bioactivity or physical properties to influence the specific interactions in cellular systems, we can apply these materials to resemble an artificial extracellular environment for cells to survive and that enable their use in mimicking native ECM, guiding stem cell's fate, and boosting induction of pluripotency in stem cell cultures.[67, 75, 100] In general, these materials are usually classified into naturally derived, hybrid hydrogels, and synthetic hydrogels, according to their origins shown in **Figure 1-11**.[101]

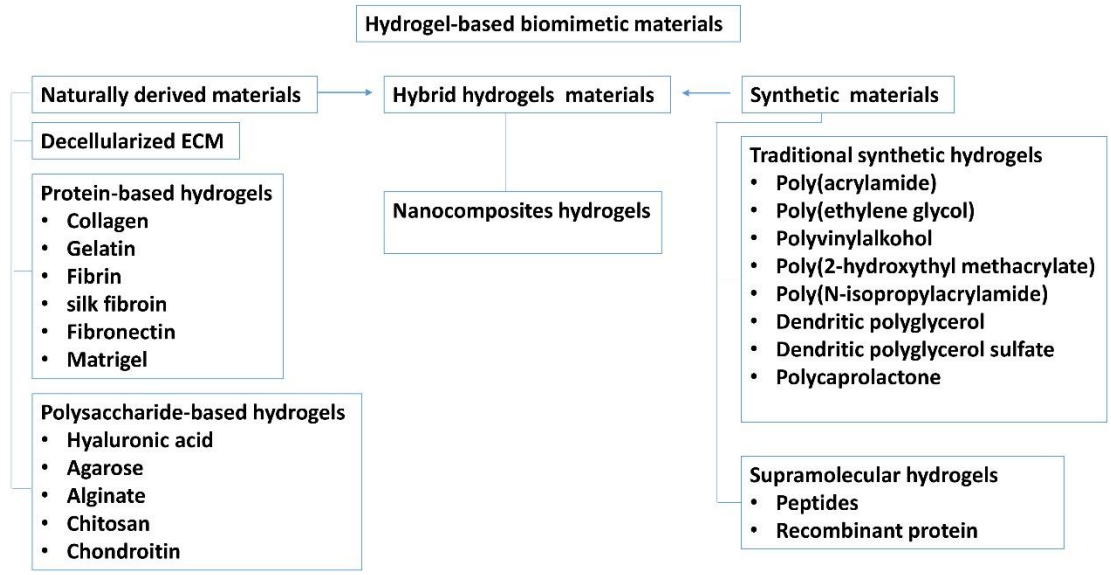

Figure 1-11. Classification of biomimetic materials for engineering 3D cell microenvironment. The biomimetic materials used for engineering cell microniche or microenvironment are based on hydrogels, which can be classified into naturally derived, hybrids, and synthetic hydrogels according to their origins and compositions. Copyright 2017, Reproduced with permission from ACS.[101]

1.2.1.1 Naturally derived and hybrid materials

Due to the biocompatibility, mechanical kinetics, tunable degradation, and the intrinsic structural resemblance to native ECM, natural biomaterials present a crucial subset of materials that can be used widely in the application of biological systems. Compared to other materials, they usually have unique advantages. For example, most of the natural biopolymers have been processed by environment friendly approaches. During their applications, the degradation process does not release cytotoxic products which will do harm to the microenvironment. And the degradation of these microenvironment can also be achieved by adjusting their formulation and processing conditions, which may strongly affect the cells' function.[96, 102, 103]

Naturally derived materials are normally divided into two kinds of materials. The protein-based materials such as collagen, silk fibroin, keratin, and fibrin are typically obtained from animal or human sources.[104-110] These materials have been widely used in many fields to build certain cell living environments, especially for stem cell culture and their regenerative applications. For polysaccharide-based materials, such as hyaluronic acid,[107, 111, 112] glucose, cellulose, chondroitin,[113] alginate,[114-118] chitin, and its derivative, chitosan[119, 120] are typically obtained from algae and these materials also been applied widely. Many specific stem cell niches are related to these materials.[96, 121]

Natural polymers usually contain some surface ligands for cell adhesion, which mediated by the specific interactions between the cells and their local surrounding environment.[86, 122] Additionally, hybrid materials have also been used to design the 3D biosynthetic hydrogel system to understand the interactions between mechanical and biochemical cues, for example, eight-arm PEG cross-linker and the functionalized proteins (HA-SH and Col-Me) as well as RGD to form bioactive hydrogels as shown in the schematic in **Figure 1-12**.[107]

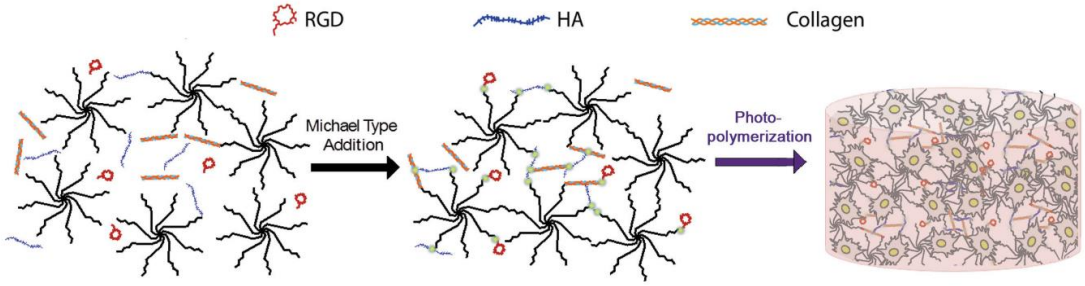

Figure 1-12. Hydrogel designed with PEG acrylates and hyaluronic acid (HA) and type I collagen (Col I) via Michael-type reaction is useful in harnessing the cell–matrix and cell–cell interactions. Copyright 2017, WILEY-VCH.[107]

Although the above-mentioned naturally derived and hybrid materials have been used widely in many fields, there are still some inevitable disadvantages and problems. Because of the source of variability and xenogeneic contamination, these poorly defined materials may pose risks for immunogenic transfer and pathogen, severely limiting the use of iPSCs for therapeutic applications.[65, 66, 123, 124] Besides, due to batch-to-batch compositional and structural variability, these poorly defined materials not only have inevitable disadvantages in segregating certain cell responses and determining exactly which signals do promote certain cell functions but also exhibit poor independent tuning of their physical and chemical properties.[48, 68] Therefore, to circumvent all of these issues, new synthetic materials and special manufacture techniques need to be employed to establish an artificial microniche that can support expansion of reliable stem cells and their scalable culture.

1.2.1.2 Synthetic materials

Synthetic materials, especially polymers, have already been widely used as templates or matrices in bioengineering. There are several advantages over the naturally derived materials.[96,125,126] In general, *in situ*-forming hydrogels based on synthetic polymers, such as PEG[77,127,128] and poly(hydroxy acids), which include PGA, PLA, and their copolymer, poly(lactic-co-glycolic acid) (PLGA),[129,130] not only can be engineered to deliver the bioactive agents in a controlled manner for the regulation to stem cells' fates, but also can be utilized as cellular micro-scaffolds. One of the important points is that

the degradation of the polymers can be achieved by simple chemical hydrolysis of the polymers and their products can be cleared away by normal metabolic pathways.[130] Besides that, it should be noted that, synthetic polymers' properties such as mechanical modulus, tensile strength, and degradation rate can be easily adjusted for certain target applications by altering the relative parameters. For example, one of these materials is PCL. Because this material has good biocompatibility and low immunogenicity, especially can be hydrolyzed under physiological conditions, PCL has attracted widely attention in biology tissue engineering. This polymer can be used either alone (PCL), or as a PCL-containing amphiphilic block copolymer, which shows excellent performance in many applications.[125, 131, 132]

Poly(N-isopropylacrylamide) (pNIPAAM) is a hydrogel that can be used for many applications.[133] Benefiting from the lower critical solution temperature (LCST) of 32 °C, an aqueous solution of pNIPAAM can be used *in situ* as scaffold in many fields. When the temperature increases to 37 °C, which is high than the LCST, it forms a reversible hydrogel. More usually, this polymer can be designed as loosely crosslinked polymers. For example, pNIPAAM can be made as copolymer of pNIPAAM and acrylic acid (pNIPAAm-co-AAc). The LCSTs of these copolymers can change some around 32 °C. For different applications, pNIPAAM can be copolymered with various other polymers, such as ethylene, lactide, and caprolactone crosslinkers.[134]

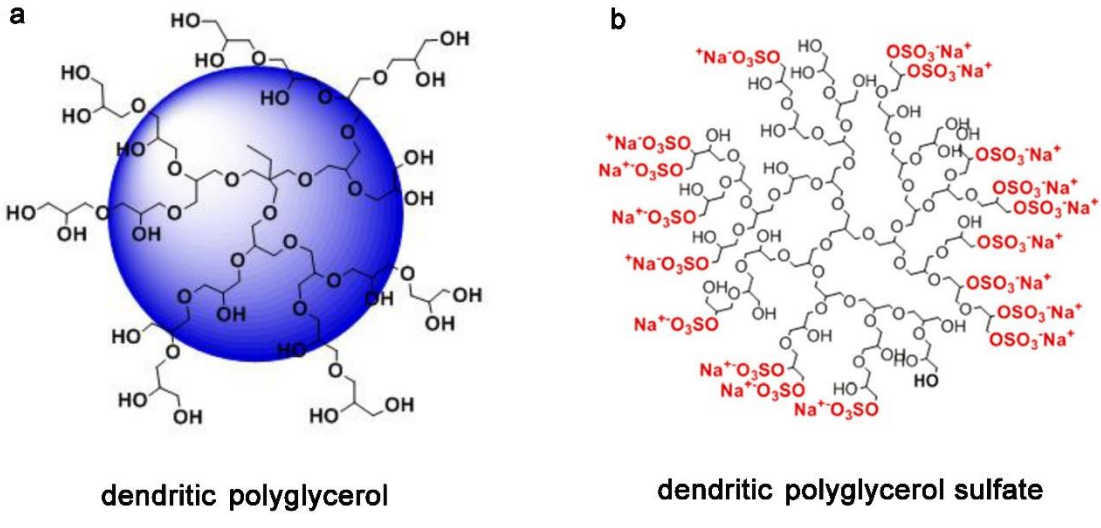

Figure 1-13. Structure of (a) dPG and (b) dPGS.[135] Copyright 2014, WILEY-VCH.

With multiple hydroxyl (OH) groups on the periphery/surface, branched structure, high-hydrophilic, non-toxic, and anti-fouling properties, dendritic polyglycerol (dPG) is an important material in bioengineering.[135-137] (**Figure 1-13a**). dPG is usually prepared by an anionic, ring-opening, ae well as multi-branching polymerization with narrow polydispersity.[138] After being sulfated, the dendritic polyglycerol can change into dendritic polyglycerol sulfate (**Figure 1-13b**). Thus, dPG and dPGs have very good characteristics to become a suitable matrix for cells encapsulation as scaffold because of their antifouling properties.[139,140] The presence of easily functionalizable hydroxyl groups on the backbone of their structure also makes them excellent candidates to prepare multifunctional polymeric network or hydrogels.[141] Crosslinking density of these networks can also be adjusted by varying their functionalization degree. Benefiting from the dendritic structure, the ligands that are responsible for cell spreading and attachment, for example, RGD (Arg-Gly-Asp), can be easy incorporated to the backbone of the dPG using the functional available groups. Thus, they can be widely used in many applications as cell scaffold materials.

1.2.1.3 Advantages and challenges of the synthetic polymers as scaffold materials

There are so many synthetic polymers such as PLGA, PCL and PCL- copolymers, PEG, PVA,[142-144] pNIPAAm and their copolymers,[145,146] polyacrylic acid, and polyvinylpyrrolidone, that have been applied in biomedicial application. With biomimetic ECM-like micro/nanoscale structures and attractive processability,[96] these materials can be easily used to manufacture various scaffolds with fully interconnected pores and certain classes that can affect cells' fate. Some of them may produce the acidic degradation products that can alter the PH around their environment. In turn, pH change in the environment will affect the cell' survival and cause some inflammatory reactions.[147,148] Due to the lack of the biologically functional domains, the synthetic materials are usually. Nevertheless, with the development of the synthesis techniques, various biologically active domains have been incorporated into synthetic polymer templates, which enable the biomimetic scaffolds with tunable but defined

composition.[149] In other cases, ECM-derived moieties also can be introduced to polymeric scaffolds by the covalent immobilization during the fabrication process to affect or adjust the cells behavior.[150] For example, the bioactive agents, such as RGD peptides, are often presented on the surfaces of the synthetic polymers template to elicit certain desired interactions between cells and materials.[151] Therefore, how to devise these polymers or copolymers systems to affect the cells' behaviors is really important, which not only provides insights into the relationships between chemistry structure and their functions but also shows great promise in utilizing these materials as much suitable cellular scaffolds instead natural derived materials.[152]

1.2.2 Strategies for gelation

Tissue engineering and 3D cells culture in an artificial scaffold are performed by seeding or encapsulating cells during the gelation process of the polymer linkers. In other words, the gelation process is also the crosslinking process. Therefore, the gelation strategies applied in the crosslinking process of the hydrogel formation are crucial in determining the cell fate, and therefore are very important in evaluating the feasibility of the scaffold establishment. Besides, the main role of the scaffolds for cells is providing enough certain mechanical stiffness, which is determined by both the crosslinking ways and the gelation approaches to a great extent and can be freely adjusted by altering the crosslinking density. There are lots of strategies and ways of crosslinking that are usually used in the polymer gelation process, such as host-guest interaction, hydrogen bond formation, supramolecular or ionic crosslinking, physical bonding crosslinking, and covalent crosslinking.

1.2.2.1 Covalent crosslinking gelation

For covalent crosslinked gelation that used in establishing cell encapsulation scaffolds, the crosslinking process need to be biorthogonal, because that does not interfere with the biological systems and has a minimum effect on the cell death. In addition, the reaction rates in the crosslinking process also need to be fast enough and the covalent reaction should be selective and with a high yield. Among all the covalent crosslinking gelation ways that can fulfill these requirements, chain growth radical crosslinking,

thiol-Michael addition, thiol-ene click reaction and the strain-promoted azide-alkyne cycloaddition are the most typical approaches that usually used in artificial cell scaffold establishment.

Firstly, due to its fast reaction kinetics, radical crosslinking is one of the most widely used strategies for hydrogel gelation. This crosslinking can usually be initiated by temperature, light and redox conditions. The most attractive advantages of this reaction are the readily available of the introduction of the reactive groups to the macro-monomers to form functional polymers and they can be applied *in vivo* because visible light can be used as initiators for it (activated by visible light).[153] However, as reported, these are intracellular reactive oxygen species format during photo crosslinking, which can increase the DNA damage tendency [53] and tissue formation[154,155] and therefore may affect the cell viability. Additionally, the light intensity decrease in deep hydrogels may also lead to inhomogeneous crosslinking density, all of which limit their applications.

Another widely used reaction is thiol-Michael addition.[156] This reaction can be performed in an aqueous medium under physiological conditions, benefiting it suitable for cell encapsulation. Since we know thiol is one of the reactive groups in this reaction and thiols are also readily available in peptides, the peptide hydrogels can be prepared by thiol-Michael addition.[157] The other reactive group can also be easily incorporated to the polymer. Therefore, this reaction can be used widely in tissue engineering.[158]

Thiol-ene reaction is a click reaction, the polymerization process is performed between a thiol and a norbornene derivative in the presence of photo initiator and light (365 nm). Compared to the free radical polymerization, this reaction can offer a more controlled radical formation.[159] In this reaction, as thiol is one of the reactive groups, peptides can easily be used as a crosslinker for hydrogel formation.[160] Sometimes too many free thiol groups will disturb the balance of the cell environment so that reduced small molecules can react with the thiols and destroy cell viability.

Strain-promoted azide-alkyne cycloaddition (SPAAC) reactions were first

reported in 2004.[161] Among the whole crosslinking chemistries, SPAAC has desirable advantageous over others because of its excellent selectivity towards substrate and very fast reaction kinetics.[162-163] Besides, the initiation of SPAAC reactions does not need any external stimuli/triggers such as photo, UV, base, pH, catalysts like metal salts, or oxidizing agents.[164] All the above properties, together with their excellent bio-orthogonal crosslinking properties, have already made them ideal candidates for 3D encapsulation of cells in tissue engineering and has been widely used in cell scaffold systems and pattern 3D cell microenvironments.[161,165]

1.2.2.2 Noncovalent crosslinking gelation

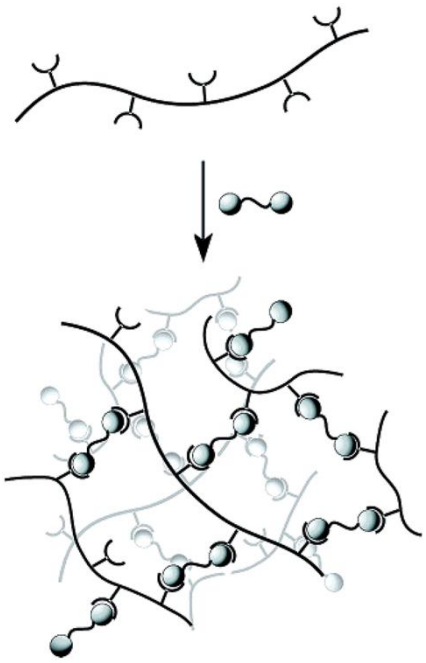

Figure 1-14. Schematic illustration of noncovalent polymer cross-linking of copolymers using complementary bifunctional cross-linkers. Copyright 2003, ACS.[167]

As reported, molecular self-assembly through noncovalent crosslinking also plays an important role in gelation.[166-168] According to this strategy, shown in **Figure 1-14**, materials with higher-order structures can be controlled formed, especially to systems about dendrimers and polymers. By using this noncovalent crosslinking methodology, diverse structures, including gels, vesicles, micelles, and other spherical aggregates, can be generated. Combined with the reversible nature of molecular recognition processes, the materials made according to noncovalent crosslinking can be designed as stimulus-

responsive recyclable materials that can be responsive to thermal,[169] photochemical,[170] or electrochemical stimuli. Therefore they supply numerous potential applications in cell encapsulation and micron-sized 3D cell-culture vessels.

1.2.3 Material design considerations for engineering 3D cell microenvironment

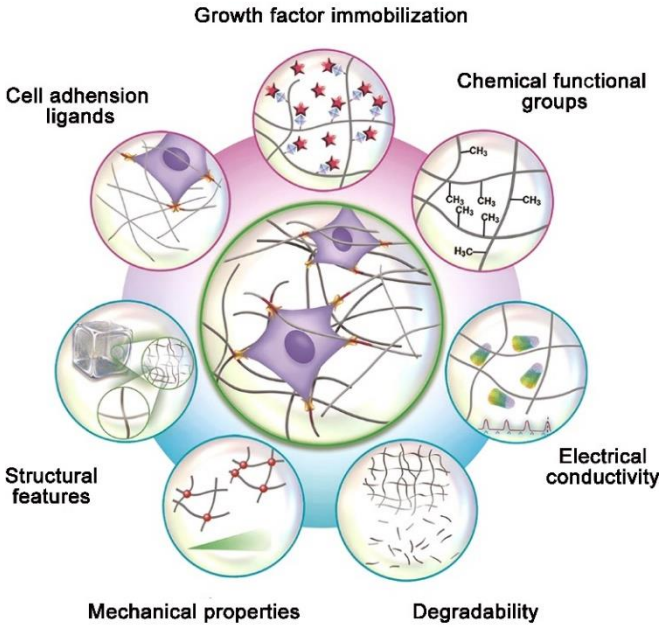

Figure 1-15. Biomimetic material design considerations for engineering the 3D cell microenvironment. Copyright 2017, ACS.[101]

In vivo cells survive in complex microenvironments called “microniches”. Though, the microenvironments of the cells are extremely diverse, but they still share many similar functions and characteristic composition features. For example, the 3D microenvironment not only briefly serves as structural supports for cells, but also offers various biochemical or physical cues that can regulate cell’s behavior together. These cues are the major concern and become crucial design considerations for the biomimetic materials in establishing artificial cell environment.

1.2.3.1 Substrate stiffness

The stiffness of the materials is usually characterized by their elastic modulus or Young’s modulus. It is often regarded as one of the most important mechanical features that can control cell fate such as adhesion, migration, and differentiation.[171] Since the

stiffness of natural tissues is usually range in 0.1 kPa to 100 kPa as shown in **Figure 1-16**, hydrogels are suitable to provide a similar 'natural' mechanical environment for cells. For example, as reported, for iPSCs culture in artificial environment, the optimal elastic modulus range are usually from 30Pa to 500Pa, during which the cells can survive and expand well.[19, 66] Cells are also usually responsive to the environment's stiffness by altering their adhesion, morphology, and migration characteristics. Therefore, stiffness parameters should be paid attention to the design of the artificial 3D cell microenvironments, as well.

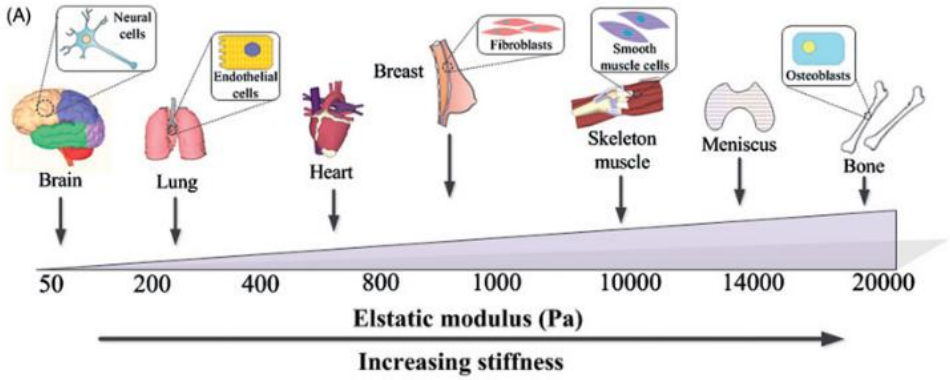

Figure1-16. Hydrogel-based methods for engineering cellular microenvironment with spatiotemporal gradients.[172] Copyright, 2017 ACS.

1.2.3.2 Substrate degradation

Most of the natural materials are enzymatically degradable. This degradation effect of the environment has a significant influence on cells' behavior, especially in a 3D microenvironment. For example, Burdick recently reported that stemness of cells was not depend on the environment's stiffness but strongly depend on degradability of the 3D hydrogel.[173] That provided an strong evidence for the important roles of degradability in maintaining neural progenitor cell in a 3D microenvironments. So, it is important to introduce degradation in establishing 3D cell microenvironments. Usually, degradation of hydrogel is usually influenced by factors like degradable linkages, cells, and the culture environment around the hydrogels.[174] The common strategies applied in designing degradation are mainly by introducing natural polymers or introducing small peptides or amino acid sequences into the backbone of the

hydrogels. Incorporation of ester bonds in the crosslinks or backbone of the polymer is a typical approach in designing hydrolytically degradable hydrogels.[175] However, the degradation profile should be optimized to complement the secretion of newly synthesized ECM, because a too quick degradation will lead to the cell-laden hydrogels dissolving, while too slow degradation will lead to the ECM depositions taking place in the pericellular region, which will affect cell function.[176]

1.2.3.3 Surface receptors and biological cues.

During the cells' living environment, there are various biochemical cues like cell–cell contact, cell adhesion and the insoluble factors around the cells. Cell behavior, including differentiation and self-renewal can easily be affected by these factors. Therefore, the precise mechanical properties and the bio cues of the links between the cells and substrates need to be essentially taken into account in the designing of the 3D microenvironment for cells by synthetic polymers that are naturally bio-inert. In that case, ECM-derived moieties can be introduced to polymeric scaffolds by the covalent immobilization during the fabrication process to affect or adjust the cells behavior.[150] For example, the bioactive agents, such as RGD peptides, are often presented on the surfaces of the synthetic polymers template to elicit certain desired interactions between cells and materials.[151] Different bio cues should be specially functionalized on the polymeric scaffolds according to certain applications. By this strategy, various biologically active domains have been incorporated into synthetic polymer templates, which provide the biomimetic scaffolds with a tunable but also defined composition, and meanwhile support the cells' survival as well.

Chapter 2. Scientific Goals

Part1

The discovery of iPSCs has opened up unprecedented opportunities for biomedical applications.[13,20,177] Because of their inherent properties, the iPSCs, as an alternative of ESCs, constitute an extremely attractive tool for therapeutic applications without immunological rejection and ethical problems.[65,70,123,124,178] However, due to the source of variability and xenogeneic contamination, the poorly defined animal-derived matrices may pose risks for pathogen and immunogenic transfer, which severely limits the cells grown in them for therapeutic applications.[65,66,123] Besides large quantities of cells, well beyond laboratory scale, are usually needed.[46,70] Obviously, conventional 2D cultures cannot meet these challenges[48,68] and novel approaches for iPSC expansion to obtain reliable cells with prolonged self-renewal ability and high pluripotency that are suitable for clinical application are urgently needed.[46,70] To circumvent all of these issues, completely synthetic materials and special manufacture techniques need to be employed to establish an artificial microniche that can support expansion of reliable iPSCs. Ideally, the manufacture processing should be engineered to realize by automatic production and support iPSCs' scalable culture. So, our research goal is to creatively establish a much more suitable surrounding environment for iPSC to survive inside a 3D scaffold similar to native ECM. To realize iPSCs' reliable expansion, we specifically engineered a novel chemically defined, artificial three-dimensional (3D) microniche with degradable polyethyleneglycol-co-polycaprolactone and RGDfk-functionalized dendritic polyglycerol hydrogel precursors by droplet-based microfluidics. The microniche engineering can allow for robust proliferation of iPSCs that maintain a high level of pluripotency expression and excellent viability but without any reproduction limits and pathogen and immunogenic transfer risks, which indicates great promise for therapeutic applications. Additionally, the fabrication process of this microniche engineering is performed under microfluidic conditions and can supply microniche scaffolds with huge efficiency. Therefore, it also shows great promise in realizing iPSCs' 3D culturing and reliable expansion on a large scale for therapeutic

applications.

Part 2

Since ECM is the natural environment for the cell growth and survival, the building of a 3D microenvironment by mimicking the properties of the ECM is a promising strategy.[19, 68] Recently synthetic materials inspired from the construction and role of ECMs in cell accommodation were produced for the cell culture applications. For example, hydrogels based on biocompatible polymers were produced which incorporated biological cues to define an artificial milieu with complex interactions that regulate and foster stem cells similar to the events occurring in a natural cellular microenvironment.[96] For example, Lutolf and coworkers reported adhesion peptide functionalized enzylatically cross-linked PEG-based hydrogels by chemical gelation for the design of 3D microenvironment to mimic the biochemical features of the native ECMs.[19] After modulating micro-environmental stiffness, degradability, and biochemical composition, this synthetic 3D 'reprogramming niche' explored for somatic cell reprogramming and iPSC generation. These synthetic matrices better represented the geometry, chemistry, and signaling environment of the natural extracellular matrix. However, these synthetic 3D system might not be suitable for the iPSC culture because enzymatic degradation will inevitably be harmful to the proliferated cells. The Haag group has previously reported a microgel construction kit and successfully realized the pH-controlled release of living cells from the hydrogel by benzacetal bond hydrolysis.[63] However, iPSCs are too sensitive to survive under pH 6 for three days and will differentiate undisputedly. Schaffer's group reported an iPSCs 3D culture system with pNIPAAm-PEG hydrogels in a different view, which was only by physical thermos-reversible gelation.[60] However, physical thermos-reversible materials are usually based on loose gelation strengths, and only under high concentration, they can support a iPSCs culture. While, under high concentrations, thermos-reversible materials have a strong preference for a defined medium and are even not stable in pure PBS solution.[36] Obviously, all of these attempts show some attractive aspects, while none of them is already proven to be the consummate template

culture method.

Within the second project, we investigate an approach to establish fully defined, thermally responsive, iPSCs' 3D artificial niche based on dPG and poly (N-isopropylacrylamide)-co-polyethylene glycol polymers via physical-chemical-co-gelation strategy. Benefiting from the cooperation of the SPAAC reaction and the physical phase transition, the co-gelation system can be adjusted with optimal stiffness and mechanical strength, which can support iPSCs cells survival well, keep self-renewal, and preserve high pluripotency. After being cultured, the cells can be easily controllably released from the niches just by adjusting their temperature. Overall, the high maneuverability and feasibility of this establishment of artificial niche engineering shows great promise in iPSCs' 3D cultures for regenerative medicine and clinical therapies.

Chapter 3. Chemically Defined Stem Cell Microniche Engineering for iPSCs' 3D Culture and Expansion

The discovery of the iPSCs has opened up unprecedented opportunities for biomedical applications. Nonetheless, the poorly defined animal-derived matrices limit the cells grown in them for therapeutic applications. Effective improvement of a cell-culturing approach and conditions for iPSCs' reliable expansion still poses a considerable challenge. Herein, we specifically engineered a chemically defined, artificial three-dimensional (3D) microniche with degradable polyethyleneglycol-co-polycaprolactone and RGDfk-functionalized dendritic polyglycerol precursors by droplet-based microfluidics for iPSCs' culturing and reliable expansion. The microniche engineering can allow for robust proliferation of iPSCs that maintain a high level of pluripotency expression and excellent viability but without any reproduction limits and pathogen and immunogen transfer risks, which indicates great promise for therapeutic applications.

3.1. Results and Discussion

3.1.1 Establishment of the chemically defined, artificial 3D microniche engineering

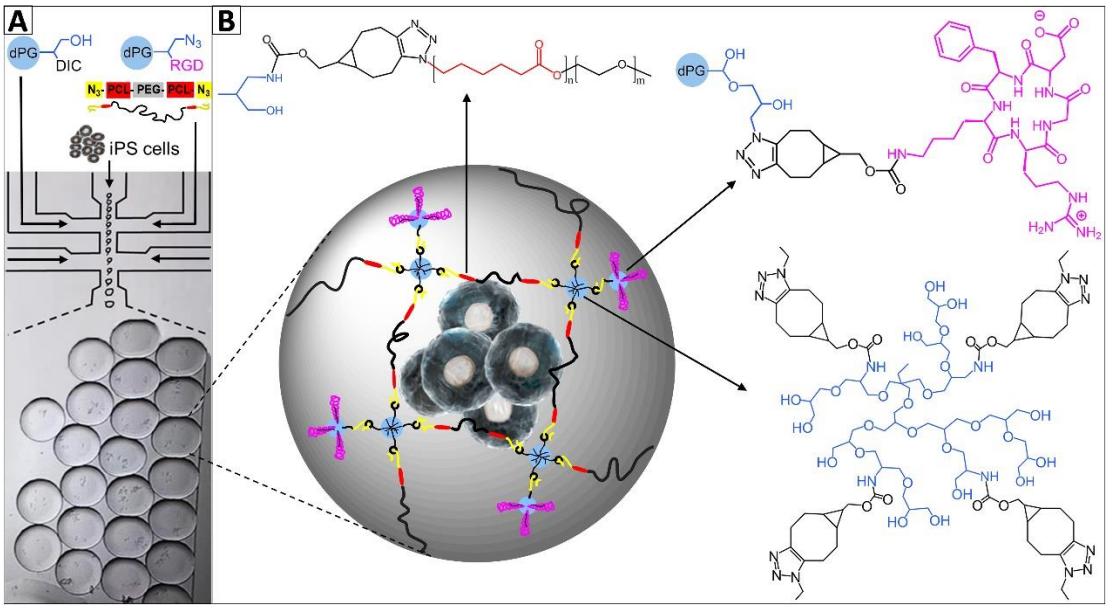

Scheme 3-1. Chemically defined artificial 3D microniche engineering. (A) A set of synthetic precursors, dPG-cyclooctyne, degradable polyethyleneglycol -co-polycaprolactone azide, and RGD-dPG-azide, were prepared. Together with these precursors, iPSCs were injected into a microfluidic device and fabricated into droplet, cell-laden microniche precursors with size of 150-200 μm. Gelation occurred inside by SPAAC during the incubation process (10 min), which then formed microniche particles with iPSCs' seeding inside. (B) dPG-PCL-PEG networks acted as the backbone of the microniche and served as structural supports for the cells. RGD supplied the microniche with cell attachment sites to promote cell survival. The hydrolysis of ester bonds from caprolactone units equipped the microniche with degradability that could stimulate iPSCs' proliferation while maintaining pluripotency.

Herein, we present a new chemically defined artificial 3D microniche engineering that can be specifically applied for iPSC culturing and reliable expansion as schematically illustrated in **Scheme 3-1**. As hydrogels composed from synthetic polymers like polyethylene glycol (PEG)[77, 128] and dendritic polyglycerol (dPG)[61, 63, 136, 179] have high biocompatibility, low batch-to-batch variability, and facile mechanical tunability, they are readily amenable to large-scale manufacture and show great promise in acting as 3D cell-culturing platforms. In this system, dPG-PCL-PEG hydrogel networks, serve as the backbone of the microniche to mimic the physical properties of the ECM, were designed according to bioorthogonal strain-promoted azide-alkyne cycloaddition (SPAAC[180-182]). To stimulate cell adhesion inside the microniche, cyclo (RGDfk), a cellular binding peptide sequence, was integrated into the polymer network as a biochemical signal.[66, 183, 184] Meanwhile, caprolactone units were introduced into the backbone to give the hydrogel degradability thus maintaining the proliferation of the iPSCs.[61] Moreover, stiffness-related physical parameters were adjusted via variations in composition and monitored by rheology tests[19] to support iPSCs' survival. In addition, a droplet-based microfluidics technique[50, 62, 63] was adapted to combine the precursors and cells with different contents into microniche particles with a certain size to let the nutrients, metabolites, and air penetrate freely. According to all of these strategies, a chemically defined microniche for iPSCs culturing was finally established.

For a holistic study of the microniche design, pivotal parameters should be coordinated and controlled to recapitulate a microenvironment that can affect cellular

responses. Among them, the stiffness plays a key role in regulating cell survival. Therefore, we primarily modulated the content and the ratios of precursors that related to hydrogel stiffness[68] and investigated the cells-behaviors. Rheology testing (**Figure 3-1A**) revealed that gels formed with precursors of PEG-PCL-N_3 and dPG-DIC in certain ratios (2:1) could support the gelation process most effectively. Additionally, the gelation time, as a crucial parameter to evaluate the gelation efficiency, was essential in determining whether the technique could be used in the microniche manufacture process. So, we further investigated the relationship between temperature and gelation time (**Figure 3-1B**). It must be emphasized that the resulting gel stiffness, i.e., viscous and elastic modulus, is independent with the change of gelation temperature. Longer gelation times would increase the incubation time in the manufacturing process and reduce cell viability, while a too short gelation time would not guarantee the even mixing of the precursors, , which would strongly influence the integrity and homogeneity of the microniche. Therefore, a gelation time of ~10 min is

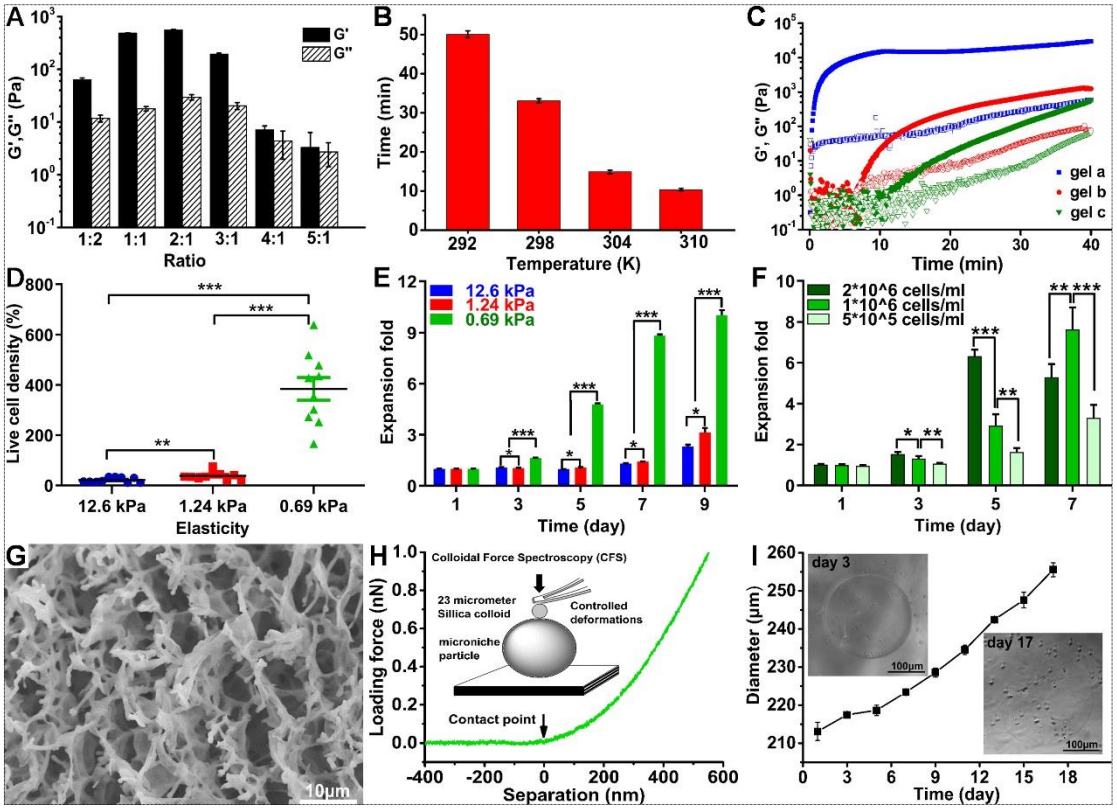

Figure 3-1. Parameter adjustment and coordinated control for establishing the 3D microniche. (A) Rheology measurements (elastic modulus G′ and viscous modulus G″

to precursor ratios: PEG-PCL-N_3 (0.1mg mL^{-1}) and dPG-DIC (0.1mg mL^{-1})). (B) Gelation time measurements under certain ratios and concentrations (Gel c in Table 1). (C) Rheology measurements to precursor concentrations (the solid line G', the hollow line G″). (D) iPSCs' viability response to microniche stiffness. (E) iPSCs' proliferation response to microniche stiffness. (F) Cell seeding density measurements. (G) SEM morphology test. (H) Colloidal force spectroscopy (CFS) is used to measure the mechanical properties of individual microniche and to extract its Young's modulus. (I) Degradability test of the microniche. *p < 0.05, **p < 0.01, and ***p < 0.001.

Table 3-1. Crosslinker concentration with gelation point, elastic moduli G', and viscous moduli G".

Sample no.	Gelation point t_g	G' [t =∞] /kPa	G" [t =∞] /Pa
Gel a	35 s	12.6	67
Gel b	5.08 min	1.24	4.713
Gel c	7.41 min	0.692	0.4874

Gel a: c_{p1} =0.2g mL^{-1}, c_{p2} =0.2g mL^{-1}; Gel b: c_{p1} =0.15g mL^{-1}, c_{p2} =0.15g mL^{-1}; Gel c: c_{p1} =0.1g mL^{-1}, c_{p2} =0.1g mL^{-1}; P1: PEG-PCL-N_3, P2: dPG-DIC.

standardized for microfluidics operation and the microniche manufacture process. Herein, 310 K was corresponded to this standard gelation time and chosen as the gelation temperature. Afterward, rheology tests (**Figure 3-1C**), according to variations in composition (**Table 3-1**), revealed that gel elasticity was inherently decided by crosslinking density and could be adjusted by precursor contents.

To assess whether the stiffness affected iPSCs' survival and proliferation, iPSCs were embedded into hydrogels precursors. Together they engineered into 150-200 μm microniche particles with different elasticity by droplet-based microfluidics technology. Benefiting from the small sphere size, the obtained microniche particles allowed oxygen and nutrients to penetrate freely and reach the compartmentalized cells. Besides, under microfluidic conditions, this fabrication strategy also showed great promise for microniche mass production. Both of the live/dead density comparison results (**Figure 3-1D**) and expansion test (**Figure 3-1E**) revealed that a softer environment allowed for iPSCs' survival and expansion well. Microniches with certain elasticity (G'=0.69 kPa) could better maintain iPSCs' renewability and higher expansion rate, which was further demonstrated by live/dead staining test (**Figure 3-S5A**) and the cell spheroids - embryoid bodies (EB) expansion measurements (**Figure 3-S5 B, C**). Besides, as

verified by Ki-67 staining (**Figure 3-S5D**), this soft microniche could also help keep iPSCs' high proliferation ability. Corresponding to the elasticity (G'=0.69 kPa) of the microniche determined by rheology, the Youngs modulus obtained with a compressing colloid was 0.56±0.43 kPa. So, it could be regarded as the best stiffness for iPSC culturing, which was consistent with previous reports.[19, 66] Moreover, cells with various densities were cultured in microniches to evaluate which cells seeding density is suitable for iPSC culture and expansion (**Figure 3-1F**). A culture system with cells seeding density of 1×10^6 cells mL^{-1} presented the optimal proliferation rate and expansion efficiency.

Next, scaffold morphology analysis (**Figure 3-1G**, **Figure 3-S3**) revealed that it took on porosity with a certain mesh size among the networks inside the microniche. As the degradation effect of microenvironments had a significant effect on cell behavior,[48, 68] we investigated the degradability of the microniche and found that the degradation period of the microniche particles was 19 days (**Figure 3-S4**). During this period, the microniche degraded gradually and disappeared slowly (**Figure 3-1I**), which demonstrated that the artificial microniche indeed has certain degradability. Therefore, during the iPSCs' culture process, unoccupied network niche space could produce and make room for the rapidly proliferated cells just in time, affording them with better proliferation ability to achieve higher expansion efficiency.

3.1.2 Overall assess to the performance of the artificial 3D microniche system

After the key physical, bioactivity, and biomechanical parameters had been optimized, all of them were systematically controlled during the manufacturing process of the chemically defined artificial microniche engineering. Afterward, cell viability, expansion efficiency, and cell quality such as the self-renewal, proliferation, and pluripotency needed to be investigated to overall assess the performance of the artificial 3D microniche system.

Primarily, iPSCs grown in 3D microniche system were monitored by live/dead staining to assess how the iPSCs respond to the artificial microniche and whether the chemically defined synthetic material-based culture system could be used in iPSCs'

reliable expansion (**Figure 3-2A**). Remarkably, except for very few dead cells, most of the cells survived very well and had great viability. Encapsulated iPSCs grew into round regular cell spheroids - EB. These results preliminarily demonstrated that our artificial microniche culture system used without pre-adsorbing proteins and cell derivatives could support iPSCs' survival and expansion. As a 3D multicellular spheroid usually formed when the iPSCs were cultured in a suspension consisting of ectodermal, mesodermal, and endodermal tissues, the embryoid body has been regarded as a means to assess the pluripotency of pluripotent stem cells.[185] To determine whether the cell spheroids were formed by big cell aggregates or grew from single cells or small clusters, we isolated single microniche particles and traced them daily (**Figure 3-2B**). By monitoring the growth process, we proved that, during the overall culture period, the cells grew from single cell or small cluster, but at least not from a big cell aggregate, to become EBs with larger sizes and finally grew out of the microniche particles resulting from the degradability of the microniche. This phenomenon also reflected that,

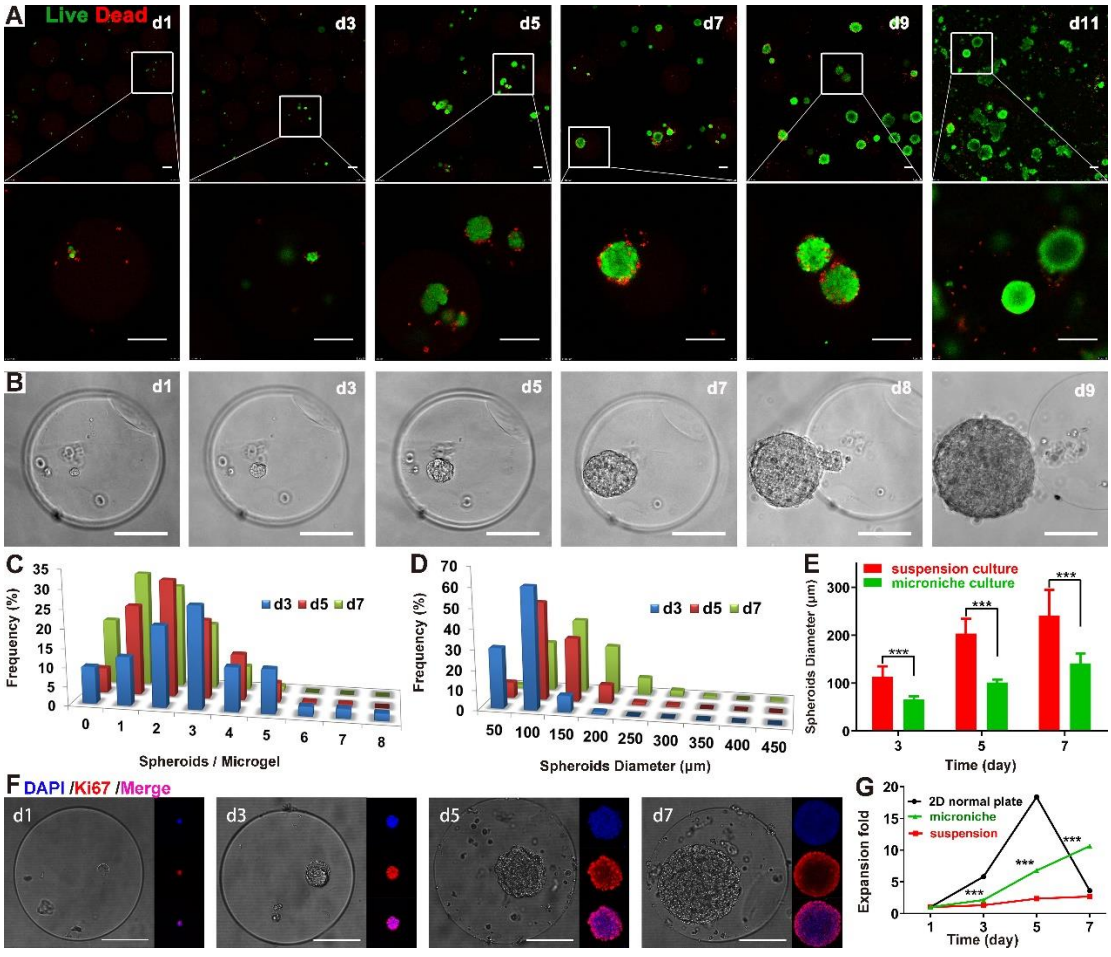

Figure 3-2. The 3D microniche supported iPSCs survival and EB formation. (A) Cell viability test monitored by live/dead staining (green-live cells, red-dead cells). (B) The morphology of the iPSCs inside the 3D microniche environment. (C) EB size statistics (green culture in a 3D microniche, red culture in suspension). (D) EB frequency to the microniche's particle size. (E) EB size measurement both in microniche and suspension. (F) Ki-67 staining (red: a marker of proliferating cells). The scale bar indicates 100 μm. (G) Expansion efficiency contrasted in different culture systems. *$p < 0.05$, **$p < 0.01$, ***$p < 0.001$.

benefiting from the biocompatibility and the degradability of the microniche, the cells could grow faster and realize expansion with high efficiency. According to the frequency statistics, the number of cell spheroids formed in each microniche particle varied from 1 to 8 and decreased along with the culture time (**Figure 3-2C**), which further proved that the cell spheroids could grow out of the microniche when they were big enough. The period of time in which the cell had grown out of the microniche finally supplied us with proper time to harvest cells.

It is well known that cell spheroid size is often regarded as one of the most important parameters to influence the proliferation and lineage-specific differentiation of pluripotent stem cells.[186] A too-large spheroid will lead to impaired proliferation and increased apoptosis due to insufficient transport of nutrients and growth factors, oxygen exchange, and metabolic waste elimination.[187] Besides, there was also unexpected cellular differentiation resulting from the ratio change of the three germ layers cells and spatial signaling alteration from cell-cell interaction or cell-environment interaction.[188, 189] Here, the statistics of cell spheroid numbers and sizes in a microniche system and suspension culture revealed that under the same cell seeding density, many more spheroids formed in the microniche system than those in suspension culture (**Figure 3-2D**). On the other hand, cell spheroids formed in the microniche system were smaller than those formed in suspension cultures (**Figure 3-2E**). Therefore, these results strongly revealed that iPSCs obtained from this microniche culture system could maintain a higher proliferation ability and better pluripotency than those from 3D suspension cultures. Beyond that, investigations of expansion efficiency and Ki-67 staining further proved that iPSCs in a microniche

culture maintained higher proliferation ability (**Figure 3-2F**) and showed better expansion rate than in suspension culture (**Figure 3-2G**). Overall, our approach demonstrated that these chemically defined 3D microniches supported iPSCs proliferation and expansion well.

To achieve the requirements of medical application, undifferentiated iPSCs must be acquired in vitro. We performed a series of pluripotency-related experiments[13] to investigate whether the pluripotency of iPSCs could still be maintained during the whole culturing process in the chemically defined 3D microniche. First, continuous high expressions of alkaline phosphatase were detected during the culture period until the seventh day (**Figure 3-3A**). Immunofluorescent staining showed that the chemically defined 3D microniche-produced iPSCs in spheroids maintained high pluripotency markers including Nanog, Sox2, Oct4, and SSEA1 expression (**Figure 3-3B**). These results demonstrated that the obtained iPSCs had prolonged self-renewal ability and simultaneously maintained high pluripotency, which also confirmed that iPSCs were still kept in an undifferentiated state. Besides, we conducted PCR analysis of marker

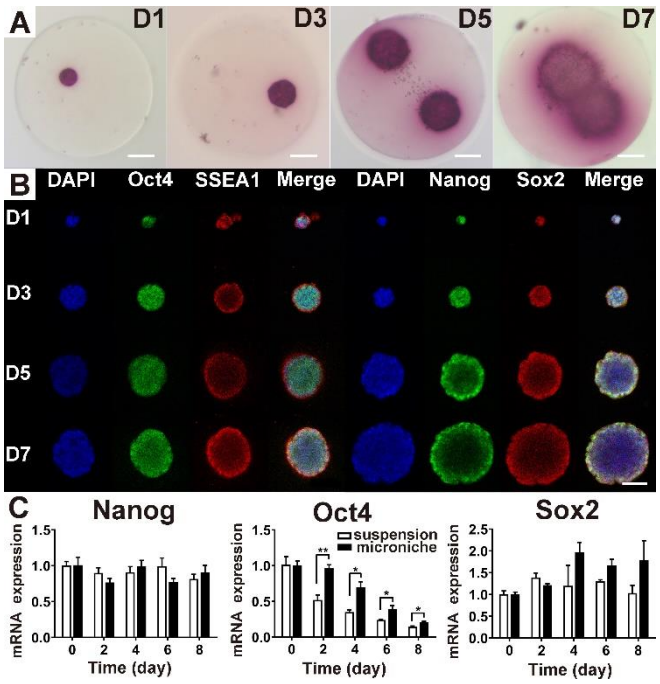

Figure 3-3. The 3D microniche supported iPSCs' maintenance of pluripotency. (A) Alkaline phosphatase (AP) staining (Scale bar = 50 μm). (B) Immunocytochemistry analysis of pluripotency markers in iPSCs from spheroids (Oct4, SSEA1, Nanog, and

Sox2). (C) PCR analysis of pluripotency marker genes (Nanog, Oct4, and SSEA1) (Scale bar = 50 μm).

genes (Nanog, Oct4, and SSEA1) and compared the pluripotency difference between iPSCs in suspension culture and the artificial microniche culture (**Figure 3-3C**). The Nanog expression levels to cells in suspension and the microniche were similar and remained stable during the culture period. While the expression of Oct4 both in suspension and microniche was decreased along with culture time, which was consistent with previous reports,[190] but the decreasing tendency in microniche was slower than that in suspension. In addition, the Sox2 expressions had a little increase in both, but there was almost no difference in suspension and microniche culture. Altogether Nanog was widely regarded as a gatekeeper to control pluripotent stem cell fate in response to signals from internal gene regulation network and external microenvironment.[191] The stable expression of Nanog and other markers indicated that iPSCs, which were obtained from this artificial microniche culturing system, could maintain high pluripotency. All of these experiments demonstrated that the chemically defined artificial microniche performed well in supporting iPSCs' reliable expansion to supply high-quality cells for therapeutic applications.

3.2 Conclusion

In summary, we have developed a novel, chemically defined artificial microniche engineering with degradable polyethyleneglycol-co-polycaprolactone and RGDfk-functionalized dendritic polyglycerol precursors by droplet-based microfluidics. This artificial 3D microniche can allow for the robust production of iPSCs with prolonged self-renewal ability and high pluripotency but without any reproduction limits and risks for pathogen and immunogen transfer. This advanced approach is meant to break through bottlenecks brought by the application of traditional poorly defined animal-derived matrices or cell derivatives and exhibits great promise for iPSCs to achieve full potential in therapeutic applications. Additionally, this microniche engineering fabrication process was performed under microfluidic conditions, which could supply

products with huge efficiency, and therefore also shows great promise in realizing iPSCs' 3D culturing and expansion on a large scale.

3.3 Materials preparation and related experiment operation

3.3.1. Synthesis procedures of materials

Synthesis of ethyl bicyclo[6.1.0]non-4-ene-9-carboxylate (BCE): the synthesis process was according to the literature with some optimization.[192] To a flask of 250 mL, after being filled with argon, 50 mL cyclooctadiene (404.37 mmol) and 1 g rhodium dimer were put inside together. Then, the flask was cooled down to 0 °C by ice bath. 5.4 mL ethyl diazoacetate (51.43 mmol) was dissolved in 30 mL DCM first and then was added dropwise into the cyclooctadiene solution under fierce stirring by injection pump in 3 hours. The temperature was brought up to room temperature and the solution was stirred for 3 days. The reaction mixture was directly added into the column and purified by the column chromatography on silica gel. The polarity of the eluent was increased slowly from 1:100 EtOAc:hexane (to 1:20) to afford *exo-endo* mixture (7.60 g, 39.08 mmol, 76%) as a colorless oil (TCL-EtOAc: hexane, 1:10).

^{1}H NMR (400 MHz, chloroform-d) δ (ppm): 1.12 – 1.17 (t, 1H), 1.18 – 1.27 (m, 7H), 1.31 – 1.40 (m, 2H), 1.40 – 1.49 (m, 3H), 1.50 – 1.59 (m, 3H), 1.63 – 1.71 (t, 1H), 1.74 – 1.86 (m, 2H), 1.96 – 2.11 (m, 5H), 2.11 – 2.22 (m, 5H), 2.22 – 2.36 (m, 3H), 2.42 – 2.54 (m, 2H), 3.97 – 4.19 (m, 5H), 5.45 – 5.70 (m, 5H). ^{13}C NMR (500 MHz, chloroform-d) δ (ppm): 174.41, 129.92, 60.23, 28.27, 27.89, 27.72, 26.65, 14.29, 14.19.

Synthesis of bicyclo[6.1.0] non-4-yn-9-ylmethanol (BCE-OH): To a 250 mL Schlenk flask, $LiAlH_4$ (1.82 g, 48.0 mmol) and 60 mL Et_2O were added, and then the suspension was cooled to 0 °C by putting the flask into the ice bath. Then a solution of compound (6.76 g, 34.89 mmol) in 60 mL Et_2O was put into a constant voltage funnel and was added dropwise into the $LiAlH_4$ suspension under fierce stirring. After that, the suspension was kept at RT for half an hour and then cooled down to 0 °C again. Water was carefully added into the suspension drop by drop until the gray solid turned into white. Anhydrous Na_2SO_4 was added to remove the redundant water. The suspension was filtered and the filtrate was concentrated by rotary evaporator to afford *exo-endo*

mixture as a colorless oil.

The colorless oil without further purification was dissolved in 200 mL DCM in a 500 mL Schlenk flask. The suspension was cooled down to 0 °C by putting the flask into ice bath. 2 mL Br_2 was resolved in 20 mL DCM before being transferred to a constant voltage funnel, and then was added dropwise into the flask until the yellow color persisted. 10% $Na_2S_2O_3$ was transferred to the constant voltage funnel and added to the solution dropwise until the yellow color disappeared. The thus obtained colorless solution was transferred to separating funnel and extracted with DCM. The organic layer was dried with anhydrous Na_2SO_4 to remove the redundant water. The solution was then filtered. The filtrate was concentrated by rotary evaporator to remove the DCM and afford exo-endo mixture (5.189 g, 34.138 mmol, 96.96%) the dibromide as a pale yellow oil.

Without further purification, the dibromide was dissolved in 100 mL THF in a flask and the solution was cooled down to 0 °C using an ice bath. A solution of KOtBu (1.6 M in THF, 66 mL) was transferred to the constant voltage funnel and added dropwise to the solution. The solution was refluxed for 2 h before being cooled down to rt and then the solution was quenched with 200 mL saturated NH_4Cl solution. After that, the THF was removed by rotary evaporator, the solution was extracted with DCM, and the yellow DCM layer was dried with anhydrous Na_2SO_4. The suspension was filtered; the filtrate was concentrated by rotary evaporator. The residue was directly added into the column and purified by the column chromatography on silica gel. The polarity of the eluent was increasingly slowed from 1:100 EtOAc: hexane (to 1:1) to afford the product exo-endo mixture (1.66 g, 11.06 mmol, 32.42%) as yellow oils (TCL-EtOAc: hexane, 1:1).

^{1}H NMR (400 MHz, chloroform-d) δ (ppm): 0.56 – 0.72 (m, 2H), 0.76 – 0.99 (m, 1H), 1.27 – 1.72 (d, J = 108.1 Hz, 4H), 2.05 – 2.46 (t, J = 44.1 Hz, 6H), 3.34 – 3.78 (d, J = 70.8 Hz, 2H). ^{13}C NMR (500 MHz, chloroform-d) δ (ppm): 130.15, 65.82, 29.02, 27.08, 22.12, 15.24.

Synthesis of bicyclo[6.1.0]non-4-yn-9-ylmethyl (4-nitrophenyl) carbonate （BCN): Without further purification, the product (0.666 g, 4.44 mmol) was dried with high

vacuum, then resolved in the 74 mL DCM in a 250 mL Schlenk flask, pyridine (0.8918 g 11.10 mmol) and 4-nitrophenyl chloroformate (1.0952 g, 5.55 mmol) were added to the solution at rt. The solution was stirred at rt for two hours, then 74 mL saturated NH_4Cl solution was added to the solution to quench the rest 4-nitrophenyl chloroformate. The obtained solution was extracted with DCM (4×150 mL); the organic layer was dried with anhydrous Na_2SO_4. After filtration, the filtrate was concentrated by rotary evaporator and purified by the column chromatography on silica gel. The polarity of the eluent was increasingly slowed from 100:1 hexane:EtOAc to 10:1, (TCL-EtOAc:hexane, 1:3), the obtained solution was concentrated by rotary evaporator to afford the *exo-endo* mixture product (1.12 g, 3.55 mmol, 80.08%) as a white solid.

^{1}H NMR (400 MHz, chloroform-d) δ (ppm): 0.69 – 1.13 (s, 3H), 1.14 – 1.30 (s, 1H), 1.33 – 1.71 (s, 5H), 2.06 – 2.61 (m, 6H), 4.14 – 4.53 (d, J = 81.5 Hz, 2H), 7.23 – 7.28 (m, 2H), 8.19 – 8.49 (d, 2H). ^{13}C NMR (400 MHz, chloroform-d) δ (ppm): δ155.69, 152.68, 145.3, 125.38, 121.85, 98.79, 98.74, 74.04, 68.09, 33.29, 29.12, 23.34, 23.05, 21.43, 21.37, 20.60, 17.32.

Synthesis of dPG- OMs: dPG was dialyzed in MeOH (dialysis tubes -2 kDa cut-off) for 2 days. After removing the MeOH, dPG (15.2343 g, 205.86 mmol OH, 20.5869 mmol of OH groups) was put in a 250 mL Schlenk flask and dried at 80 °C overnight under high vacuum. Then, it was dissolved in anhydrous DMF (200 mL) and cooled to 0 °C by ice bath. 4.292 mL Et_3N was added to the solution and the solution was cooled down to 0 °C by ice bath. Then MsCl (1.338 mL, 24.7043 mmol, 1.2 eq. with respect to all OH groups) in DMF (10 mL) was added dropwise over 1 hour under fierce stirring using an injection pump. After 2 hours, the ice bath was removed and the mixture was allowed to recover room temperature and was kept being stirred for 1 day. Then, DMF was removed by rotary evaporator and the resulting mixture was dialyzed in MeOH (pre-wetted RC tubing (MWCO: 1kD)) to afford 13.612 g of dPG-OMs as a honey-like product. Degree of functionalization (DF) = 8.0%, quantified by ^{1}H NMR. Yield = 82.40%.

^{1}H NMR (400 MHz, deuterium oxide) δ (ppm): 0.77 (m, CH_3 core), 1.26 (m, CH_2 core); δ 3.10 – 3.16 (s, 1H, CH_3 mesyl), 3.37 – 4.34 (m, 22H, CH_2 and CH, PG scaffold). IR

(film): ν = 3030, 2941, 2361, 1709, 1457, 1362, 1184, 971, 813, 753 cm^{-1}.

Synthesis of dPG- N_3: dPG-OMs (6.8057 g, 6.785 mmol OMs) was dissolved in 50 mL DMF and added to a 250 mL Schlenk flask equipped with a reflux condenser. Argon was purged into the flask slowly for five minutes to remove the air. NaN_3 (2.21 g, 33.92 mmol, 5 eq. to OMs group) was added to the solution, and then the solution was stirred for 3 days at 60 °C. After the reaction, the solution was cooled down to room temperature and filtered with the filter paper (Rotilabo-folded filters, type 600P) to remove the resulting salts. The filtrate was concentrated by rotary evaporator to remove the redundant DMF. The residue was dialyzed in H_2O for two days by pre-wet RC tubing (MWCO: 1kD) to afford the product of dPG- N_3 in water. After concentrated, 5.1781 g product was obtained. DF = 8%, conversion: quantitative (determined by ^1H NMR). Yield= 79.0%.

^1H NMR (400 MHz, deuterium oxide) δ (ppm): 0.77 (m, CH_3 core), 1.27 (m, CH_2 core), 3.27 – 3.92 (m, CH_2 and CH, PG scaffold). IR (film): ν = 2097 (-N_3) cm^{-1}.

Synthesis of dPG- NH_2: dPG-N_3 (4.35 g, 58.78 mmol) was dissolved in 200 mL of THF+H_2O (7:3) in a 250 mL Schlenk flask. Argon was purged into the flask slowly for five minutes to remove the air and PPh_3 (7.2 g, 27.6 mmol) was added to the flask. THF and H_2O were alternately added to keep the solution always clear. The reaction was monitored by IR and did not stop until the –N_3 peak at around 2097cm^{-1} absolutely disappeared. Then, the flask with solution was put in 4 °C in fridge for 2 hours. The white precipitate was removed by the filtration with the filter paper (Rotilabo-folded filters, type 600P). The residue was extracted with $CHCl_3$ and the water layer was dialyzed in MeOH by pre-wet RC tubing (MWCO: 1kD) for 2 days. The solution was concentrated and afforded 3.55 g as a pale yellow product. Yield = 83.92%.

^1H NMR (400 MHz, deuterium oxide) δ (ppm): 0.76 (m, CH_3 core), 1.26 (m, CH_2 core), 2.02 - 2.28 (d, J = 46.1 Hz, 1H), 2.53 - 2.85 (s, 3H), 3.19 - 3.24 (s, 10H, OCH-NH_2 and CH_2-NH_2), 3.33 - 4.00 (m, 69H, CH_2 and CH, PG scaffold).

Synthesis of dPG- BCN: dPG-NH_2 (1.1785 g, 15.925 mmol) was first dissolved in 20 mL MeOH and put in a 250mL flask. After the MeOH was removed from the flask by HV, dry DMF was added into the flask to dissolve the dPG-NH_2 and argon was slowly

purged into the flask for five minutes to remove the air. $E_{t3}N$ (0.2656 mL, 1.911 mmol, 1.5 eq) and BCN (0.486g, 1.529 mmol, 1.2 eq) were added to the solution. The reaction was kept for overnight at rt. After that, the DMF was removed by rotary evaporator. The residue was dialyzed first in acetone and H_2O, and then in pure Milli-Q water for four days with a molecular weight cut off (MWCO) of 2000 and collected by freeze-drying. Then, 0.8217g product was afforded. Yield = 71.28%.

^{1}H NMR (400 MHz, deuterium oxide) δ (ppm): 0.55 – 0.93 (m, 1H), 1.13 – 1.56 (d, J = 80.2 Hz, 1H), 1.96 – 2.37 (m, 1H), 2.69 – 4.21 (m, 12H, CH_2 and CH, PG scaffold).

Synthesis of PEG-PCL-OH: Poly(ethylene glycol) (PEG) (12 g, 0.002 mol) with an average molecular weight (Mw) of 6000 g mol^{-1} was put in a 250 mL Schlenk flask and dried under high vacuum and stirring at 70 °C at least for 12 hours. Argon was purged into the flask slowly for five minutes to remove the air and 150 mL dry toluene was added to the flask to dissolve the PEG. 40.5 mg stannous 2-ethylhexanoate was dissolved in toluene and added to the solution. Then 1.1414 g ε-caprolactone was dissolved in 5 mL toluene and added dropwise to the solution using an injection pump. After being equipped with a reflux condenser, the solution was refluxed under 135 °C for 2 days under fierce stirring and an argon balloon was added on the top of the condenser. After the reaction, the solution was cooled down and added dropwise to a mixture solution of hexane and diethyl ether in an ice bath. The product was slowly precipitated. The precipitate was filtered by suction funnel and after being dried with high vacuum for 12 hours, 12.69 g product was obtained as a white solid. Yield = 96.05%.

^{1}H NMR of PEG (400 MHz, chloroform-d) δ (ppm): 3.56 – 3.64 (m, PEG-backbone), ^{13}C NMR (500 MHz, chloroform-d) δ (ppm): 70.63 PEG-backbone.

^{1}H NMR of PEG-PCL-OH (400 MHz, chloroform-d) δ (ppm): 0.88 (m, CH_3 core), 1.33 – 1. 1.72 (m, PCL-backbone), 2.29 – 2.36 (m, PEG–CH2–O–CO–$\underline{CH_2}$–PCL), 3.49 – 3.80 (m, PEG-backbone, terminal –$\underline{CH_2}$–OH from PCL), 4.01 – 4.11 (t, PCL-$\underline{CH_2}$-O-CO-)), 4.19 – 4.26 (t, 1H PEG– $\underline{CH_2}$–O–CO–CH_2–PCL). ^{13}C NMR (500 MHz, chloroform-d) δ(ppm): 173.61 (PEG–CH_2–O–$\underline{C}$O–CH_2–PCL), 72.59 (PEG–O–$\underline{CH_2}$–CH_2–OH), 69.21-70.62 (PEG-backbone), 63.49 (PEG–O–CH_2–$\underline{CH_2}$–O–CO–PCL),

62.54 (PCL–CH_2–$\underline{C}H_2$–OH), 61.76 (PEG–O–CH_2–$\underline{C}H_2$–OH), 34.18, 32.37, 28.39, 25.58, 24.62 (PCL-backbone). $\nu_{C=O}$ (FTIR) = 1735 cm^{-1}.

Synthesis of PEG- PCL-OMs: 12.0 g (1.859 mmol) PEG- PCL-OH was added to a Schlenk flask with 200 mL dry DCM. After being absolutely dissolved, the solution was cooled to 0 °C by an ice bath. Argon was slowly purged into the flask for five minutes to remove the air and 2.667 mL TEA was added to the solution. 1.6457 g (7.435 mmol) methylsufonyl chloride dissolved in 10 mL DCM was added dropwise using an injection pump. Then removing the ice bath, the reaction was kept at 25 °C for 24 hours under fierce stirring. After the reaction, the solution was extracted by 200 mL DCM and 200 mL brine. The organic layer was dried with anhydrous Na_2SO_4 and filtrated. The filtrate was concentrated by rotary evaporator and precipitated in diethyl ether in ice bath. The precipitate was washed several times with diethyl ether and filtered by suction funnel. After dried with high vacuum for 12 hours, 10.5976 g product was obtained as a white solid. Yield = 77.56%.

^{1}H NMR (400 MHz, chloroform-d) δ (ppm): 1.30 – 1.47 (m, PCL-backbone), 1.57 – 1.67 (m, PCL-backbone), 1.68 – 1.80 (m, PCL-backbone), 2.20 – 2.37 (m, PCL–$\underline{CH_2}$–OCO–), 2.95 – 3.02 (s, C$\underline{H}_3$ mesyl-PCL), 3.03 – 3.08 (s, C$\underline{H}_3$ mesyl-PEG), 3.41 – 3.82 (m, PEG-backbone), 3.99 – 4.09 (m, PCL–$\underline{CH_2}$–OCO–), 4.16 – 4.24 (m, PEG–$\underline{CH_2}$–OCO–CH_2–PCL, PCL–$\underline{CH_2}$–OMs), 4.31 – 4.40 (m, PEG–CH_2–$\underline{CH_2}$ –OMs). ^{13}C NMR (500 MHz, chloroform-d) δ (ppm): 173.56 (PEG–CH_2–O–$\underline{C}$O–CH_2–PCL), 69.21-70.62 (PEG backbone), 63.49-64.17 (PEG–O–CH_2–$\underline{C}H_2$–O–CO–PCL), 37.43 (PCL–$\underline{CH_3}$) 34.02, 28.39, 25.57, 24.61 (PCL-backbone). $\nu_{C=O}$ (FTIR) = 1735 cm^{-1}.

Synthesis of PEG- PCL-N_3: 10.20 g (1.544 mmol) PEG-PCL-OMs was added to a Schlenk flask with 100 mL dry DMF. 1.1 g (16.92 mmol) Na_3N was added into the flask. Argon was slowly purged into the flask for five minutes to remove the air and the reaction was kept at 40 °C under stirring for 24 hours. Then the solution was concentrated by rotary evaporator remove the DMF and the obtained solid was dissolved in 20 mL DCM. The DCM solution was extracted with water (100 mL ×2). The organic layer was dried with anhydrous Na_2SO_4. After filtration, the filtrate was concentrated by rotary evaporator and precipitated in diethyl ether in ice bath. The

precipitate was washed with diethyl ether and filtered by suction funnel (pro4). After being dried with high vacuum overnight, the solid was purified by dialysis in Milli-Q water for two days with a molecular weight cut off (MWCO) of 2000 and collected by freeze-drying. Then, 6.9324 g product was obtained as a white solid. Yield = 69.03%.

^{1}H NMR (400 MHz, chloroform-*d*) δ (ppm): 1.30 – 1.44 (m, PCL backbone), 1.52 – 1.71 (m, PCL backbone), 2.24 – 2.38 (m, PCL–$\underline{CH_2}$ –OCO–), 3.26 (t, PCL–$\underline{CH_2}$ –N_3), 3.37 (t, *J* = 10 MHz, PEG–O–CH_2–$\underline{CH_2}$ –N_3), 3.42 – 3.83 (m, PEG backbone), 4.01 – 4.08 (m, PCL–$\underline{CH_2}$–OCO–), 4.17 – 4.24 (m, PEG–$\underline{CH_2}$–OCO–CH_2–PCL). ^{13}C NMR (500 MHz, chloroform-d) δ (ppm): 173.55 (PEG–CH_2–O–$\underline{C}$O–CH_2–PCL), 69.21-70.62 (PEG backbone), 64.19 (PCL–CH_2–$\underline{C}H_2$–CO), 63.48 (PEG–O–CH_2–$\underline{C}H_2$–O–CO), 51.26 ($\underline{C}H_2$–N_3), 34.02, 28.39, 26.28, 25.58, 24.61 (PCL backbone). $\nu_{C=O}$ (FTIR) = 1735 cm^{-1}, ν_{N3} (FTIR) = 2097 cm^{-1}.

Synthesis of dPG-RGD: BCN-RGD was synthesized based on the cyclic pentapeptide c[RGDfK], which was linked to BCN through its lysine residue without hindering its biological performance.[193-195] Cyclic Arg(Pmc)-GlyAsp(OtBu)-D-Phe-Lys(Boc) (20 mg, 0.03312 mmol)was dissolved in 8 mL DMF, followed by addition of 16 uL (3 eq) TEA. A solution of BCN (10.95 mg, 0.03477 mmol, 1.05 eq) dissolved in 8 mL DMF was added into the RGD solutions and kept being stirring for 16 hours at rometemperature. Then, the BCN-RGD was directly added to the solution of dPG-N_3 (DF = 8%, 62.928 mg, 0.828 mmol) in 10 mL DMF. The reaction was kept at room temperature overnight. After that, the DMF was removed by rotary evaporator, and the residue was purified by dialysis in Milli-Q water for two days with a molecular weight cut off (MWCO) of 2000 and collected by freeze-drying. After that 74.254 mg product N_3-dPG-RGD (-N_3, 4%; -RGD 4%) was obtained. Yield = 84 %

^{1}H NMR (500 MHz, deuterium oxide) δ: 0.60 – 1.13 (s, 10H), 1.24 – 1.42 (m, 3H), 1.47 – 1.55 (s, 5H), 1.58 – 1.69 (s, 5H), 1.77 – 1.90 (s, 1H), 2.09 – 2.64 (d, J = 76.5 Hz, 5H), 2.74 – 2.89 (s, 2H), 2.85 – 3.25 (s, 6H), 3.30 – 4.52 (backbone of PG), 4.36 – 4.55 (t, J = 19.4 Hz, 3H), 7.11 – 7.64 (m, 5H).

3.3.2 Surfactant preparation

Synthesis of PEG-NH_2: PEG with molecular weight of 600 g mol^{-1} (10.0 g, 33.32 mmol of OH group) was added to a Schlenk flask and melted in 65°C overnight under HV to remove traces of water. After having cooled to room temperature, the solution was dissolved in 60 mL dry DCM. Then, the solution was cooled down to 0 °C with ice bath. Argon was slowly purged into the flask for five minutes to remove the air and 23.2 mL (166.7 mmol, 5 eq) TEA was added to the solution. 15.276 g (133.36 mmol, 4 eq) methylsufonyl chloride dissolved in 10 mL DCM and then was added dropwise using an injection pump. After removing the ice bath, the reaction was kept at 25 °C for 24 hours under fierce stirring. After the reaction, the solution was extracted by 200 mL DCM and 200 mL brine. The organic layer was dried with anhydrous Na_2SO_4 and allowed to filtrate. The filtrate was concentrated by rotary evaporator and precipitated in diethyl ether in ice bath. The precipitate was washed several times with diethyl ether and filtered by suction funnel. After drying with high vacuum for 12 hours, the product was obtained as a white solid. All of the homobifunctional PEG-OMs was added to a Schlenk flask with 100 mL 25% aqueous ammonia solution and kept being stirred for 4 days at room temperature. Then, the ammonia was evaporated and the PH was adjusted to 13.0 with base of 1 M NaOH. The solution was extracted with 150 mL DCM and 300 mL brine for 3 times and the organic layer was concentrated and precipitated in diethyl ether. After drying in HV, 5.525 g desired product was yielded as white solid. ^{1}H NMR (500 MHz, D_2O, 25 °C) δ (ppm): 3.82 (m, 4H, -O$\underline{CH_2}$-CH_2), 3.75-3.65 (m, PEGbackbone), 3.63 (t, 4H, -$\underline{CH_2}$-CH_2-NH_2), 3.54 (m, 4H, -OCH_2-$\underline{CH_2}$), 2.93 (t, 4H, -$\underline{CH_2}$-CH_2-NH_2).

Synthesis of Krytox-PEG-Krytox: The three-block-structure surfactant was synthesized and characterized according to the literature.[196] The Krytox polymer with a carboxylic acid functionality (60.8 g, 15.145 mmol, M = 4013 g/mol) was dissolved in 100 mL HFE-7100 and kept being stirred for 2 h at room temperature. Under Ar atmosphere, oxalyl chloride (19.22 g, 151.45 mmol) was added dropwise by glass pipette and was kept being stirred for 12 hours at room temperature. The solution was put in oil bath 70 °C to remove the rest of the oxalyl chloride and HFE7100 under HV by a neutralizer of 2M KOH solution. The desired product was yielded as colorless solution.

Homobifunctional PEG -NH_2 (5.0g, 8.33 mmol) was dissolved in 50 mL DCM and 50 mL HFE-7100 in flask, (-NH_2 (amino group) 1.1 eq to -COCl), and the whole colorless desired product in 50mL HFE-7100 was followed added dropwise into the solution. The flask was put on the rotation evaporator overnight with elevated temperature 40-50 °C without vacuum. After the reaction, the DCM and HFE-7100 were removed by a rotation evaporator. The rest was transferred into 50 mL falcon tubes into which was added unmodified PEG. Under the mixture solutions, PEG was supposed to bind with the excess homobifunctional PEG -NH_2 to form solid plug. After centrifugation, the bottom fraction was clear. By cutting with a razor into the bottom of the tube and let the sample drip out. The desired product was obtained as a more viscous colorless solution.

The molecular structure of the Krytox-PEG-Krytox surfactant was determined by ^{19}F NMR spectroscopy. Figure S23 reveals assignments for different fluorine signals used to characterize the material for molecular structure. By inspecting the NMR region at -131.5 to -133.5 ppm, it was found that approx. 81% of the acid chloride end groups of the PFPE had converted to the non-ionic amide coupling to PEG. The balance of the PFPE carboxylate is an ionic species, which can be indicated by the broad multiplet at -126.5 to -128 ppm.

^{19}F NMR (376 MHz, C_6F_6 + MeOD) δ (ppm): -147.82 – -146.25 (35F), -133.14 – -132.80 (1F), -132.66 – -132.53 (2F), -83.48 – -81.52 (394F).

3.3.3 Cell culture

The mouse iPS cell line PhiC31 was obtained from System Biosciences (Catalog# SC211A-1), and maintained on laminin (Cultrex, #3400-010-01)-coated plate with complete clonal grade medium (Merck Millipore, #SF001-500P) containing GSK3β inhibitor. The medium was changed daily and the cells were passaged every 3-4 days with accutase (Merck Millipore, #SCR005).

For traditional suspension culture, iPSCs were trypsinized with accutase for around 3 min into single cells and then reseeded on uncoated plate with defined concentration. The medium was changed daily by gently centrifuging the cell spheroids into the bottom of the tubes and carefully aspirating the supernatant until ready to use.

For the 3D microniche culture, iPSCs were trypsinized with accutase into single cells and then mixing with a density gradient medium (Sigma, #D1556) to prevent the cell aggregation form before carrying out the microfluidics devices. Please refer to the microfluidic encapsulation section about the detailed microniche encapsulation process. The microniche particles containing iPSCs were harvested and filtered through 100 μm cell strainer (Corning, #352326) to remove unencapsulated cells. And then the cells embedded into microniche particles were reseeded on normal plate. The medium was changed daily by carefully inclining the plate and aspirating the supernatant without disrupting the floating microniche particles. The cells in microniche particles were imaged by normal or fluorescent microscope at specific time points and the cell spheroids' numbers and diameters were counted and measured by Image J software.

3.3.4 Microniche Engineering

Microfluidic Devices

The devices of the microfluidic were made by soft lithography.[197] First a silicon wafer was made by patterning with SU-8 photoresist. Then, poly (PDMS) and the crosslinker (Sylgard 184 elastomer kit, Dow Corning, ratio of base and crosslinker was 10:1) were thoroughly mixed by a rotational vibration mixer for three minutes before being poured onto the silicon wafer. The whole device was put in a drying vessel under high vacuum for half an hour to remove the air bubbles. After solidificated in the oven at 65℃ overnight, the device was cut and punched to produce pore canals. The device was washed with isopropanol and water and dried with oven again. The dry PDMS device was fabricated on to the glass slide by the oxygen-plasma bonding machine. After solidification in the oven at 65 ℃ overnight, the device was treated with Aquapel® (PPG, Pittsburgh, PA, USA.), a commercial windshield treatment in a drying vessel under high vacuum to render the inter surface of devices hydrophobic and suitable for the hydrophilic–hydrophobic water-in-oil emulsification. After the hydrophobic treatment, the channel device was washed with ethanol and isopropanol to make it clean and put under the 48w UV exposure overnight to kill all the bacteria and make the encapsulation process avoid bacterial infections.

Microniche particles engineering

For the fabrication of the microniche particles, we proceeded it in stepwise manners: First, we prepared two sets of aqueous precursors, one solution containing dPG with an average molecular weight (Mw) of 5.3 kDa functionalized with BCN groups, and the other containing PEG- PCL-N_3 with molecular weights (6.5 kDa) and hPG-N_3 -RGD. (Keep the final concentration of c[RGDfK] in precursors mixtures as 1mM).[182] Then, both precursor solutions were injected into the microfluidic device at different concentrations, along with a cell culture media containing iPSCs with varying density. (The microniche elasticity was controlled by the molecular weight of the PEG-cross-linker and by the total precursor concentration. To optimize the microniche properties for the encapsulation of iPSCs, the influence of the microniche elasticity on the viability of the encapsulated cells and polymers concentration to the elasticity have been studied in advance) This way, premicroniche droplets could be formed, which were easy to gel, and yielded cell-laden microniche particles through the strain-promoted azide−alkyne cycloaddition. After formation in microfluidic device, the microniche particles were dispersed in the oil phase (HFE-7100) with Krytox-PEG-Krytox (2% wt). Then the EP pipe was put in 37 ℃ water bath and used as a receiver. After incubation in a carbon-dioxide cell incubator for 10 min (optimized by gelation time in rheology test), the microniche particles were washed with surfactant solutions to remove the HFE on the surface and transferred into the cell culture media. With their special 3D microenvironment structure, the microniche particles were manufactured with iPSCs embedded inside. According to the strategy of coordinated control the physical and chemical properties to influence the specific interactions with cellular systems, this fully chemically defined artificial 3D microniche engineering was designed to tailored a new proper microenvironment niches that could work as 3D matrices for iPSC culturing. As a result, we created a novel approach for an iPSC expansion to get reliable cells with prolonged self-renewal ability and high pluripotency suit for clinical applications.

3.3.5 Cell viability assay

A Live/Dead Viability Kit (Thermo, #L3224) measured the viability of the iPSCs that were cultured in microniche particles, which then were collected and washed with PBS. A freshly prepared staining solution was added to microniche particules. After incubation for 30 min, the microniche with cells was imaged by confocal microscope (Leica SP8). Green-fluorescent calcein-AM indicated live cells and red-fluorescent ethidium homodimer-1 showed the dead cells.

3.3.6 Proliferation assay

A Cell Counting Kit - 8 (Sigma, #96992) measured the expansion rate of the iPSCs growing in the microniche. After harvest, the same amount of microniche particles were seeded in plate (24-well) and cultured for several days. At an indicated time period, one tenth of the volume of CCK-8 reagent of the used medium was added to each well of the plate, and then incubated in the plate for 1-4 hours. After incubation, the supernatants were transferred to 96-well plate, and a microplate reader measured the absorbance at 450 nm.

3.3.7 Immunofluorescent staining

The cells in microniche were collected and washed with PBS at specified time periods. Then the micronice particles with cells were fixed with 4% PFA for 15-30 min, which was followed by permeabilization for 10-20 min (bigger cell spheroids need longer time). After washing with PBS for 3 times, the cells were blocked with 10% goat serum at temperature of 37 ℃ for 30 min to cover nonspecific sites. Then they were incubated with defined primary antibodies (anti-Nanog, 1:400, Abcam, #ab80892; anti-Oct4, 1:400, Abcam, #ab19857; anti-SOX2, 1:1000, Abcam, #ab97959; anti-SSEA1, 1:200, ThermoFisher, #MA1-022; anti-Sox2, 1:400, CST, #4900; anti-Ki-67, 1:400, CST, #9129) at 4℃ overnight. The second day microniche particles with cells were washed by PBS for 3 times and then incubated with second antibodies (goat anti-rabbit IgG H&L (Alexa Fluor 488, 1:400, Abcam, #ab150077; goat anti-mouse IgG H&L (Cy5), 1:1000, Abcam, #ab6563) at 37℃ for 1 hour. They were washed by PBS again and then

stained with DAPI at room temperature for 10-20 min. In the end, all the microniche particles with cells were imaged by sp8 confocal microscope.

3.3.8. RT-qPCR reaction

After several days' culture, both microgels containing iPSCs and EBs under traditional suspension culture were collected by centrifuging at 200 g for 5 minutes. Cell total RNA were lysed and extracted by Trizol Reagent (Thermo Fisher Scientific, #15596026) and then reversely transcribed into cDNA with a SuperScript™ IV VILO™ Master Mix Kit (Thermo Fisher Scientific, #11756050) according to the manufacture's instruction. The real time PCR reaction tests were performed using Power SYBR™ Green PCR master mix (Thermo Fisher Scientific, #4367659) by the PikoReal Real-Time PCR device following the respective user manuals. The primers used: Gapdh-F: 5′-TTC ACC ACC ATG GAG AAG GC-3′, Gapdh-R: 5′-CCC TTT TGG CTC CAC CCT-3′; Nanog-F: 5′-CAG GTG TTT GAG GGT AGC TC-3′Nanog-R: 5′-CGG TTC ATC ATG GTA CAG TC-3′; Oct4-F: 5′-TCT TTC CAC CAG GCC CCC GGC TC-3′, Oct4-R: 5′-TGC GGG CGG ACA TGG GGA GAT CC-3′; Sox2-F: 5′-TAG AGC TAG ACT CCG GGC GAT GA-3′, Sox2-R: 5′-TTG CCT TAA ACA AGA CCA CGA AA-3′. The data were obtained by PikoReal Software 2.2 and analyzed by the Comparative Ct method (ΔΔCt). The value of 2^-ΔΔCt were analyzed with the GraphPad Prism 5 software by the unpaired Student's t-test method. The results were normalized by treating the data of d0 as the reference value.

3.3.9 ALP staining

ALP staining was performed to confirm the pluripotency of iPSCs by following the instructions of an alkaline phosphatase detection kit (Merck Millipore, #SCR004). Briefly, cells in the microniche particles were collected and washed by PBS, and then fixed by 4% PFA for very short time followed by PBS washing. Next, enough stain solution was added to the tube and then incubated in dark at room temperature for 15

min. After 3 times' washing by PBS, the images were observed and acquired by a color microscope.

3.3.10. AFM tests

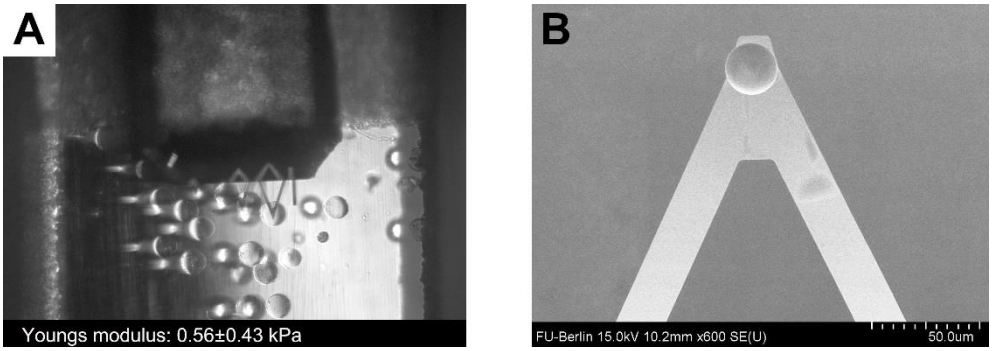

Figure 3-S1. Young's modules and the morphology of the microniche particles. (A) The real time morphology of the microniche particles under detection. (B) The tips for the detection.

For the assessment of the stiffness properties of the 3D microenvironment, the material properties of microniche particles were investigated with an atomic force microscope (JPK Nanowizzard 4, Berlin, Germany GmbH) in a force spectroscopy mode using the technique known as colloidal force spectroscopy (CFS). In this technique, a micro-sized silica colloid glued at the end of a tipless cantilever is used as a force sensor device to induce controlled compressions. The advantage of using a well-defined geometry to perform deformations against another well-defined interface (microgel) is that the contact models exist to extract the elasticity parameter Y or Young's modulus of the tested material. Silica colloids of 23 μm in diameter (microParticles GmbH Berlin, Germany) were glued with 2-component Plus Endfest epoxy to tipless cantilevers D (model MLCT-O10 from Bruker) with a nominal spring constant of 0.03N/m. Prior to any force measurements, the probe cantilever+colloid, was used to compress the hard surface of mica and obtain the sensitivity of the cantilever. Afterwards, the thermal noise method was used to determine the spring constant of the probe cantilever+colloid. Calibration of the probe and all force

measurements were performed inside a fluid chamber in Milli-Q water.

The microniche particles were first deposited onto a glass slide (Carl Roth, Karls Ruhe, Germany) and identified through optical microscopy. Then a colloidal probe was positioned directly on top and at the center of the particles. At least 3 repetitive approach-retraction cycles were taken per microparticle with a maximal applying loading force of 1000 pN. For this loading force, deformations were fully reversible and within a range of 200-300 nm. An approach-retraction velocity of 500 nm/s was used. During the testing process, the real time morphology of the microniche particles was also tested (Figure 3-S1 A).

The JPK software for data processing was used for posterior surface analysis. All obtained force-separation curves were baseline corrected and converted from force-piezo displacement to force-separation curves that were then further analyzed. The model of the contact of Hertz was used for a rigid sphere's compressing a planar semi-space, where only deformations of no more than 100 nm were considered for analysis. Since deformations were less than ~10% of the radius of the indenter (here about 11.5 µm), the Hertz model allowed determination of the Young´s modulus when a fit was applied to the first 100 nm of the approach curve after the contact point. In addition, a soft PDMS surface provided in the Bruker Peak Force kit with a modulus of 2.5 MPa was used as a control for Young's modulus determination. Finally, the Young's modulus of the microniche particle (gel c) was 0.56±0.43 kPa.

3.3.11 Rheology tests

The gel-gelation process could be monitored by rheological measurements. The gelation temperature, the gelation time, and elastic and viscous moduli could be investigated. During the test, PL08 probe was chosen to detect the amplitude sweep strain controlled, frequency sweep strain controlled, and the single frequency strain controlled. For parameters, the gap was set as 2 nm, the amount of each polymer was 50 uL. For the amplitude sweep, the scan range was set as 0.01-10% at 1 Hz. For frequency sweep, the frequency scan range was set as 0-10 Hz at 1%. Three distinct regions in the rheological curves can be identified under three conditions: Firstly, during the initiation period, G' (t) and G" (t) were low. The details could be identified because both moduli were under the detection limit of the instrument. During this period, polymerization was low and the network could not form. Then, a sudden increase of G'

(t) and G" (t) period meant the polymerization began and a covalent network formed. When G' (t) remains constant, independent from the gel composition and temperature the gelation process is completed. During the test, all the samples according to Table 3-1 were tested at constant temperature.

3.3.12 Gelation efficiency to precursor ratios

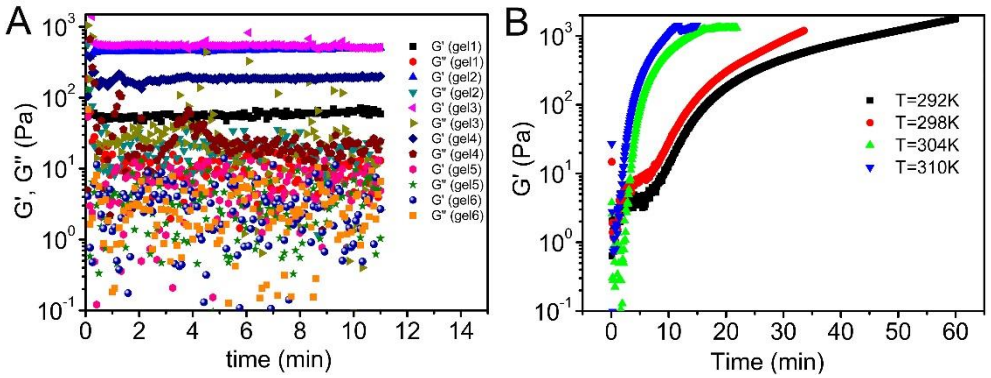

Figure 3-S2. (A) Time dependence of the elastic modulus (G′) and viscous modulus (G″) during gelation with variations in precursor ratios of PEG-PCL-N_3 to dPG-DIC (PEG-PCL-N_3 =0.1g mL^{-1}, dPG-DIC = 0.1g mL^{-1}). (B) Time dependence of the elastic modulus (G′) during gelation process under different temperatures.

Since the synthesized microniche were constructed by precursors of PEG-PCL-N_3 and dPG-DIC, the ratio of the precursors to form the microniche determined the content of each of them, which had a close relationship to the crosslinker type. To investigate the effect of the content of precursors to stiffness, the rheology measurement was performed and the elastic and viscous moduli were investigated accordingly. As shown in Figure S2 A, the elastic and viscous moduli of the synthesized hydrogels (gel 1 to gel 6) formed by precursors with different ratios presented varied values. By comparing these gels with each other, it could be found obviously that gel 3 with content ratio of 2:1 had the higher value of both elastic and viscous moduli, which demonstrated that precursor ratios strongly influenced the gelation effectively.

Additionally, gelation time is also an important parameter to investigate and evaluate the gelation efficiency capable of determining the strategy of the following microgel manufacture. As we know, temperature is also important factor for the gelation process, especially because the principle of which in this project is based on

SPAAC reaction. Azide-alkyne cycloaddition kinetics can be controlled with temperature variation. Accordingly, the gelation kinetics also shows a strong temperature dependence. To investigate the effect and relationship of temperature and gelation time, gelation process with same precursor concentration under different temperatures was followed by rheological measurements. As shown in Figure S2 B, during gelation under different temperatures at certain ratios and concentration, the time-dependent elastic modulus G′ takes on different rheological curves. Gelation time, the time required for the elastic modulus to approach constant, was respectively 50, 35, 15, and 10 min accordingly under the temperature of 292 K, 298 K, 304 K, and 310 K. It is worth noting that temperature has a remarkable effect on the gelation time but no effect on viscous modulus and very little effect on elastic modulus.

3.3.13 SEM test

The morphologies of the poly (ethylene glycol) - poly (ε-caprolactone azide) (PEG-PCL-N_3) and dendritic poly (glycerol dicyclooctyne) hydrogels were characterized by scanning electron microscopy (SEM) after formation of the hydrogel. The formed hydrogel was first put in a cell culture media overnight to make it swollen absolutely. After the swollen hydrogel was freeze-dried and then gold-sputtered for moment on the clean mica tablet, and their morphology was viewed using a Hitachi SU 8030sem operated at 5.0 kV accelerating voltage.

3.3.14 Morphology property of the microniche

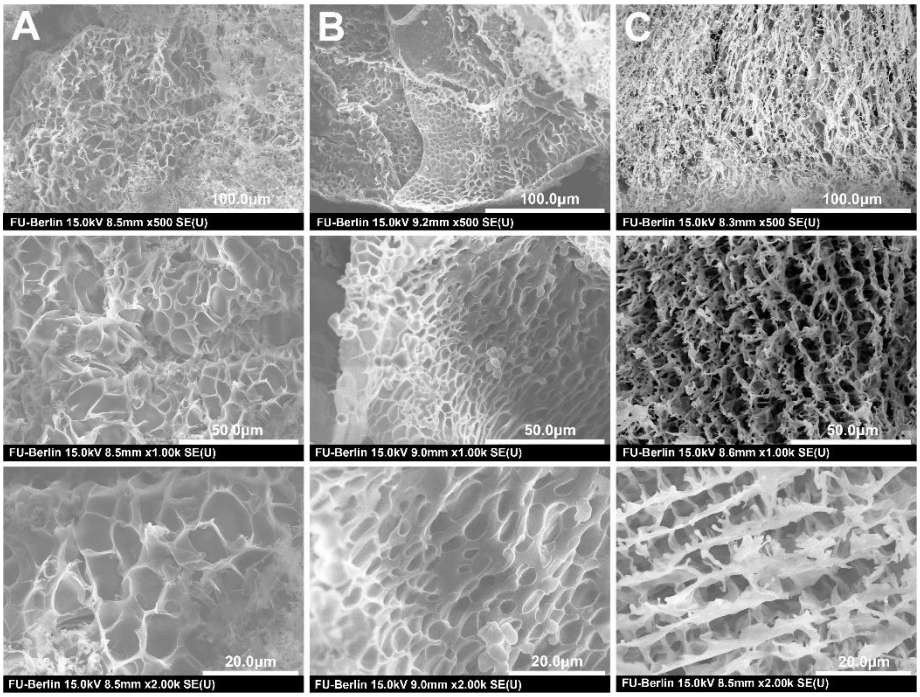

Figure 3-S3. SEM micrographs of gel a (A), gel b (B), and gel c (C).

The morphology property inside the 3D microniche was characterized by SEM. Gels were processed with freeze-drying by a lyophilizer before they were tested by the SEM. As shown in Figure 3-S3, gel a, gel b and gel c show different mesh sizes and the networks of the microniche took on many holes with different sizes. After removal of all the water from the microniche gel by lyophilization, gels made of high concentration proceeded to take on larger poles morphology among the polymeric network, which also demonstrated that there was close relationship between mesh size and poles among the networks and the concentrations of the precursors that were used to construct the polymeric gels.

3.3.15 Degradability characterization of the microniche particles

For the degradation test, the microniches were prepared according to the following Table 1 gel c at 37 ℃. After gelation, the samples were transferred into the used iPSCs culture DMEM and incubated in the cell incubator. The DMEM was changed once a day, and the morphologies and the size of the microniche particles were monitored by microscope day by day. After degradation, the size of the microniche particles was

changed which correspondingly led to the expansion of the microniche particle. The degradation test was carried on until the microniche particles was absolutely decomposed.

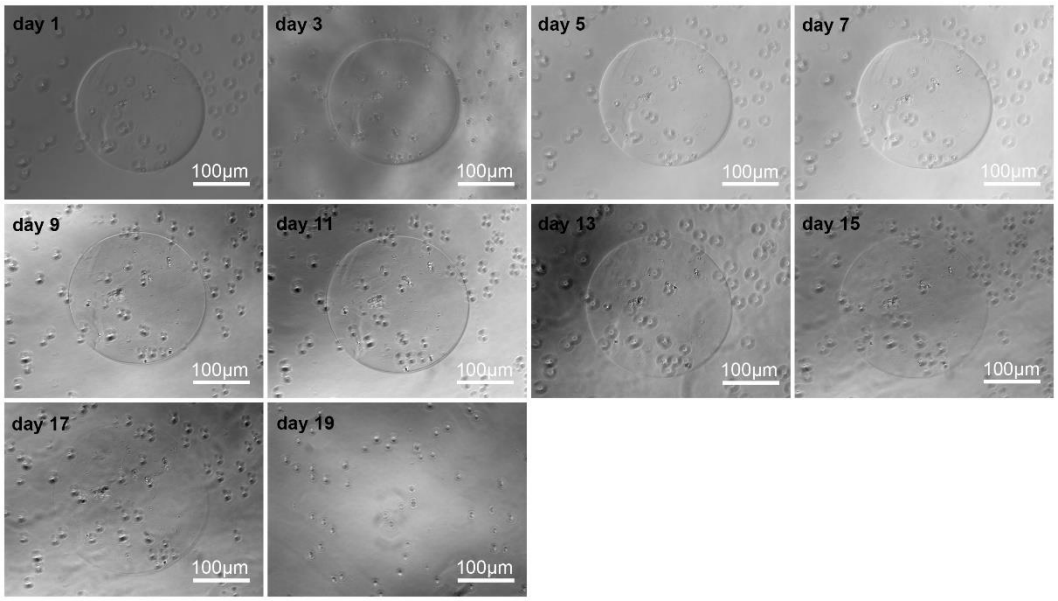

Figure 3-S4 Degradability test and the morphology monitor during the degradation of the microniche particles in DMEM containing 10% FCS and PBS at 37 ℃.

Degradability of the microenvironment is an important property in regulating cell behavior. In this project, the degradability of the 3D microniche was designed by functionalizing caprolactone units on both terminals of the PEG linker to form homobifunctional PEG-PCL polymer linker, of which the ester bond hydrolysis would have afforded the microniche with degradability under culture conditions. The degradation efficiency was investigated by real time morphology monitoring with microscope. As shown in Figure 3-S4, the size of the microniche particle increased slowly over time until the 19th day, when the morphology of whole particle disappeared completely. This could be explained by hydrogel swelling and the ester bond hydrolysis, which obviously demonstrated that the artificial microniche indeed had degradability. During the degradation process, much more unoccupied space occurred around the niche, which make room for the rapidly expanding cells just in time, giving them the advantage for survival and keeping better proliferation.

3.3.16 iPSCs' response to microniche stiffness

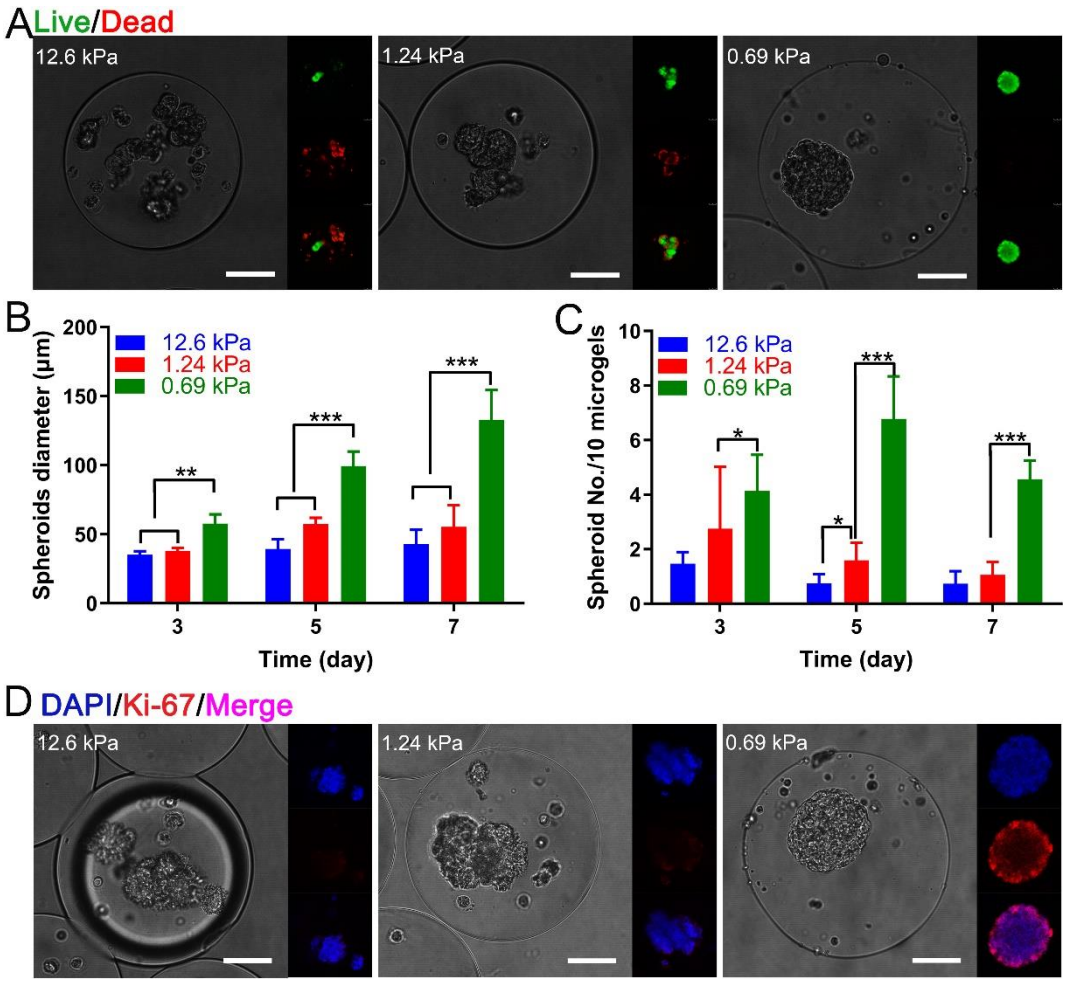

Figure 3-S5 Microniche elasticity affect iPSCs proliferation. (Scale Bar=100μm) (A) live/dead staining in different elasticity (green-live cells, red -dead cells). (B) EB diameter changes with culture time. (C) EB numbers changes with time. (D) Ki-67 staining (red: a marker of proliferating cells).

To determine the microniche elasticity of iPSCs survival and proliferation, three kinds of microniche particles with different elasticity of 0.69 kPa, 1.24 kPa, and 12.6 kPa were prepared with iPSCs embedded inside and then investigated by monitoring the live/dead staining, EB growth conditions as well as Ki-67 staining. Apparently, soft environments were more advantageous for the iPSCs survival. The softer the microniche was, the more iPSCs survived (Figure 3-5 A). Cells in soft microniche with elasticity of 0.69 kPa grew and survived much better than that in other stiff microniches. The diameter and the numbers of the EB in three different elasticity microniche particles were measured and counted after culturing for 3, 5, and 7 days (Fig. 3-S5 B

and C). Obviously, the EB cells grew faster in lower elastic microniches than that in higher ones. Ki-67 staining (Fig. 3-S5 D) results revealed that cells in microniche with elasticity of 0.69 kPa presented higher levels of proliferation markers expression than that in others, which means that cells got from this soft microniche with high proliferating potency. We can also imagine that the iPSCs almost did not expand in the stiff microniche because of the lack of proliferation ability (Figure 3-S5 C). From all of above, we can get to the conclusion that stiffness parameters are an important physical property for cell survival, Low elastic moduli-related 3D microenvironment (0.69 kPa) allowed iPSCs 3D culturing well.

3.3.17 Optimal seeding density for iPSCs microniche culturing.

Many factors can affect whether you can acquire enough high quality spheroids among which, the cell density must be the most important one. Previous study has proved that too low cell seeding density was not enough to form spheroids[198] while too high seeding density lead to spheroids agglomeration, which means separate spheroids merged and formed a larger spheroid. Therefore the spheroid formation efficiency was decreased and the spheroid quality was reduced.[199] To optimalize the suitable cell concentration for the encapsulated iPSCs culture in microniche particles. The iPSCs with three different concentrations of 2×10^6, 1×10^6, and 5×10^5 cells /mL were involved in the microniche fabrication process. The cellular growths were continuously observed during the culture time and the results showed that the more cells were seeded in the microniches, the faster iPSCs grew and the more cell spheroids formed (Figure 3-S6 A) However, too high concentration may lead to the aggregation and fusion of iPSCs spheroids and the generation of super big spheroids which would extrude out of the microniche particles after 5 days' culture. This also explained very well the decrease expansion rate and smaller spheroid diameter at d 7 under concentration of 2×10^6 cells /mL than that of 1×10^6 cells /mL (Figure 3-S6 B and C). Notably, too low cell concentration led to very little iPSCs spheroids which indicated that certain high cell concentration were needed to form embryoid bodies during the microniche particles' fabrication process. We concluded that cell concentration of 1×10^6 cells /mL was the

best density for iPSCs to survive in the microniche, to grow in a great expansion rate, and to form more and enough high quality spheroids while avoiding the spheroids agglomeration.

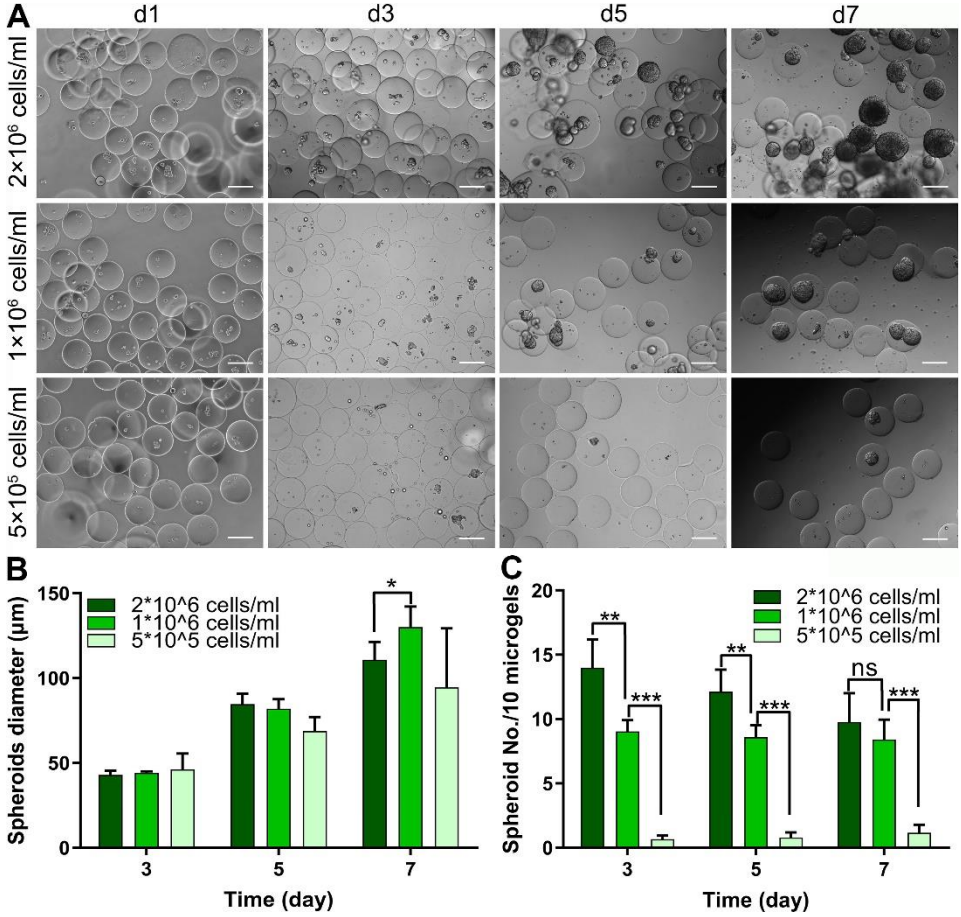

Figure 3-S6. (A) Optimize the cell density for iPSCs encapsulation (Scale bar = 200 μm). (B) Spheroids' diameter change with culture time. **(**C) Spheroid density changes with culture time.

Chapter 4. Advanced controlled-releasable iPSCs' 3D artificial niches based on dendritic polyglycerol and poly(N-isopropylacrylamide)-co-polyethylene glycol polymers via physical-chemical-co-gelation strategy

The recently emerging stem cell artificial niche engineering in iPSCs' 3D culture has provided enormous opportunities to fully utilize the potential of these cells in biomedical applications. Although a fully chemically defined niche environment could supply cells with desirable safety for clinical use, establishing an artificial degradable niche environment for the controlled release of proliferated cells under mild conditions is still a big challenge. Here we reported an advanced controlled releasable iPSCs' 3D artificial niche based on dendritic polyglycerol and poly(N-isopropylacrylamide)-co-polyethylene glycol polymers via physical-chemical co-gelation strategy. Benefiting from the chemically-defined synthetic materials and their precise cooperation by covalent crosslinking and physical phase transition, the co-gelation-based artificial niche system can be adjusted with optimal parameters and high cell biocompatibility to support the robust production of high quality iPSCs with an excellent expansion efficiency. Moreover the expanded cells can be released out of their niche environment controllably only by adjusting the temperature. Overall, this controlled releasable artificial niche scaffold engineering shows great promise in iPSCs' 3D culture for downstream applications.

4.1. Results and Discussion

4.1.1 Establishment of control-releasable 3D Hydrogel based artificial Niche microenvironment by ECM mimicking

In order to overcome all the limitations mentioned above, we presented an advanced approach for engineering a synthetic and control-releasable iPSCs' 3D artificial niche environment according to a physical-chemical cogelation strategy for

iPSCs culture **(Figure 4-1)**. To achieve this goal, we tailored a 3D microenvironment with two specially designed biocompatible linkers: dPG-bicycloalkyne and poly(N-isopropylacrylamide) co-polyethylene glycol azide (pNIPAAm-co-PEG-N_3) polymers in two steps. First, under room temperature, the two polymers could form a hydrogel by strain-promoted azide-alkyne cycloaddition (SPAAC) reaction.[63] After being transferred to culture conditions (37 ℃), in which the temperature was higher than the lower critical solution temperature (LCST), the N-isopropylacrylamide co-polyethylene glycol polymers undergo physical gelation and further form a reversible hydrogel. Under physic-chemical synergistic gelation conditions, the formed dPG-pNIPAAm-co-PEG can work as the backbone and be used to mimic the physical property of the ECM. Additionally, rfRGD was introduced as biochemical signal to promote self-renewal and pluripotency.[200-202] After all the foremost parameters about precursor ratios (dPG-DIC (100 mg/mL) and pNIPAAm-co-PEG-N_3 (100 mg/mL)), elastic modulus (physical stiffness),[48, 68] and cell seeding density were optimized, an optimalcondition for cell culture was achieved. Therefore the culture system could support iPSCs' fast expansion and maintain high quality about proliferation capacity and high pluripotency, which can be characterized by the test of Ki-67 staining,[203] alkaline phosphatase (ALP) staining,[204] and pluripotency immunostaining.[13, 60, 205] Upon cooling down to the room temperature (＜LCST), the physical gelation affect despair leaving alone the covalent bond based gelation affect. This mechanism precisely benefits the culture system with the ability of controlled release of the cells and to harvest them with the high maneuverability and feasibility. Overall, this work provides an advanced control-releasable artificial niche scaffold engineering approach and shows great promise in the field of iPSCs' 3D culture.

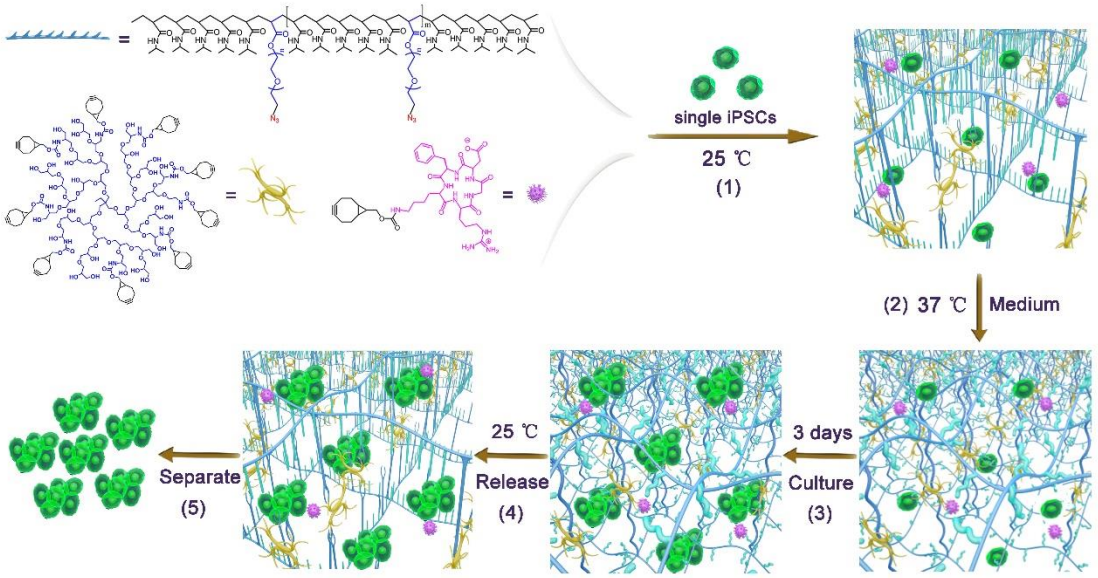

Figure 4-1. Schematic representation of the work mechanism in iPSCs' 3D culture for the artificial niche built based on dPG and pNIPAAm-co-PEG polymers via physical-chemicalcogelation strategy: first, a set of synthetic precursors, dPG-cyclooctyne, pNIPAAm-co-PEG azide, and RGD-cyclooctyne, was formed. (1) Together with these precursors, iPSCs were seeded into the system, and they preliminarily produced a niche only by chemical gelation. (2) After being transferred into 37 °C, physical gelation also occurred and created a reversible hydrogel. (3) Under these conditions, a stable niche was formed by physical-chemical cogelation strategy, which supported iPSCs' survival and quick expansion, then culture the cells for 3days. (4) After being cultured for certain time, the system could be transferred to 25 °C again, and the physical gelation disappeared, the niche was loosened, and then the cells released out of the niches. (5) Cells harvest by centrifugation.

The native ECM, which works as a key constitutive part of the microniche and plays an essential role in regulating cell behavior, is a complicated system.[48] Establishing an artificial niche microenvironment by mimicking the physical and biochemical characteristics of such an extracellular matrix, involves the optimization of several parameters, for example, chemically defined cell-compatible material synthesis, concentration-related hydrogel stiffness, cell seeding density, and adhesion-

relative biochemical cues.[128] Furthermore, finding efficient methods and related vital factors for the design of 3D cell culture niche environment that better represent the geometry, chemistry, and signaling environment suitable for iPSCs' survival and expansion is crucial. All optimal parameters and conditions of the above factors and conditions should be coordinated to control the influence of specific interactions with cellular systems. After these conditions have been modulated, the quality of the expanded cells obtained from the niche culture system should be further assessed. Moreover, the controlled release ability of this niche for the loaded cells needs to be investigated as well.

4.1.2 Precursors synthesis and the fabrication of novel hydrogel scaffold niche

For the establishment of a chemically defined niche environment for iPSC culturing, materials that are used to tailor their backbone and supply the cells' physical properties to capture are crucial.[68, 206] Thus, the design and the specific preparation of the synthetic precursors are the primary steps.[207] Polyethylene glycol (PEG)[116, 208] and dendritic polyglycerol (dPG),[63] because of their high biocompatibility, low batch-to-batch variability, as well as their readily amenable scalability have shown great promise to act as cellular scaffold.[209] Stimuli-responsive polymer materials are powerful tools in establishing dynamic or control reversible microenvironment, especially in cell biology.[210] Among various stimuli triggered factors, thermoresponsiveness which can be easily controlled is the most potential one to engineer materials for cell loaden or release. Poly(N-isopropylacrylamide) (PNIPAM) has been widely applied as a temperature-sensitive polymer with reversible gelation at the lower critical solution temperature (LCST) of 32 °C.[211-213] In order to combine the advantages of both, we designed synthesized a pNIPAAm-co-PEG polymer, as illustrated in **Figure 4-2a**. The stimuli-responsive illustration was revealed (**Figure 4-2b**), and its LCST was shown in **Figure 4-S1**. After azidation, the pNIPAAm-co-PEG polymer can be applied to program the hybrid hydrogel with dendritic polyglycerol cyclooctyne (dPG-DIC) (**Figure 4-2c**) by the *in situ* crosslinking approach by the bioorthogonal SPAAC reaction.[63] The synthesis and characterization of other macro-monomers and details of their characterization are shown in the experimental section. Benefiting from the

cogelation strategy, dPG- pNIPAAm -PEG hydrogel networks serve as the backbone of the microniche for supporting cells (**Figure 4-2e**) better than the pNIPAAm-co-PEG hydrogel networks. On the one hand, they overcome the disadvantage caused by a single pNIPAAm-co-PEG polymer, which physically crosslinked hydrogels fail to show strength and are not stable enough to serve as a cell scaffold for covalently crosslinked systems. On the other hand, one must introduce pNIPAAm, which has been equipped with a microniche with degradable and controlled-release properties. For stimulating cell adhesion inside the microniche, cyclo (RGDfk), a cellular binding peptide sequence was integrated into the polymer network as a biochemical signal to mimic the biological cues' features of native ECMs in stimulating colony formation that support iPSCs' survival and support proliferation[200-202] (**Figure 4-2d**). Finally, all of these precursors together preliminarily form the artificial scaffold niche environment **(Figure 4-2e)**, during which certain parameters, such as stiffness-related elastic modules and precursor's contents, still need to be further adjusted.

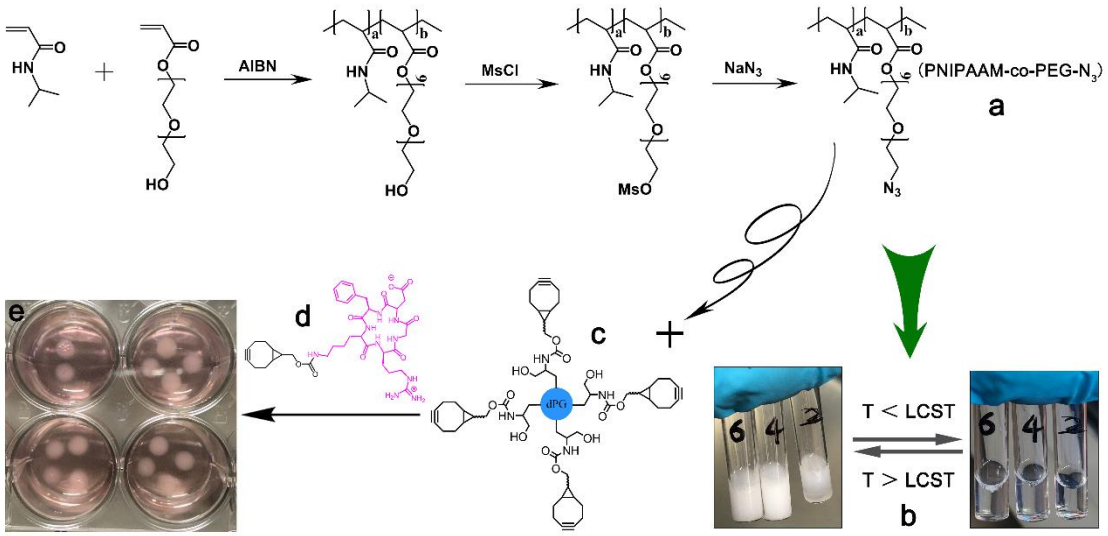

Figure 4-2. Synthesis of the precursors and fabrication process of the hydrogel scaffold's niche: (a) synthesis process of the pNIPAAm-co-PEG-N_3 and its thermos-reversible hydrogel properties. (a:b=5:1), (b) the thermoreversible phase-change phenomenon of the pNIPAAm-co-PEG-N_3 (LCST≈31 °C), (c) dPG-DIC (6%), (d) RGD-DIC, and (e) the finally formed scaffold niche with iPSCs culture inside under

37 °C in a cell culture incubator (within ESGRO medium).

4.1.3 Stiffness characterization of the hydrogel niche formed with various precursors' ratios and concentrations

Substrate stiffness, typically characterized by the elastic modulus, has emerged as one of the important mechanical features in controlling cell fate.[48] To tailor a microenvironment with proper physical strength, it is essential to optimize the stiffness parameters by adjusting the related affecting factors. Because the synthesized hydrogels-based niche was constructed by two precursor polymers, i.e. pNIPAAm-co-PEG-N_3 and dPG-DIC, the mechanical stiffness of the hydrogel networks was regulated by the respective ratios and overall concentration of the precursor. Influence of both of these parameters on the stiffness of hydrogel networks were studied which led to the establishment of an ideal artificial niche for iPSC loading and proliferation **(Figure 4-2)**. Primarily, precursor ratios were not only related to the content of different materials but also have a close relationship with their crosslink type and density, which together determine the final compatibility and stiffness of the whole niche environment.[19, 214] To assess the effect of precursor ratios, the elastic and viscous moduli were investigated by performing the rheological measurements. The ratios of precursors (dPG-DIC to pNIPAAm-co-PEG-N_3) for gel 1 to gel 6 were accordingly preset as 1:3, 1:2, 2:3, 1:1, 2:1, 3:1, and 2:3. Obviously, the elastic and viscous moduli of the hydrogel responded sensitively to the variation of precursor ratios and their data presented a curvilinear distribution. Compared to other gels, gel 3 and gel 4 with content ratio 2:3 and 1:1 respectively, presented a high value of both elastic and viscous modulus. It could be referred from these data analyses that only under certain precursor ratio, the synthesized hydrogel-based niche environment could be formed with high efficiency and possessan optimal stiffness, especially when the ratio (dPG-DIC and pNIPAAm-co-PEG-N_3) was 1:1 or 2:3.

Besides the precursor ratios, the polymers' concentration was another crucial parameter that could affect the stiffness.[214] To further investigate the stiffness parameter affected by polymer concentration, a rheological test was performed by

varying the polymer concentrations under constant ratio (**Figure 4-3b and 4-3d**). The rheological curves of all the gels that with different concentrations of dPG-DIC and pNIPAAm-co-PEG-N_3 indicated that the strength of the elastic modulus was in accordance with the concentration of the polymer under a specific polymer precursor ratio. Therefore we had significant instruction in searching for suitable stiffness-related physical parameters for constructing an artificial cell niche. Also, the gelation time, as a crucial parameter to evaluate the gelation efficiency, was essential in determining whether the technique could be used in the niche manufacturing process and supplied us with an appropriate incubation time during the initial period of cell seeding and cultivation. Thus, from the time-dependent elastic modulus G′ and viscous modulus G″ test, the effect and relationship of temperature and gelation time were also investigated during the gelation process. As shown in **Figure 4-3b**, gelation time, the time needed for the elastic modulus to approach constant was respectively about 120 s under the temperature of 37 °C. It demonstrated that, in consideration of the operation and 3D scaffold niche manufacture process, 120 s is the best choice for the parameters of gelation time for this project. On the whole, these results demonstrated that the mechanical properties of the artificial extracellular environment were governed by a complex interplay of dPG-DIC and pNIPAAm-co-PEG-N_3. Moreover, cells might be regulated by modulating the ratios and content of these polymers.

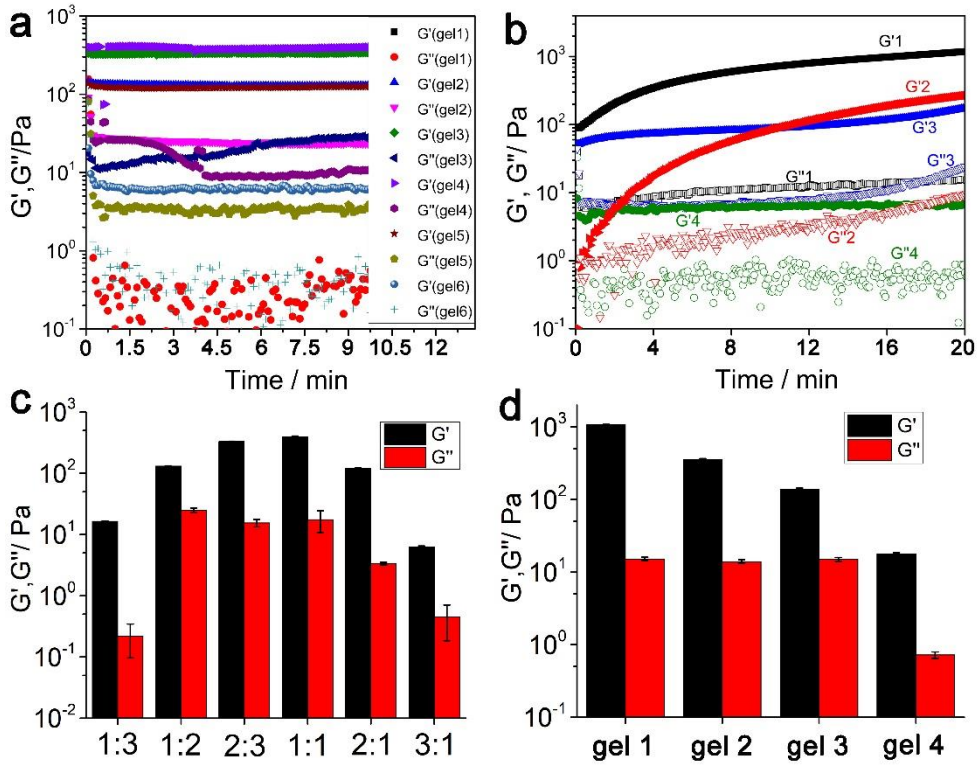

Figure 4-3. (a) The elastic modulus G′ and viscous modulus G″ was tested for the pre-formed hydrogel with variable volume ratio of dPG-DIC to pNIPAAm-co-PEG-N_3 ($C_{pNIPAAm\text{-}co\text{-}PEG\text{-}N3}$ =100 mg mL^{-1}, $C_{dPG\text{-}DIC}$ =100 mg mL^{-1}) at a constant temperature (37 °C). (b) Time-dependent gelation test for system with four different precursor concentrations under a certain ratio (1:1). (c) The rheology data of hydrogels niche under various precursor ratios. (d) The rheology data of hydrogels niche (gel 1- gel 4) with various precursors' concentrations under certain ratios.

4.1.4 iPSCs' response to the precursors ratios of materials for establishing a 3D niche environment

For a holistic study of the artificial 3D niche environment design, pivotal parameters should be coordinated and controlled to recapitulate a microenvironment that can affect cellular responses. In spite of the dPG-DIC and pNIPAAm-co-PEG-N_3 exhibiting good gelling mechanical strength by modulating their ratios, how the iPSCs' respond to the materials, especially to the extracellular niche environment resembled by precursors with different ratios, is still unclear. Since this application requires more than

mechanical versatility from hydrogels,[67] it requires cell compatibility based on biomimicry of ECM. Therefore, to assess the influence of the material type and proportion to iPSCs, we next investigated the cells' behavioral response to the resembled extracellular niche environment. Due to the precursor ratios that would determine the hydrogel composition and topography, we primarily performed the artificial extracellular niche's interior morphology analysis (**Figure 4-4a)**. The results revealed that it took on porosity with a certain mesh size among the networks inside the niche and the density and order would also change accordingly with variations of their elastic modulus. This means that the hydrogel and their composition indeed have a deep influence on the interior structure of the niche. To assess whether the different ratios of precursors affect iPSCs' survival and proliferation, iPSCs were further embedded into hydrogels precursors with six different ratios (R_1 - R_6) and cultured in an incubator under 37 °C. During the culture process, the cell survival and morphology features were monitored by live/dead staining day by day. The investigations' results (**Figure 4-4b**) indicated that cells' behavior in the artificial niche environment was significantly affected by the forming and ratios of their precursors. In a niche environment with precursor ratio of R_1 (dPG-DIC : pNIPAAm-co-PEG-N_3 = 1:3, E～16 Pa), most of the cells soon died and only very few cells survived and aggregated with each other. After three days of culture (day 3), there were obviously dead cells on the surface on the cell agglomeration. Until day 5, serious cell agglomeration occurred and formed EB with a super large size (more than 300 μm). The fact revealed that a niche environment with precursor ratio R1 could not support iPSCs' culture. These phenomena can be explained by the fact that, under this precursor ratio (3:1), the content of dPG-DIC is much lower than that of pNIPAAm-co-PEG-N_3, which would lead to predominant physical gelation rather than chemical SPAAC gelation within the cogelation system. It additionally also indicated that, with peristalsis phenomena, the physical gelling of pNIPAAm gel could not supply enough strength to prevent cell agglomeration, especially in the scaffold formed with pure or too much pNIPAAm physical gelation. Compared to the situation of R_1, cells in niche environment with the precursor ratio of R_2 (dPG-DIC : pNIPAAm-

co-PEG-N_3 = 1:2, E～120 Pa) and R_3 (dPG-DIC : pNIPAAm-co-PEG-N_3 = 2:3, E～330 Pa) survived better. Especially under R_3, culturing cells in a niche environment formed dense uniform and small spheroids with really high cell viability. This phenomenon showed that the hydrogel's niche with the current precursor ratio could better support iPSCs' survival. During this situation, it also revealed that, under a certain ratio (2:3), coordination and balance of the chemical and physical gelation could be achieved precisely to prevent cell agglomeration, which meanwhile worked as a scaffold to support iPSCs' survival and expansion. While the situation of R_4, R_5, and R_6, with the content increase of dPG-DIC and the content decrease of pNIPAAm-co-PEG-N_3, benefitted from the adequate SPAAC reaction and chemical covalent gelation, the niche environment could still prevent cell agglomeration. However, they could not support the cells to simultaneously keep high viability as well, because the poor degradability of their network would limit the cells' growth and loose hydrogel with too weak stiffness would break down easily and thus would be insufficient to support the iPSCs keep in 3D interspace. Besides, the expansion test (**Figure 4-4c**) further revealed that a niche with a precursor ratio of 2:3 shows the best for iPSCs' survival and expansion. Especially, after 3 days, the niche environment with these precursor ratios could better maintain iPSCs' renewability and has a higher expansion rate. So, overall, iPSCs' viability was indeed a response to the precursor ratio of 2:3 (dPG-DIC : pNIPAAm-co-PEG-N_3) and it could be regarded as the best ratio to form the niche environment for iPSC culturing, which was chosen as the standard parameters during in the following experiments.

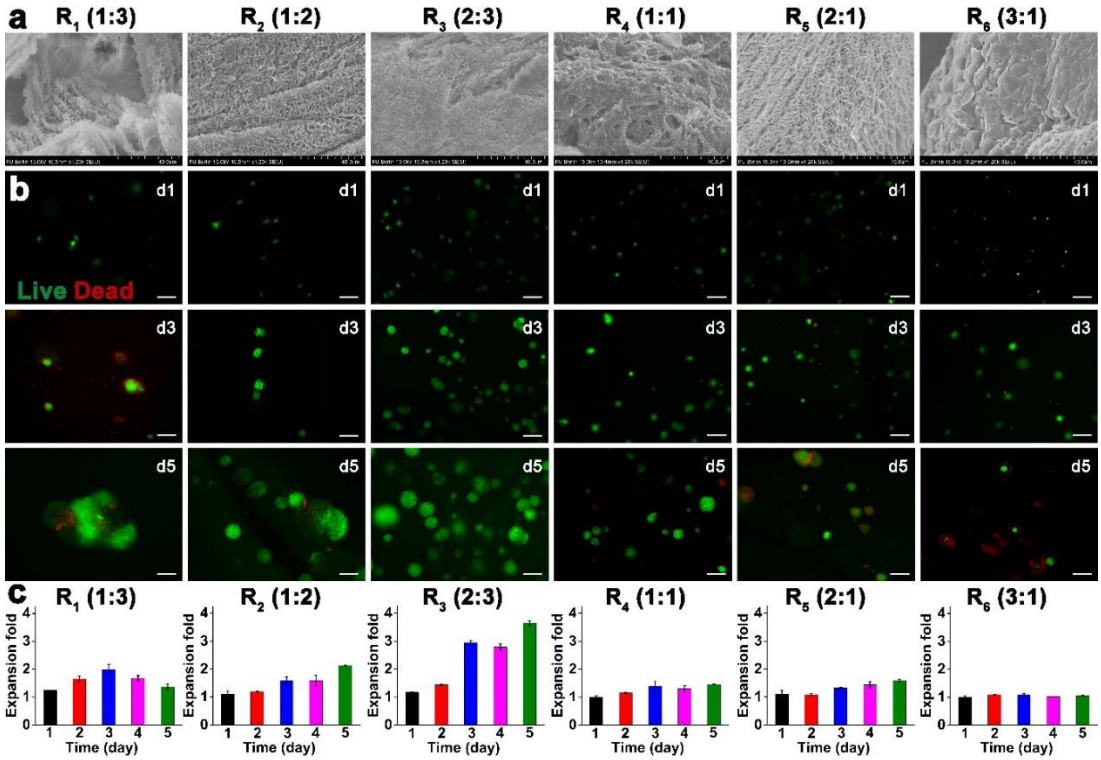

Figure 4-4. The response of iPSCs' viability and scaffold environment morphology to precursor ratios of the hydrogels niche. (a) SEM morphology test response to the precursor ratios of the hydrogel niche. The scale bar indicates 40 μm. (b) Cell viability tests depending on the precursor ratios of the hydrogel niche was monitored by live/dead staining (green - live cells, red - dead cells). The scale bar indicates 100 μm. (c) The iPSCs' proliferation as performance response to the precursor ratio of the hydrogel.

4.1.5 iPSCs' viability response to the stiffness and precursor content of the 3D niche environments

Previous studies reported that signals from the extracellular environment, especially the mechanical feedback of the linkage between cell and substrate, play a key role in regulating stem-cell fate.[171] The extracellular environment varies not only in composition but also in physical parameters, including stiffness, which typically is characterized by the elastic modulus and topography.[215] So, it is essential to investigate how the cells are influenced by the topography and stiffness in our artificial niche

environment. Control of the polymer concentration or crosslinking density varies topography and hydrogel stiffness.[68] Therefore the morphology properties of the niche environment with various polymers were adapted to test how their morphology was affected by crosslinking density. Alterations in the concentration ratio of the various polymers influenced the cell fate (**Figure 4-5**). The morphology analysis (**Figure 4-5a**) of concentrations should be studied first. However, as mentioned above, the precursor ratios also showed a particular effect in determining the stiffness of the niche environment. To circumvent the stiffness change caused by ratio variation, all the niche environment was performed by SEM, the results revealed that the inside niche environment took on a porous cellular structure. Whereas, in all of the niche environments with different stiffness, the hole's morphology varied according to elastic modules. In a slightly less crosslinked gel's niche environment (E_3～139 Pa) and E_4～17.8 Pa), the hole's size was a little larger. While, conversely, in slightly more crosslinked gels' niche environment (E_1～1070 Pa) and E_2～357 Pa), the hole's size was a little smaller. This study demonstrates that there is a close relationship between mesh size of holes within the networks and stiffness related precursor concentrations that were used to construct the polymeric gels.

To assess whether the different stiffness of the niche scaffold affected iPSCs' survival and proliferation, iPSCs were embedded into hydrogels precursors with high, medium, low, and really low concentrations, respectively, of which the elastic modulus are from 1070 -17.8 Pa accordingly. Meanwhile, cells were cultured in the ESGRO medium, and their survival conditions were monitored at least for 3 days (**Figure 4-5b**). The results revealed that cell behavior in this artificial niche was significantly affected by the stiffness of their microenvironment. Firstly, cells can form dense uniform spheroids under all the stiffness at the beginning, which demonstrated that the biocompatibility of the materials, both of the dPG-DIC and pNIPAAm-co-PEG-N_3 could support iPSCs' survival. However, specific stiffness is essential for niche microenvironment to prevent cells from agglomerating. Without enough stiffness, the microenvironment was insufficient to support the cell spheroids - embryoid bodies (EB), such as situations that occurred in E_3 (139 Pa) and E_4 (17.8 Pa), and these EB would

aggregate with each other and formed supersize agglomerations. Once the supersize agglomerations formed, oxygen, nutrients, and metabolites do not easily penetrate freely and reach or leave the center of the dense EB, which would inevitably lead to cell death. These were further demonstrated in the cell expansion test (**Figure 4-5d**). In the low stiffness niche environment, almost no cell expansion occurred. Compared to these, culturing cells in the niche with medium stiffness, uniform spheroids quickly could form and these iPSCs proliferated fast. The average size of the EB could reach 44.8 μm (day 3) from 24 μm (day 1) (**Figure 4-5c**), and the expansion rate could reach 6.5-fold (day 4) from 3.5 fold (day 4) (**Figure 4-5d**). While under high elastic modulus-environment E_1 (1075 Pa), most iPSCs still survived but with a lower cell survival rate and relative poor expansion efficiency. Not only the average EB sizes were only 19.3 μm and 39.4 μm for day 1 and day 3, but also the number and density of the EB were much lower than that in medium elastic modulus environment (**Figure 4-5c**). This was also revealed from the expansion test (2.3- and 3.3-fold for day 1 and day 3, respectively) (**Figure 4-5d**). Overall, this study revealed that only a certain stiffness environment allows for iPSCs' survival and expansion. Therefore, during the iPSCs' culture process, the elastic modulus of 357 Pa was chosen as the standard stiffness parameters for the dPG-pNIPAAm-co-PEG-based 3D niche environment culture system.

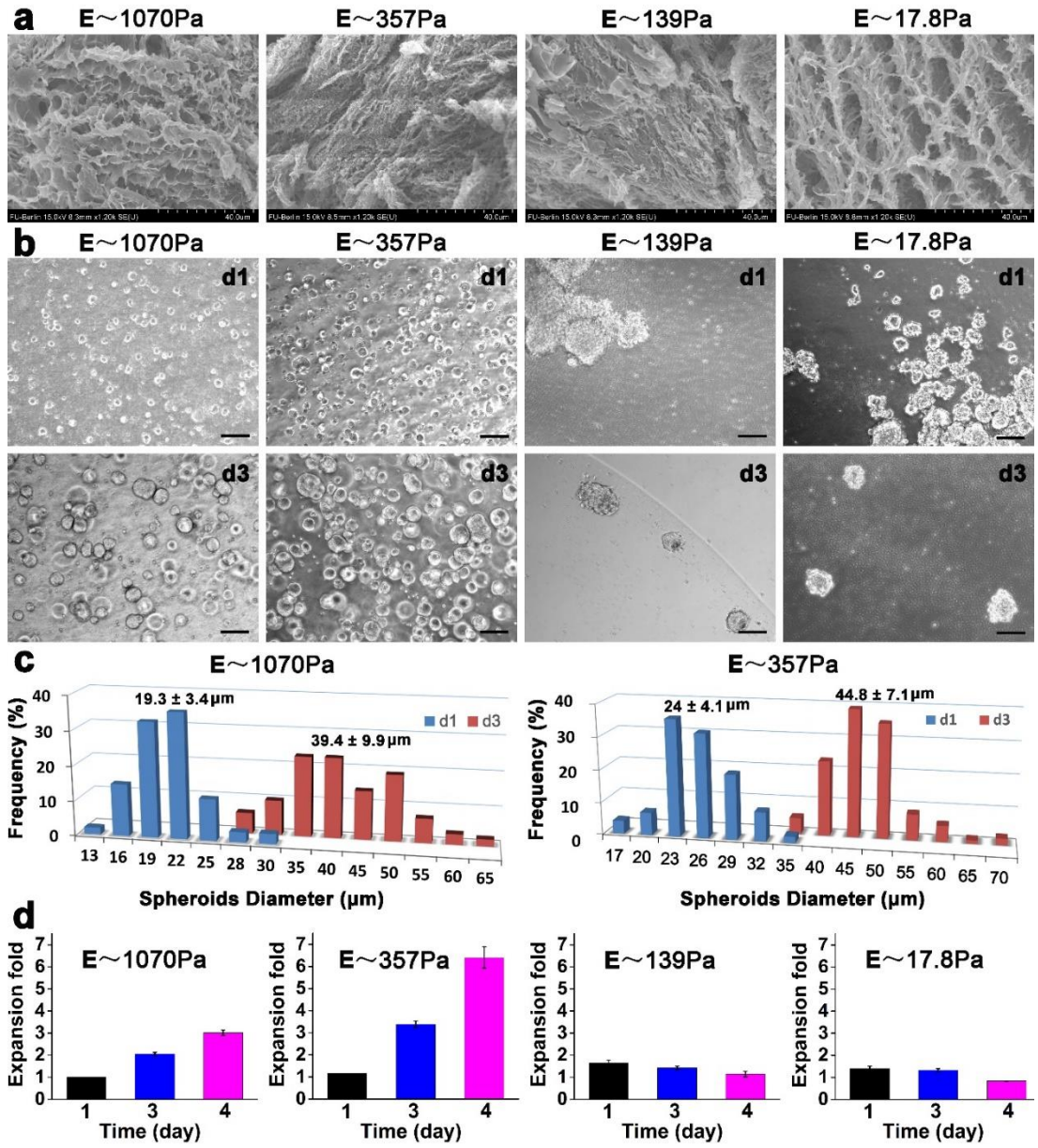

Figure 4-5. The iPSCs' viability and artificial niche environment morphology response to the stiffness and precursor content of the hydrogels. (a) SEM morphology response to the stiffness and precursor content of the hydrogels niche (with elastic modulus of 1070 Pa, 357 Pa, 139 Pa and 17.8 Pa, accordingly). The scale bar indicates 40 μm. (b) Cell viability to the stiffness and precursor content of the hydrogels niche were monitored by bright field microscopy. The scale bar indicates 100 μm. (c) EB size distribution and frequency in different culture days. (d) The iPSCs' proliferation efficiency response to the stiffness of the hydrogel niche environment.

4.1.6 iPSCs' viability and expansion efficiency response to cell seeding density

3D artificial scaffolds produced by hydrogel gelation techniques have proven their high value for cell culture applications due to their ability to support single cells in a three-dimensional environment. Nevertheless, in the extracellular environment, cells do not live alone. They can secrete substances that affect surrounding cells and keep sensing with each other.[48, 215] Thus, cell distribution and seeding density work as crucial determiners that not only affect the cell-cell contact but also affect cells' survival and expansion in the artificial niche environment. To further investigate the relationship between the iPSCs' seeding density and expansion efficiency in this fully chemically defined dPG- pNIPAAm-co-PEG niche environment and finally determine the optimum seeding density, cells with different concentrations of 2×10^6, 1×10^6, 3×10^5 cells /mL were separately seeded in three scaffold niches with the same elastic modulus (357 Pa) and specific precursor ratios (dPG-DIC: pNIPAAm-co-PEG-N_3 = 2:3). Furthermore, the morphology of the cells that survived in the artificial niche environment was monitored day by day (**Figure 4-6a**). Remarkably, under high or medium seeding density, the cells cultured in this dPG- pNIPAAm-co-PEG-based 3D microenvironment grew very fast and formed EB soon, while, under low seeding density, the cells expanded and grew into spheroids slowly. According to the statistical analysis, EB formed in the niche microenvironment with medium seeding density took on a much narrower size distribution than that under low and high seeding density conditions (**Figure 4-6b**). During day 1, the average EB sizes for high, medium, and low seeding density were 38.7 μm, 23.2 μm, and 13.2μm, respectively, which seemed that high cell seeding density could support cells expanding better. While, until day 3, average EB sizes for high, medium, and low seeding density niche environments reached 54.4 μm, 50.3 μm, and 16.4 μm, respectively. This can be explained by the fact that it is much easier for high-density cells to form small clusters from the beginning. However, it is precisely the formation of EB, both from small clusters and single cells, which seriously affects both of the EB size' homogeneous and uniform distribution, and their viability and expansion rates. In detail, the degree of EB sizes increase has been shown to support that the medium seeding density promoted a higher proliferation rate

(23.2 μm at day 1 to 50.3 μm at day 3). The further expansion tests revealed that the expansion rates of iPSCs in niche with seeding density of 1×10^6 cells /mL was 3.82 fold and 5.83 fold at day 3 and day 4, respectively (**Figure 4-6c**), and was higher than those with seeding densities of 2×10^6 cells /mL (3.54-fold and 5.47-fold at day 3 and day 4, respectively) and 3×10^5 cells /mL (1.82-fold and 1.16-fold at day 3 and day 4, respectively).

Additionally, EB size distribution in niche with medium seeding density was 16 – 32 μm on day 1 and 35 – 70 μm on day 3, which were much narrower than those in niche with high seeding density (20 – 90 μm on day 1 and 30 – 110 μm on day 3) or low seeding density (10 – 25 μm on day 1 and 10 – 45 μm on day 3) (**Figure 4-6b**). Based on the comprehensive consideration both of the EB size distribution and cells expansion efficiency, it is clear that the cells cultured in the 3D microenvironment grew very fast and formed EB quickly under a high seeding concentration, while the cells grew and expanded slowly under a low seeding concentration. Nevertheless, after being cultured for three days, cells under medium seeding concentration (1×10^6 cells /mL) had a much higher expansion efficiency than those under high seeding concentration (2×10^6 cells /mL). This can be explained by the fact that too much high seeding density caused the formed EB to aggregate with each other and limited their rapid expansion. Besides, it can be inferred from the results, culture system with a low seeding concentration of 3×10^5 cells /mL could not support iPSC expansion well in this 3D microenvironment. Overall, considering all the above factors, a seeding concentration of 1×10^6 cells /mL can be chosen as the most reasonable seeding density for the iPSCs expansion in this 3D chemically defined dPG-pNIPAAm-co-PEG niche culture system.

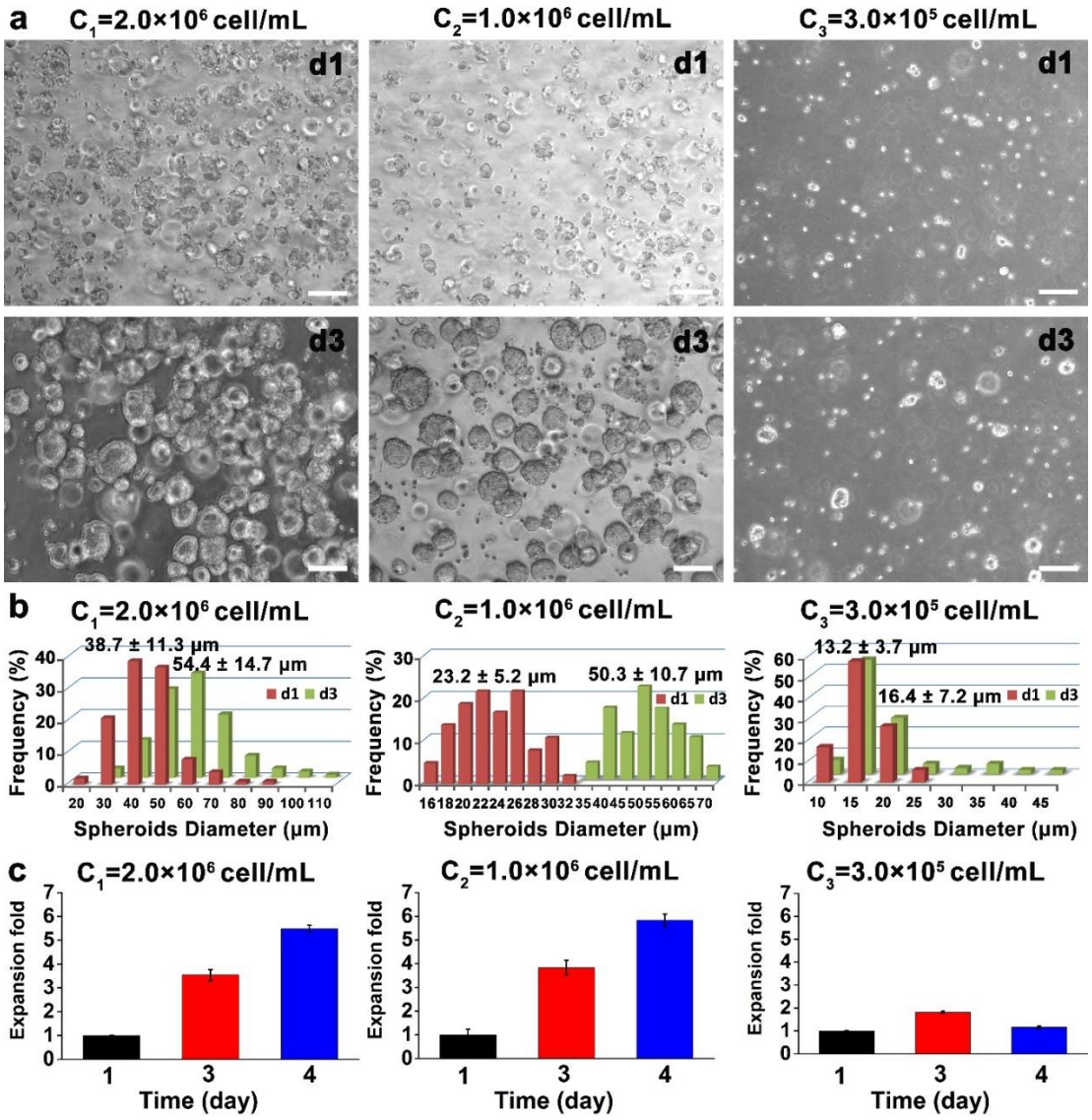

Figure 4-6. Optimization of the cell seeding density for iPSCs expansion in dPG-pNIPAAm-co-PEG niche 3D culture system (scale bar = 100 um). (a) Cell viability test of the cell seeding density was monitored by bright field microscope. (b) EB size distribution and frequency in different culture days to cell seeding density. (c) The iPSCs' proliferation efficiency response to culture time under different cell seeding densities in the artificial niche environment.

4.1.7 Overall performance of dPG-pNIPAAm-co-PEG 3D niche culture system in supporting iPSCs' proliferation

As reported, *in vivo* cells reside in a complex "microniche" environment. This

microenvironment generally not only serves as a structural support for cells but also offers various biochemical cues that regulate cell behavior.[48] Among these cues, the cell's adhesion site, which has a close relationship with cell density, is essential in determining cells' viability and proliferation because cells can sense their environment. To stimulate cell adhesion inside the microniche, cyclo (RGDfk), a cellular binding peptide sequence, was here integrated into the polymer network as a biochemical signal.[202, 203] The concentration of the RGDfk was adjusted to 1 mM, which was reported as the conmon's reasonable concentration.[216] Afterward, the multifactor optimization thus resulted in an effective, completely defined system for iPSC culture, which was then characterized under systematically controlling of all the key physical, bioactivity, and biomechanical parameters. Taking into account all the factors of optimal parameters, we embedded iPSCs (1×10^6 cells /mL) with precursors (dPG-DIC and pNIPAAm-co-PEG-N_3, both of their concentration were 100 mg/mL, the ratio of them was 2:3, cyclo (RGDfk) 1mM) into the culture system (E_2～357 Pa), again to investigate the cell viability and expansion efficiency and overall assess the performance of the artificial 3D niche environment in iPSCs' culture (**Figure 4-7**). Under optimal conditions, single iPSCs cultured in the 3D microenvironment (with RGDSK culture medium) grew very fast and soon grew into dense, uniform, and small spheroids. Then, these spheroids expanded quickly and took on narrow size distribution (**Figure 4-7 a-c**). Furthermore, the live/dead staining test indicated that cells cultured in this artificial environment had a high viability. Except for very few dead cells, most cells kept their renewal ability (**Figure 4-7 d-e**). This was also demonstrated by the expansion test (**Figure 4-7f**). Under optimal conditions, the expansion rates of iPSCs in this niche's culture system can achieve efficiency as high as 4.9- and 7.18-fold at day 3 and day 4, respectively. The study revealed that the dPG-pNIPAAm-co-PEG niche 3D culture system could allow for the robust proliferation of iPSCs with high viability. To investigate whether the dPG-pNIPAAm-co-PEG niche has a strong preference for defined medium, the niche 3D culture system was also performed both in E8 and ESGRO medium. The results revealed that despite iPSCs' having a strong preference for defined medium, the dPG-pNIPAAm-co-PEG did not show any preference for

defined medium. Overall, the cogelation of dPG-pNIPAAm-co-PEG-based culture system with optimal parameters could support iPSCs proliferation with excellent expansion efficiency but without preference for defined medium.

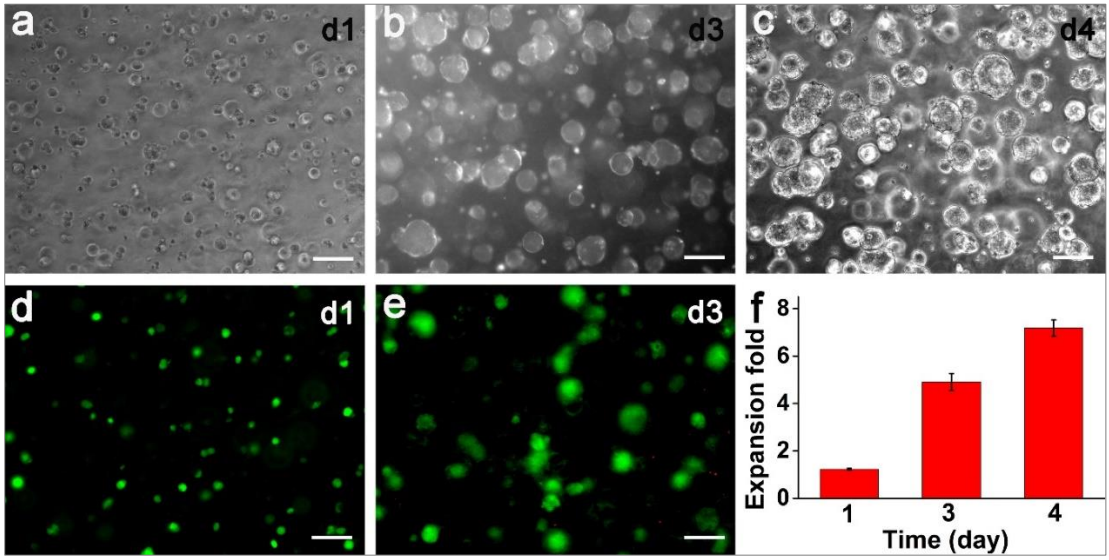

Figure 4-7. The dPG- pNIPAAm-co-PEG niche scaffold-based 3D culture system support iPSCs' expansion well under optimized conditions (scale bar = 100 um). (a) - (c) Cell viability and morphology during the culture process at day 1, day 3, and day 4, respectively. (d) - (e) Cell viability test at day 1 and day 3 was monitored by live/dead staining (green-live cells, red-dead cells). (f) iPSCs' proliferation efficiency under optimal conditions.

4.1.8 Control release and cells' harvest

Hydrogels represent an essential class of biomaterials for applications in 3D cell culture because their mechanical properties are similar to those of many objects in a living system.[63,96] However, in spite of availability of supplying high biocompatibility, low batch-to-batch variability, facile mechanical tunability, and amenable large-scale manufacturing and showing a great promise in acting as 3D cell-culturing scaffolds, the degradation of this scaffold and how to release the expanded cells with precise control and appropriate rate is still a crucial challenge in these applications.[174] To achieve the goal of hydrogel degradation, different strategies for cleaving chemical bonds in the hydrogels networks have been applied. For example, photolytic,[217] hydrolytic,[218]

enzymatic degradation,[200] and hydrolysis under acidic pH[218] have a great potential for degradation mechanisms which have been tried for controlled release applications.[63] However, for these strategies, the photo energy, the hydrolytic initiator, enzyme, and the acidic pH environment would inevitably damage the viability of the cell and might also lead to cell differentiation. To circumvent such an obdurate problem, we introduced a degradation property by the mechanism of thermos-reversible gelation into covalent crosslinking gelation and we finally formed a physical and chemical cogelation system. Thus, in this way, the cogelation degree of the niche scaffold could be adjusted by temperature (LCST), which could be used as a strategy to realize a controlled release of the iPSCs from their culture system (**Figure 4-8**). During this work, iPSCs were firstly embedded with precursors and together formed a niche scaffold culture system. After that, they were cultured for three days in cell incubator (37 °C) (**Figure 4-8a**). To release the expanded cells, the culture medium was replaced by the PBS, and the culture dish was put in 25 °C (＜ LCST) for 5 min. During this process, because the temperature was lower than the LCST, the thermos-gelation disappeared, leaving behind a loose network because of only covalent crosslinking gelation (**Figure 4-8b**). After the morphology of the niche scaffold changed from the white turbid solid to transparent and colorless, cells with a niche scaffold were together transferred into a centrifuge tube (**Figure 4-8c**). By centrifugation, iPSCs' EB that were formed in the niche environment were released, collected, and finally reached cell harvest (**Figure 4-8d**). According to the preliminary proliferation test, continuous high expressions of alkaline phosphatase were detected during the culture period until the seventh day (**Figure 4-8e**). This revealed that iPSCs' EB harvested from the extracellular environment still maintained proliferation ability well. The whole study here revealed that the chemically defined dPG- pNIPAAm-co-PEG cogelation niche scaffold culture system not only offers many features that benefit iPSC cultures, such as supporting cells' rapid growth and prevention of forming large cell aggregation, but also supplies thermoreversible degradation that could benefit the expanded cells to be controllably released from their culture system. Moreover, the controlled release can be achieved by only adjusting the temperatures, which shows substantial convenience and

maneuverability. We strongly expect that this principle can be generalized for the construction of controllably releasable iPSCs' 3D artificial niche for cell culture.

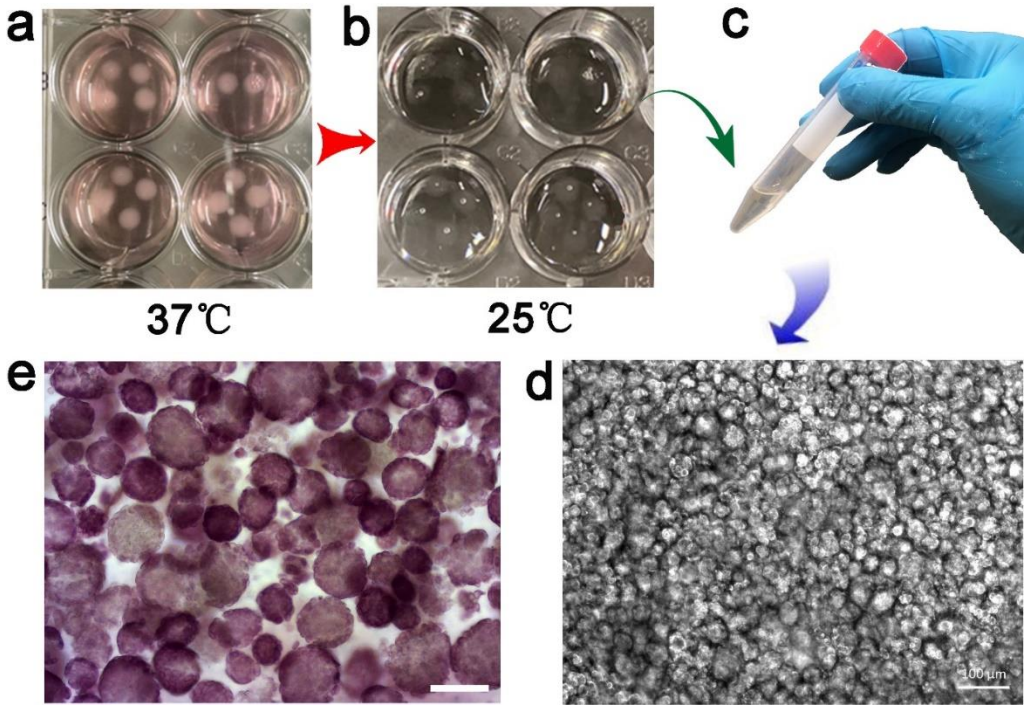

Figure 4-8. Controlled release and harvest of the expanded iPSCs from the dPG-pNIPAAm-co-PEG cogelation niche culture system**.** (a) iPSCs were embedded with precursors into the culture system and cultured for certain time. (b) Culture medium was replaced by the PBS, and the culture dish was put in 25 °C (＜LCST) for 5 min to release the expanded cells. (c) iPSCs EB purify and collection by centrifugation. (d) EB cells were cultured for three days (scale bar = 100 μm). (e) Alkaline phosphatase (ALP) staining (scale bar = 50 μm).

4.1.9 Cell quality characterization

To further assess the performance of the chemically defined dPG- pNIPAAm-co-PEG co-gelation niche scaffold culture system, we also performed Ki-67 staining test (**Figure 4-9**) and the immunocytochemistry analysis of pluripotency markers **(Figure 4-10)** to investigate their proliferation ability and whether iPSCs could maintain pluripotency during the whole culturing process. Firstly, investigations of Ki-67

staining from day 1 to day 5 showed that iPSCs in the spheroids maintained a high expression of Ki-67 proliferation markers. It means that the dPG- pNIPAAm-co-PEG cogelation niche scaffold culture system could support the expanded cells to keep high proliferation ability. Beyond that, immune-fluorescent staining revealed that the chemically defined cogelation 3D niche-produced iPSCs in spheroids maintained high expression of pluripotent markers,[13, 80] including Nanog, Sox2, Oct4, and SSEA1 (**Figure 4-9**). In summary, together with the consistent cell growth and ALP staining (**Figure 4-8d**), the uniform expression of these proliferation and pluripotent markers deeply revealed that the current system highly expanded iPSCs with high quality, density, and efficiency. Overall, our approach demonstrated that this chemically defined dPG-pNIPAAm-co-PEG cogelation niche scaffold culture system 3D supported iPSCs' proliferation and expansion well.

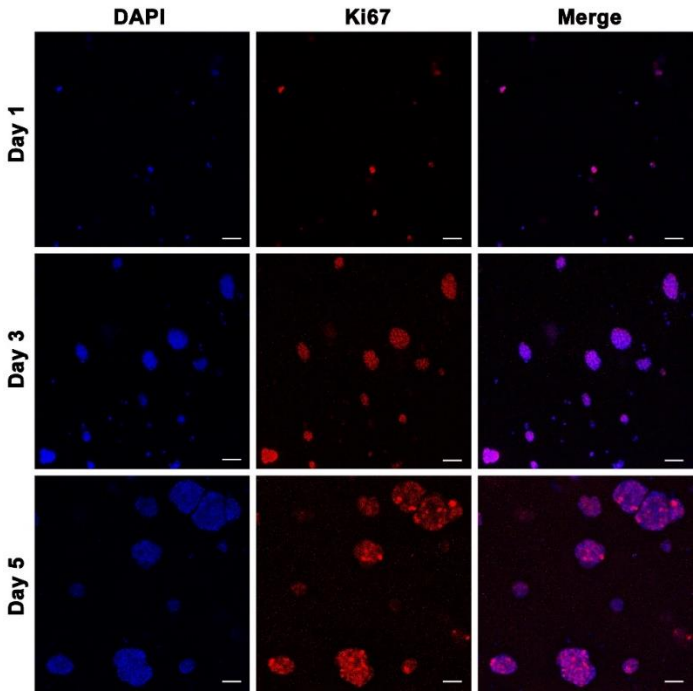

Figure 4-9. Ki-67 staining of the iPSCs' EB after having been cultured for 1, 3, and 5 days, respectively. (Blue: DAPI, red: a marker of proliferating cells). (scale bar = 100 μm).

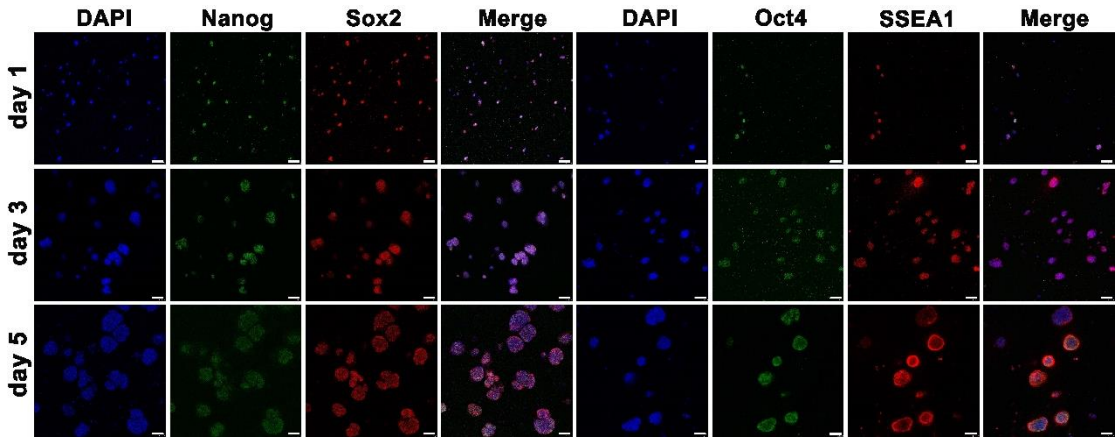

Figure 4-10. Immunostaining of the spheroids shows that the majority of cells expressed the pluripotent markers of Nanog, Sox2, Oct4, and SSEA1. All the staining tests were performed after the iPSCs' EB were cultured for 1, 3, and 5 days, respectively (scale bar = 100 μm).

4.2. Conclusion

In summary, we developed an advanced controlled-release iPSCs' 3D artificial niche based on dPG and pNIPAAm-co-PEG polymers *via* physical-chemical-co-gelation strategy. This chemically defined niche environment can support robust production of iPSCs with strong maintenance of pluripotency and self-renewal ability. Their expansion efficiency could reach as high as 4.9- and 7.18-folds only in 3 and 4 days' culture, respectively. Due to the fully chemically defined property, this 3D culture system can supply iPSCs without any reproduction limits and risks for pathogen and immunogenic transfer that might be caused by the application of traditional poorly defined animal-derived matrices or cell derivatives. Therefore it exhibits great promise for iPSCs to keep full potential in downstream biomedical applications. Furthermore, our system obtained from the optimized physical-chemical-co-gelation strategy substantially overcome the strong preference for defined medium and the collapse, which is caused by utilizing only thermo-reversible physical gelation and would lead to being insufficient for preventing cells agglomeration. Most important of all, the introduction of thermo-reversible crosslinkage to the covalently crosslinked networks equip the final 3D co-gelation niche culture system with specific thermos-reversible

degradation, which precisely enables the system for controlled release of the expanded cells. This dramatically simplifies the process of collecting cells. Overall, this work provides an advanced, controlled-release, defined, artificial niche engineering approach based on the physical-chemical-co-gelation strategy that shows great promise in the field of iPSCs' 3D culture.

4.3 Materials preparation and related experiment operation

4.3.1. Synthetic procedures of materials

Materials: Anhydrous solvents and all the chemicals were purchased from Acros or Sigma (Germany) and used as received, unless otherwise noted. N-isopropylacrylamide (NIPAAM) (Aldrich) was purified by recrystallization from hexanes and dried under high vacuum overnight (yield 80%). CH_2Cl_2, THF, and toluene were taken from a MBraun MB SPS-800 solvent purification system; poly(ethylene glycol) -acrylate with an average molecular weight (Mw) of ～360. 2, 2'-azobis(isobutyronitrile) (AIBN) was recrystallized from methanol. Dendritic polyglycerol (dPG) with a number average molecular weight (Mn) of 5 kDa, a weight average molecular weight (Mw) of 8 kDa and a degree of branching of 64% was synthesized by procedure reported previously and characterized by gel-permeation chromatography (GPC).

Methods: Nuclear magnetic resonance spectroscopy (NMR) spectra were measured on a Jeol ECX 400 or Jeol ECP 500 MHz and 100 MHz spectrometer, respectively. IR spectra was recorded with a Nicolet AVATAR 320 FT-IR 5 SXC (Thermo Fisher Scientific, Waltham, MA, USA) with a DTGS detector from 4000 to 650 cm^{-1}. Ultrasonic bath was used to disperse materials in solvents. Optical and fluorescence micrographs of all the resultant microniche particles with cells encapsulated inside were recorded on a ZEISS microscope. The cell viability was measured using a TECAN Infinite M200 Pro microplate reader. Confocal laser scanning microscopy was recorded by Leica TCS SP8 with 5×, 10×, and 20× oil-immersion objective lens and disposed by Leica confocal software.

Synthesis of poly(NIPAAm-co-PEG)-acrylate: the synthesis process was according to

the literature with some optimization.[219] To a flask of 250 mL, after being filled with argon, 4.982g NIPAAM (44.028 mmol) and 1.585g *PEG-acrylate* were together dissolved in 5 mL THF. Then, the flask was plug in Ar again. 80mg AIBN (51.43 mmol) was dissolved in 5 mL THF and then was added into the mixture solution under fierce stirring by injection pump. The temperature was brought up to 65°C temperature and the solution was stirred for 24h. The reaction mixture was precipitated directly in Et_2O and the product was got by suction filtration. The copolymer was then dialyzed, frozen, and lyophilized as a white solid (4.9634g, 76%).

Synthesis of Synthesis of poly(NIPAAm-co-PEG)-N_3: To a 250 mL Schlenk flask, poly(NIPAAm-co-PEG)-acrylate (5g,) was added, and then dried under high vacuum overnight. Then a solution of DMF (100mL) was added into the flask, suspension under fierce stirring. After that, 1.122mL Et_3N was added into the flask, and the flask was cooled down to 0 °C. 0.9247g MsCl in 15 mL DMF Water was carefully added into the suspension drop by drop. Then, remove the ice bath and keep the reaction overnight. After the reaction was kept in room temperature for 2 days, 3.4986g NaN_3 was added into the solution and mixture was heated to 65 °C. After kept reaction for 2days, the mixture solution was then dialyzed by 2K Da tube a mixture of water and methanol. The copolymer azidiation was then frozen, and lyophilized as a white solid (4.01g, 80%). ^{1}H NMR (500 MHz,) δ (ppm) was tested in different temperature (298K -313K) and as shown in Figure S1. The mole ratio of NIPAAm and PEG was calculated from the integration ratio between the methyl protons (6H)($(CH_3)_2CHNHCO$-) of NIPAAm and the methylene protons (2H)(H $OCH_2CH_2(OCH_2CH_2)$n OCH_2CH_2OCO-) of PEG appearing at 1.1 and 3.65 ppm, respectively. From the ^{1}H NMR tests in different temperature, the signals of both of them disappeared when the temperature to its lower critical solution temperature (LCST). Therefore, from these tests with under different temperature, it can be inferred that the FTLC of the synthetic poly(NIPAAm-co-PEG)-N_3 was about 301K (31°C). Besides that, the azide functional group of the poly(NIPAAm-co-PEG)-N_3 was also characterized by IR test as shown in Figure 4-2. The GPC information of the poly(NIPAAm-co-PEG)-N_3 was shown in Figure 4-3 and Figure 4-4.

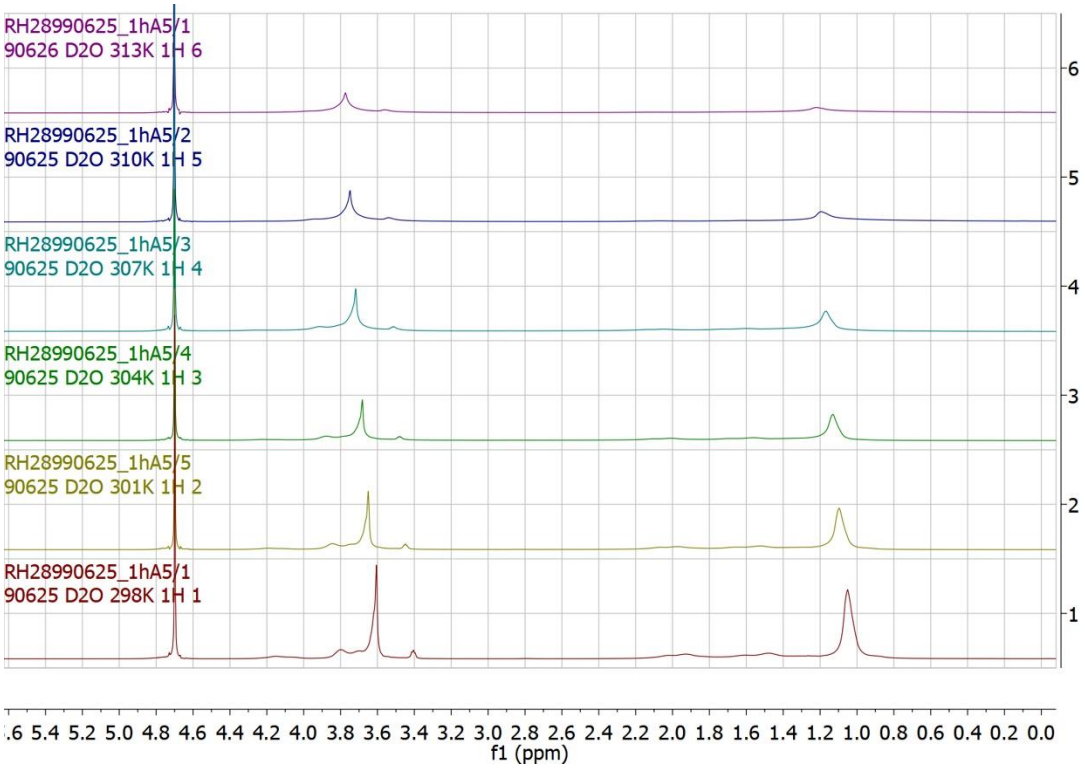

Figure 4-S1. ^{1}H NMR of poly(NIPAAm-co-PEG)-acrylate in different temperature.

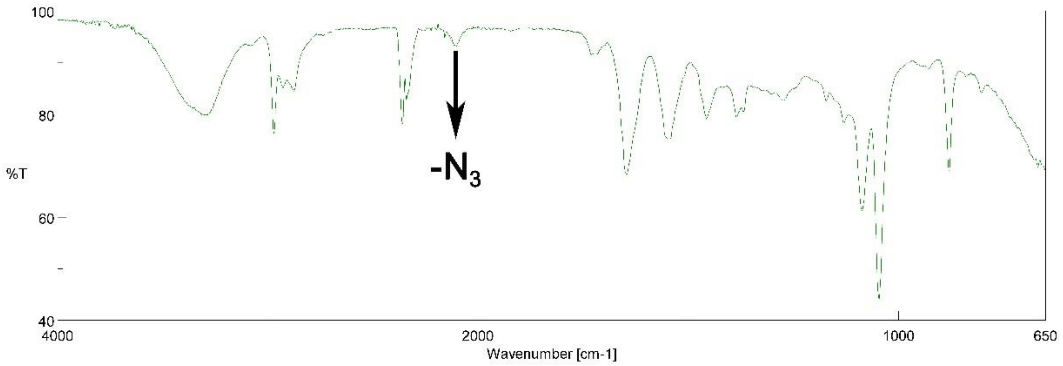

Figure 4-S2. IR of the poly(NIPAAm-co-PEG)-N_3.

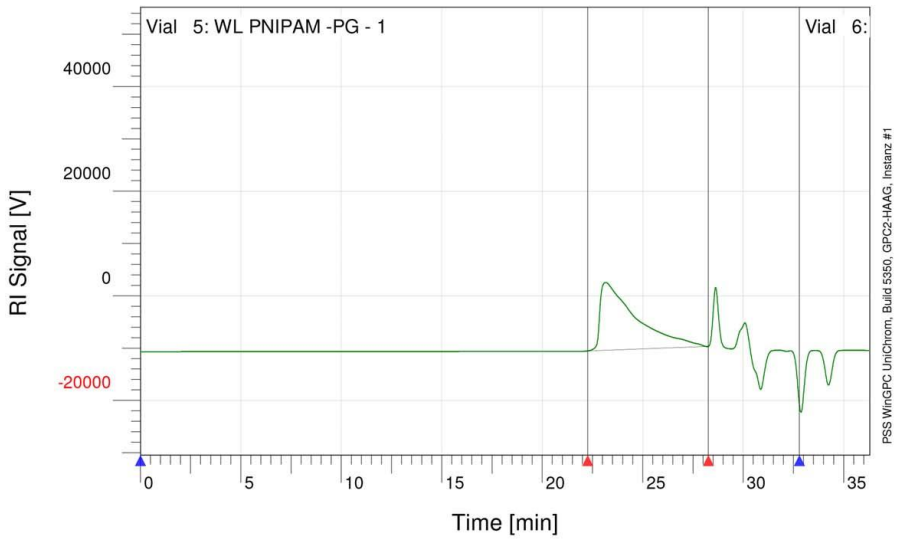

Probe :	Vial 5: WL PNIPAM -PG - 1	**Methode :**	C:\GPC-Daten\Methoden\PS_80bar_180709.MET
Basislinie von :	22.263 ml	**bis :**	28.265 ml
Integration von :	22.647 ml	**bis :**	26.856 ml
Kalibration :	Polystyrol 190408 82bar.CAL	**Eluent :**	THF
MHK - A (Kal.):	0.000E+0	**MHK - K (Kal.):**	1.000E+0 ml/g
Int.Stand.-K :	28.640 ml	**Int.Stand.-M :**	28.637 ml
Pumpe :	PSS SECcurity	**Flussrate :**	1.000 ml/min
Konzentration :	3.000 g/l	**Injektvolumen :**	100.000 ul
Säule 1 :	PL Gel 5µm Vorsäule	**Temperatur :**	25.000 °C
Säule 2 :	PL Gel 5µm mix-C	**Temperatur :**	0.000 °C
Säule 3 :	PL Gel 5µm mix-C	**Temperatur :**	0.000 °C
Säule 4 :	PL Gel 5µm mix-C	**Temperatur :**	0.000 °C
Detektor 1 :	I1: RID 1, RI Signal	**Versatz :**	0.000 ml
Detektor 2 :	I1: IsoPump 1, Pressure	**Versatz :**	0.000 ml
Operateur :	Administrator	**Messintervall :**	1.000 sec

Figure 4-S3. RI signal of the poly(NIPAAm)-co-PEG for GPC test.

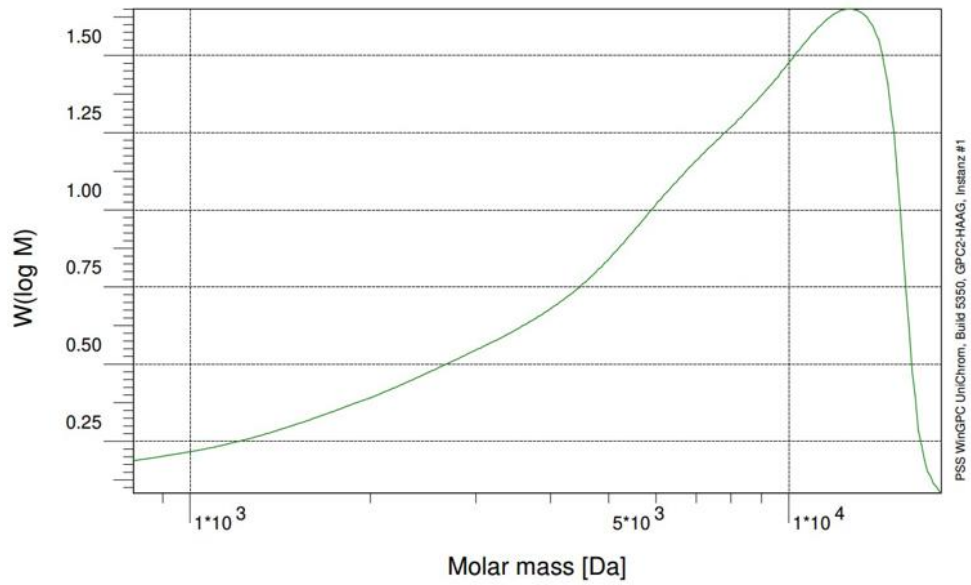

Mn: 4.3759 e3 g/mol
Mw: 7.508 e3 g/mol
D: 1.7158

Figure 4-S4. GPC test for poly(NIPAAm)-co-PEG linkers.

Chapter 5. Summary & Conclusion

The poorly defined animal-derived matrices severely limit a reliable culture for further therapeutic application, because these animal-derived matrices may pose risks for pathogen and immunogenic transfer due to their variable source and xenogeneic contamination. Thereby, to construct a fully chemically designed stem cell microniches for the alternative of the poorly defined animal-derived matrices for iPSCs culturing is urgently needed. *In vivo*, stem cells reside in an intricate, specialized microniche, which not only serves as a structural support for the cells but also offers various biochemical or physical cues that together regulate their behavior. As cells can sense and respond to a myriad of signals from their microenvironment, which can control the cell fate to some extent, 3D microenvironment engineering is particularly important in establishing a cell environment. The research strategy should be to establish a much more suitable surrounding environment for iPSC to survive inside, like 3D scaffold similar to the native ECM.

In my first project, the novel chemically defined, artificial 3D microniche was engineered with degradable polyethyleneglycol-co-polycaprolactone and RGDfk-functionalized dendritic polyglycerol hydrogel precursors by coordinately controlling over physical properties and bioactivity to keep specific interactions with cellular systems. In this way, the behavior of iPSC was indeed completely maintained by the artificial microniches and they also kept a high level of pluripotency expression and excellent viability without any pathogen and immunogenic transfer risks, which indicates great promise for therapeutic applications. Additionally, the fabrication process of the microniches was performed under microfluidic conditions and could supply microniche scaffold with huge efficiency. Therefore, it shows great promise in realizing iPSCs' 3D culturing and reliable expansion in chemically defined synthetic microniches on a large scale.

In my second project, I described an approach to establish fully defined, thermally responsive, iPSCs' 3D artificial niches based on dPG and poly (N-

isopropylacrylamide)-co-polyethylene glycol polymers via physical-chemical cogelation strategy. Benefiting from the cooperation of the SPAAC reaction and the physical phase transition, the cogelation system could be adjusted with optimal stiffness and mechanical strength and also supported iPSCs' survival well, maintained self-renewal, and preserved high pluripotency. After being cultured, the cells can easily controllably release from the niches just by adjusting the temperature. Overall, the high maneuverability and feasibility of this establishment of artificial niche engineering shows great promise in iPSCs' 3D culture for regenerative medicine and clinical therapies.

Chapter 6. Zusammenfassung

Die wenig definierten Matrizen tierischer Herkunft schränken die zuverlässige Kultivierung der Zellen für die weitere therapeutische Anwendung stark ein, da diese Matrizen aufgrund ihrer Variabilitätsquelle und heterogenen Kontamination Risiken für den Pathogen- und Immunogentransfer bergen können. Daher ist es dringend erforderlich, eine vollständig chemisch entworfene Stammzell-mikronische als Alternative für die wenig schlecht definierten Matrizen tierischer Herkunft für die Kultivierung von iPSCs zu konstruieren. In vivo befinden sich Stammzellen in einer komplizierten, spezialisierten Mikronische, die nicht nur als strukturelle Unterstützung dient, sondern auch verschiedene biochemische und biophysikalische Hinweise bietet, die zusammen das Zellverhalten regulieren. Da Zellen eine Vielzahl von Signalen aus ihrer Mikroumgebung erfassen und darauf reagieren können, wodurch das Zellschicksal in gewissem Maße gesteuert werden kann, ist die 3D-Mikroumgebung besonders wichtig. Die Forschungsstrategie sollte darin bestehen, eine geeignetere Umgebung für iPSC zu schaffen, um darin überleben zukönnen, wie beispielsweise ein 3D-Gerüst, das mit nativem ECM vergleichbar ist.

In meinem ersten Projekt wurde die neuartige chemisch definierte künstliche 3D-Mikronische mit abbaubaren Polyethylenglykol-Co-Polycaprolacton- und RGDfk-funktionalisierten dendritischen Polyglycerin-Hydrogelvorläufern hergestellt, indem die physikalischen Eigenschaften und die Bioaktivität koordiniert kontrolliert wurden, um spezifische Wechselwirkungen mit zellulären Systemen aufrechtzuerhalten. Auf diese Weise wurde das Verhalten von iPSC von den künstlichen Mikronischen vollständig eingehalten. Darüber hinaus können sie ein hohes Maß an Pluripotenz-Expression und eine hervorragende Lebensfähigkeit ohne jegliches Risiko für Pathogen- und Immunogentransfer aufrechterhalten, was für therapeutische Anwendungen vielversprechend ist. Weiterhin hinaus wird der Herstellungsprozess der Mikronischen unter mikrofluidischen Bedingungen durchgeführt und kann ein Mikronischengerüst mit einer ehohen Effizienz liefern. Daher ist es vielversprechend,

die 3D-Kultivierung von iPSCs und die zuverlässige Expansion in chemisch definierten synthetischen Mikronischen in großem Maßstab zu realisieren.

Zusammenfassend haben wir eine fortschrittliche künstliche 3D-Nische entwickelt, die auf dPG- und pNIPAAm-Co-PEG-Polymeren mittels einer physikalisch-chemischen Co-Gelierungsstrategie zur kontrollierten Freisetzung von iPSCs basiert. Diese chemisch definierte Nischenumgebung kann die robuste Produktion von iPSCs mit starker Aufrechterhaltung der Pluripotenz und der Fähigkeit zur Selbsterneuerung unterstützen. Ihre Expansionseffizienz, die bis zu 4,9 und 7,18 erreichen könnte, lässt sich nur durch 3 bzw. 4-tägige Kultur verdoppeln. Aufgrund der vollständig chemisch definierten Eigenschaft kann dieses 3D-Kultursystem iPSCs ohne jegliche Reproduktionsgrenzen und Risiken für den Pathogen- und Immunogentransfer liefern, die durch die Anwendung traditioneller, schlecht definierter Matrices oder Zellderivate aus tierischen Quellen verursacht werden könnten, was für iPSCs vielversprechend ist, um das volle Potenzial in nachgeschalteten biomedizinischen Anwendungen zu erhalten. Durch die physikalisch-chemische Ko-Gelierungsstrategie konnte dieses System die starke Vorliebe für definiertes Medium und den Kollaps, der nur durch die Verwendung von thermoreversibler physikalischer Gelierung verursacht wird und zu einer unzureichenden Verhinderung der Zellagglomeration führen würde, im Wesentlichen überwinden. Am wichtigsten ist jedoch, dass durch die Einführung einer thermoreversiblen Vernetzung in die kovalent vernetzten Netzwerke das endgültige 3D-Co-Gelierungs-Nischen-Kultursystem mit einem spezifischen thermoreversiblen Abbau ausgestattet wird, der genau die Eigenschaft aufweist, die es dem System ermöglicht, die expandierten Zellen kontrolliert freizusetzen. Dies vereinfacht den Prozess des Sammelns von Zellen dramatisch und seine hohe Manövrierfähigkeit und Durchführbarkeit sind bei der Zellernte während der 3D-Kultur vielversprechend. Insgesamt bietet diese Arbeit einen fortschrittlichen, von der Steuerung lösbaren, definierten Ansatz für die Konstruktion künstlicher Nischen, der auf der Strategie der physikalisch-chemischen Ko-Gelierung basiert und im Bereich der 3D-Kultur von iPSC vielversprechend ist.

Chapter 7. Outlook

Fully chemically defined artificial microniche engineering with degradable polyethyleneglycol-co-polycaprolactone and RGDfk-functionalized dendritic polyglycerol precursors by droplet-based microfluidics has been achieved. This artificial 3D microniche can allow for the robust production of iPSCs with prolonged self-renewal ability and high pluripotency but without any reproduction limits and risks for pathogen and immunogenic transfer. This advanced approach that breaks through bottlenecks brought by the application of traditional poorly defined animal-derived matrices or cell derivatives exhibits great promise for iPSCs to obtain their full potential in therapeutic applications. Additionally, this microniche engineering fabrication process was performed under microfluidic conditions, which could supply products with huge efficiency, and therefore also shows great promise in realizing iPSCs' 3D culturing and expansion on a large scale. By using a physical-chemical-co-gelation strategy, the co-gelation system can be adjusted with an optimal stiffness and mechanical strength, which can support iPSCs to survive well, keep self-renewal and preserve high pluripotency. After they were cultured, the cells could be easily controllably released out of the niches only by adjusting the temperature. Overall, the high maneuverability and feasibility of this establishment of artificial niche engineering shows great promise in iPSCs' 3D culture for regenerative medicine and clinical therapies.

Chapter 8. Reference

[1] K. D. Wilson, J. C. Wu, *JAMA* **2015**, *313*, 1613-1614.

[2] A. J. Becker, E. A. Mcculloch, J. E. Till, *Nature* **1963**, *197*, 452-454.

[3] L. Siminovitch, E. A. Mcculloch, J. E. Till, *Journal of Cellular and Comparative Physilogy* **1963**, *62*, 327-336.

[4] The Nobel Prize in Physiology or Medicine **2012** http://nobelprize.org

[5] J. A. Thomson, J. I. Eldor, S. S. Shapiro, M. A. Waknitz, J. J. Swiergiel, V. S. Marshall, J. M. Jones, *science* **1998**, *282*, 1145-1147.

[6] K. Takahashi, K. Tanabe, M. Ohnuki, M. Narita, T. Ichisaka, K. Tomoda, S. Yamanaka, *Cell* **2007**, *131*, 861-872.

[7] K. Takahashi, S. Yamanaka, *Development* **2015**, *142*, 3274-3285.

[8] I. J. Fox, G. Q. Daley, S. A. Goldman, J. Huard, T. J. Kamp, M. Trucco, *Science* **2014**, *345*, 889.

[9] D. A. Robinton, G. Q. Daley, *Nature* **2012**, *481*, 295-305.

[10] V. C. Chen, S. M. Couture, J. Ye, Z. Lin, G. Hua, H. I. Huang, J. Wu, D. Hsu, M. K. Carpenter, L. A. Couture, *Stem Cell Res* **2012**, *8*, 388-402.

[11] M.J. Evans, M.H. Kaufman, *Nature* **1981**, *292*, 15-156.

[12] G. R. Martin, *PNAS* **1981**,*78*,7634-7638.

[13] K. Takahashi, S. Yamanaka, *Cell* **2006**, *126*, 663-676.

[14] D. Jing, A. Parikh, J. M. Canty, Jr., E. S. Tzanakakis, *Tissue Eng Part B Rev* **2008**, *14*, 393-406.

[15] M. Eiraku, K. Watanabe, M. Matsuo-Takasaki, M. Kawada, S. Yonemura, M. Matsumura, T. Wataya, A. Nishiyama, K. Muguruma, Y. Sasai, *Cell Stem Cell* **2008**, *3*, 519-532.

[16] J. A. Thomson, J. I. Eldor, S.S. Shapiro, M. A. Waknitz, J. J. Swiergiel, V. S. Marshall, J. M. Jones, *Science* **1998**, *282*, 1145-1147.

[17] L. A. Boyer, T. I. Lee, M. F. Cole, S. E. Johnstone, S. S. Levine, J. P. Zucker, M. G. Guenther, R. M. Kumar, H. L. Murray, R. G. Jenner, D. K. Gifford, D. A. Melton, R. Jaenisch, R. A. Young, *Cell* **2005**, *122*, 947-956.

[18] Y. H. Loh, Q. Wu, J. L. Chew, V. B. Vega, W. Zhang, X. Chen, G. Bourque, J. George, B. Leong, J. Liu, K. Y. Wong, K. W. Sung, C. W. Lee, X. D. Zhao, K. P. Chiu, L. Lipovich, V. A. Kuznetsov, P. Robson, L. W. Stanton, C. L. Wei, Y. Ruan, B. Lim, H. H. Ng, *Nat Genet* **2006**, *38*, 431-440.

[19] M. Caiazzo, Y. Okawa, A. Ranga, A. Piersigilli, Y. Tabata, M. P. Lutolf, *Nat Mater* **2016**, *15*, 344-352.

[20] K. Takahashi, S. Yamanaka, *Development* **2013**, *140*, 2457-2461.

[21] M. Bellin, M. C. Marchetto, F. H. Gage, C. L. Mummery, *Nat Rev Mol Cell Biol* **2012**, *13*, 713-726.

[22] J. Y. Yu, M. A. Vodyanik, K. S. Otto, J. A. Bourget, J. L. Frane, S. L. Tian, J. Nie, G. A. Jonsdottir, V.Ruotti, R. Stewart, I. I. Slukvin, J. A. Thomson, *Science* **2007**, *318*, 1917-1920.

[23] G. M. Roomans, *European Cells and Materials* 2010, *19*, 284-299.

[24] S. Kusuma, S. Gerecht, *Expert Rev Cardiovasc Ther* **2010**, *8*, 1433-1445.
[25] D. Xu, F. Wang, H. Gu, J. Wang, Q. Guo, Y. Zhang, Z. Wang, *Cell Mol Biol Lett* **2010**, *15*, 451-472.
[26] S. F. Badylak, D. Taylor, K. Uygun, *Annu Rev Biomed Eng* **2011**, *13*, 27-53.
[27] M. Eiraku, N. Takata, H. Ishibashi, M. Kawada, E. Sakakura, S. Okuda, K. Sekiguchi, T. Adachi, Y. Sasai, *Nature* **2011**, *472*, 51-56.
[28] H. Suga, T. Kadoshima, M. Minaguchi, M. Ohgushi, M. Soen, T. Nakano, N. Takata, T. Wataya, K. Muguruma, H. Miyoshi, S. Yonemura, Y. Oiso, Y. Sasai, *Nature* **2011**, *480*, 57-62.
[29] P. W. Burridge, G. Keller, J. D. Gold, J. C. Wu, *Cell Stem Cell* **2012**, *10*, 16-28;
[30] H. Liu, S. C. Zhang, *Cell Mol Life Sci* **2011**, *68*, 3995-4008.
[31] O. Lindvall, Z. Kokaia, A. Martinez-Serrano, *Nat Med* **2004**, *10 Suppl*, S42-50.
[32] T. Nishimura, S. Kaneko, A. Kawana-Tachikawa, Y. Tajima, H. Goto, D. Zhu, K. Nakayama-Hosoya, S. Iriguchi, Y. Uemura, T. Shimizu, N. Takayama, D. Yamada, K. Nishimura, M. Ohtaka, N. Watanabe, S. Takahashi, A. Iwamoto, H. Koseki, M. Nakanishi, K. Eto, H. Nakauchi, *Cell Stem Cell* **2013**, *12*, 114-126.
[33] R. Vizcardo, K. Masuda, D. Yamada, T. Ikawa, K. Shimizu, S. Fujii, H. Koseki, H. Kawamoto, *Cell Stem Cell* **2013**, *12*, 31-36.
[34] K. Hayashi, H. Ohta, K. Kurimoto, S. Aramaki, M. Saitou, *Cell* **2011**, *146*, 519-532.
[35] K. Hayashi, S. Ogushi, K. Kurimoto, S. Shimamoto, Hiroshi Ohta, M. Saitou, *Science* **2012,** *338*, 971-975.
[36] A. Trounson, N. D. DeWitt, *Nat Rev Mol Cell Biol* **2016**, *17*, 194-200.
[37] S. C. Desbordes, L. Studer, *Nat Protoc* **2013**, *8*, 111-130.
[38] A. D. Ebert, P. Liang, J. C. Wu, *J Cardiovasc Pharmacol* **2012**, *60*, 408-416.
[39] A. D. Ebert, J. Yu, F. F. Rose, Jr., V. B. Mattis, C. L. Lorson, J. A. Thomson, C. N. Svendsen, *Nature* **2009**, *457*, 277-280.
[40] V. K. Singh, M. Kalsan, N. Kumar, A. Saini, R. Chandra, *Front Cell Dev Biol* **2015**, *3*, 2.
[41] J. A. Efe, S. Hilcove, J. Kim, H. Zhou, K. Ouyang, G. Wang, J. Chen, S. Ding, *Nat Cell Biol* **2011**, *13*, 215-222.
[42] N. Zhang, Michael, J. Bevan, *Immunity* **2011**, *35*, 161-168.
[43] mP. D. Potdar, Y. D. Jethmalani, *World J Stem Cells* **2015**, *7*, 839-851.
[44] A. Faulkner-Jones, C. Fyfe, D. J. Cornelissen, J. Gardner, J. King, A. Courtney, W. Shu, *Biofabrication* **2015**, *7*, 044102.
[45] A. J. Want, A. W. Nienow, C. J. Hewitt, K. Coopman, *Regen. Med* **2012**, *7*, 71-84.
[46] M. Serra, C. Brito, C. Correia, P. M. Alves, *Trends Biotechnol* **2012**, *30*, 350-359.
[47] M. Schutte, B. Fox, M. O. Baradez, A. Devonshire, J. Minguez, M. Bokhari, S. Przyborski, D. Marshall, *Assay Drug Dev Technol* **2011**, *9*, 475-486.
[48] M. Bao, J. Xie, W. T. S. Huck, *Adv Sci* **2018**, *5*, 1800448.
[49] L. G. Villa-Diaz, A. M. Ross, J. Lahann, P. H. Krebsbach, *Stem Cells* **2013**, *31*, 1-7.

[50] A. S. Mao, J. W. Shin, S. Utech, H. Wang, O. Uzun, W. Li, M. Cooper, Y. Hu, L. Zhang, D. A. Weitz, D. J. Mooney, *Nat Mater* **2017**, *16*, 236-243.
[51] M. Serra, C. Correia, R. Malpique, C. Brito, J. Jensen, P. Bjorquist, M. J. Carrondo, P. M. Alves, *PLoS One* **2011**, *6*, e23212.
[52] R. Peerani, B. M. Rao, C. Bauwens, T. Yin, G. A. Wood, A. Nagy, E. Kumacheva, P. W. Zandstra, *EMBO J* **2007**, *26*, 4744-4755.
[53] M. Bissell, *Nature* **2003,** 424, 870.
[54] K. G. Chen, B. S. Mallon, R. D. McKay, P. G. Robey, *Cell Stem Cell* **2014**, *14*, 13-26.
[55] T. C. McDevitt, S. P. Palecek, *Curr Opin Biotechnol* **2008**, *19*, 527-533.
[56] R. Zweigerdt, R. Olmer, H. Singh, A. Haverich, U. Martin, *Nat Protoc* **2011**, *6*, 689-700.
[57] Y. Nie, V. Bergendahl, D. J. Hei, J. M. Jones, S. P. Palecek, *Biotechnol Prog* **2009**, *25*, 20-31.
[58] A. K. Chen, X. Chen, A. B. Choo, S. Reuveny, S. K. Oh, *Stem Cell Res* **2011**, *7*, 97-111.
[59] G. R. Souza, J. R. Molina, R. M. Raphael, M. G. Ozawa, D. J. Stark, C. S. Levin, L. F. Bronk, J. S. Ananta, J. Mandelin, M. M. Georgescu, J. A. Bankson, J. G. Gelovani, T. C. Killian, W. Arap, R. Pasqualini, *Nat Nanotechnol* **2010**, *5*, 291-296.
[60] Y. Lei, D. V. Schaffer, *PNAS* **2013**, *110*, E5039-5048.
[61] P. Dey, S. Hemmati-Sadeghi, R. Haag, *Polymer Chemistry* **2016**, *7*, 375-383.
[62] T. Rossow, J. A. Heyman, A. J. Ehrlicher, A. Langhoff, D. A. Weitz, R. Haag, S. Seiffert, *J. Am. Chem. Soc.* **2012**, *134*, 4983-4989.
[63] D. Steinhilber, T. Rossow, S. Wedepohl, F. Paulus, S. Seiffert, R. Haag, *Angew Chem Int Ed* **2013**, *52*, 13538-13543.
[64] C. M. Madl, B. L. LeSavage, R. E. Dewi, C. B. Dinh, R. S. Stowers, M. Khariton, K. J. Lampe, D. Nguyen, O. Chaudhuri, A. Enejder, S. C. Heilshorn, *Nat Mater* **2017**, *16*, 1233-1242.
[65] R. Cruz-Acuna, M. Quiros, A. E. Farkas, P. H. Dedhia, S. Huang, D. Siuda, V. Garcia-Hernandez, A. J. Miller, J. R. Spence, A. Nusrat, A. J. Garcia, *Nat Cell Biol* **2017**, *19*, 1326-1335.
[66] N. Gjorevski, N. Sachs, A. Manfrin, S. Giger, M. E. Bragina, P. Ordonez-Moran, H. Clevers, M. P. Lutolf, *Nature* **2016**, *539*, 560-564.
[67] D. Seliktar, *Science* **2012**, *336*, 1124-1128.
[68] J. Thiele, Y. Ma, S. M. C. Bruekers, S. Ma, W. T. Huck, *Adv. Mater.* **2014**, *26*, 125-147.
[69] N. Di Maggio, E. Piccinini, M. Jaworski, A. Trumpp, D. J. Wendt, I. Martin, *Biomaterials* **2011**, *32*, 321-329.
[70] M. X. Doss, A. Sachinidis, *Cells* **2019**, *8*.
[71] K. Lee, E. A. Silva, D. J. Mooney, *J R Soc Interface* **2011**, *8*, 153-170.
[72] D. Dado, S. Levenberg, *Semin Cell Dev Biol* **2009**, *20*, 656-664.

[73] D. Hubmacher, S. S. Apte, *Curr Opin Rheumatol* **2013**, *25*, 65-70.
[74] J. J. Song, H. C. Ott, *Trends Mol Med* **2011**, *17*, 424-432.
[75] A. D. Celiz, J. G. Smith, R. Langer, D. G. Anderson, D. A. Winkler, D. A. Barrett, M. C. Davies, L. E. Young, C. Denning, M. R. Alexander, *Nat Mater* **2014**, *13*, 570-579.
[76] A. L. Sisson, D. Steinhilber, T. Rossow, P. Welker, K. Licha, R. Haag, *Angew Chem Int Ed* **2009**, *48*, 7540-7545.
[77] T. Bai, F. Sun, L. Zhang, A. Sinclair, S. Liu, J. R. Ella-Menye, Y. Zheng, S. Jiang, *Angew Chem Int Ed Engl* **2014**, *53*, 12729-12734.
[78] R. Edri, I. Gal, N. Noor, T. Harel, S. Fleischer, N. Adadi, O. Green, D. Shabat, L. Heller, A. Shapira, I. Gat-Viks, D. Peer, T. Dvir, *Adv Mater* **2019**, *31*, e1803895.
[79] R. A. Perez, S.-J. Choi, C.-M. Han, J.-J. Kim, H. Shim, K. W. Leong, H.-W. Kim, *Progress in Materials Science* **2016**, *82*, 234-293.
[80] M.W. Lensch, L. Daheron, T. M. Schlaeger, *Stem Cell Rev* **2006**,185-201.
[81] Yoshida, M. Takeichi, *Cell* **1982**, *28*, 217-224.
[82] K. A. D'Amour, A. D. Agulnick, S. Eliazer, O. G. Kelly, E. Kroon, E. E. Baetge, *Nat Biotechnol* **2005**, *23*, 1534-1541.
[83] A. M. Eastham, H. Spencer, F. Soncin, S. Ritson, C. L. Merry, P. L. Stern, C. M. Ward, *Cancer Res* **2007**, *67*, 11254-11262.
[84] M. A. Wozniak, C. S. Chen, *Nat Rev Mol Cell Biol* **2009**, *10*, 34-43.
[85] D. A. Williams, M. Rios, C. Stephenst, V. P. Patel, Nature **1991,** *352*, ***438-441*.**
[86] R. McBeath, D. M. Pirone, C. M. Nelson, C. S. Chen, K. Bhadriraju, *Developmental Cell* **2004,** *6***,** 483-495.
[87] P. M. Gilbert, K. L. Havenstrite,1 K. E. G. Magnusson, A. Sacco, N. A. Leonardi, P. Kraft, N. K. Nguyen, S. Thrun, M. P. Lutolf, H. M. Blau, *Science* **2010**, *329*, 1078-1081.
[88] T. E. North, W. Goessling, M. Peeters, P. Li, C. Ceol, A. M. Lord, G. J. Weber, J. Harris, C. C. Cutting, P. Huang, E. Dzierzak, L. I. Zon, *Cell* **2009**, *137*, 736-748.
[89] J. Holst, S. Watson, M. S. Lord, S. S. Eamegdool, D. V. Bax, L. B. Nivison-Smith, A. Kondyurin, L. Ma, A. F. Oberhauser, A. S. Weiss, J. E. Rasko, *Nat Biotechnol* **2010**, *28*, 1123-1128.
[90] W. Kimura, H. A. Sadek, *Cardiovasc Diagn Ther* **2012**, *2*, 278-289.
[91] C. E. Forristal, I. G. Winkler, B. Nowlan, V. Barbier, G. Walkinshaw, J. P. Levesque, *Blood* **2013**, *121*, 759-769.
[92] C. Muscari, E. Giordano, F. Bonafè, M. Govoni, A. Pasini, C. Guarnieri, *Journal of Biomedical Science* **2013**, *20*, 63.
[93] S. Mendez-Ferrer, D. Lucas, M. Battista, P. S. Frenette, *Nature* **2008**, *452*, 442-447.
[94] S. Cosson, E. A. Otte, H. Hezaveh, J. J. Cooper-White, *Stem Cells Transl Med* **2015**, *4*, 156-164.
[95] S. W. Lane, D. A. Williams, F. M. Watt, *Nat Biotechnol* **2014**, *32*, 795-803.
[96] F. M. Chen, X. Liu, *Prog Polym Sci* **2016**, *53*, 86-168.

[97] K. Sadtler, A. Singh, M. T. Wolf, X. Wang, D. M. Pardoll, J. H. Elisseeff, *Nature Reviews Materials* **2016**, *1*.

[98] J. Malda, J. Visser, F. P. Melchels, T. Jungst, W. E. Hennink, W. J. Dhert, J. Groll, D. W. Hutmacher, *Adv Mater* **2013**, *25*, 5011-5028.

[99] P. Dey, T. Bergmann, J. L. Cuellar-Camacho, S. Ehrmann, M. S. Chowdhury, M. Zhang, I. Dahmani, R. Haag, W. Azab, *ACS Nano* **2018**, *12*, 6429-6442.

[100] J. Lee, M. J. Cuddihy, N. A. Kotov, *Tissue Eng Part B Rev* **2008**, *14*, 61-86.

[101] G. Huang, F. Li, X. Zhao, Y. Ma, Y. Li, M. Lin, G. Jin, T. J. Lu, G. M. Genin, F. Xu, *Chem Rev* **2017**, *117*, 12764-12850.

[102] W. L. Stoppel, C. E. Ghezzi, S. L. McNamara, L. D. Black, 3rd, D. L. Kaplan, *Ann Biomed Eng* **2015**, *43*, 657-680.

[103] A. N. Renth, M. S. Detamore, *Tissue Eng Part B Rev* **2012**, *18*, 341-362.

[104] K. Lin, D. Zhang, M. H. Macedo, W. Cui, B. Sarmento, G. Shen, *Advanced Functional Materials* **2019**, *29*.

[105] M. B. Oliveira, C. A. Custodio, L. Gasperini, R. L. Reis, J. F. Mano, *Acta Biomater* **2016**, *41*, 119-132.

[106] A. T. Neffe, B. F. Pierce, G. Tronci, N. Ma, E. Pittermann, T. Gebauer, O. Frank, M. Schossig, X. Xu, B. M. Willie, M. Forner, A. Ellinghaus, J. Lienau, G. N. Duda, A. Lendlein, *Adv Mater* **2015**, *27*, 1738-1744.

[107] B. Carrion, M. F. Souzanchi, V. T. Wang, G. Tiruchinapally, A. Shikanov, A. J. Putnam, R. M. Coleman, *Adv Healthc Mater* **2016**, *5*, 1192-1202.

[108] A. S. Lee, M. Inayathullah, M. A. Lijkwan, X. Zhao, W. Sun, S. Park, W. X. Hong, M. B. Parekh, A. V. Malkovskiy, E. Lau, X. Qin, V. R. Pothineni, V. Sanchez-Freire, W. Y. Zhang, N. G. Kooreman, A. D. Ebert, C. K. F. Chan, P. K. Nguyen, J. Rajadas, J. C. Wu, *Nat Biomed Eng* **2018**, *2*, 104-113.

[109] G. Thrivikraman, A. Athirasala, R. Gordon, L. Zhang, R. Bergan, D. R. Keene, J. M. Jones, H. Xie, Z. Chen, J. Tao, B. Wingender, L. Gower, J. L. Ferracane, L. E. Bertassoni, *Nat Commun* **2019**, *10*, 3520.

[110] L. Shi, F. Wang, W. Zhu, Z. Xu, S. Fuchs, J. Hilborn, L. Zhu, Q. Ma, Y. Wang, X. Weng, D. A. Ossipov, *Advanced Functional Materials* **2017**, *27*.

[111] K. Xu, K. Narayanan, F. Lee, K. H. Bae, S. Gao, M. Kurisawa, *Acta Biomater* **2015**, *24*, 159-171.

[112] Z. Wei, D. M. Lewis, Y. Xu, S. Gerecht, *Adv Healthc Mater* **2017**, *6*.

[113] L. Karumbaiah, S. F. Enam, A. C. Brown, T. Saxena, M. I. Betancur, T. H. Barker, R. V. Bellamkonda, *Bioconjug Chem* **2015**, *26*, 2336-2349.

[114] M. F. Leong, H. F. Lu, T. C. Lim, K. Narayanan, S. Gao, L. Y. Wang, R. P. Toh, H. Funke, M. H. Abdul Samad, A. C. Wan, J. Y. Ying, *Tissue Eng Part C Methods* **2016**, *22*, 884-894.

[115] D. L. Amaral, R. S. Zanette, C. G. Almeida, L. B. Almeida, L. F. Oliveira, R. F. Marcomini, B. V. Nogueira, M. O. Santos, H. M. Brandao, C. Mc Maranduba, M. Munk, *Biomed Mater* **2019**, *14*, 035011.

[116] S. Nam, R. Stowers, J. Lou, Y. Xia, O. Chaudhuri, *Biomaterials* **2019**, *200*, 15-24.

[117] W. Jia, P. S. Gungor-Ozkerim, Y. S. Zhang, K. Yue, K. Zhu, W. Liu, Q. Pi, B.

Byambaa, M. R. Dokmeci, S. R. Shin, A. Khademhosseini, *Biomaterials* **2016**, *106*, 58-68.

[118] Z. Luo, S. Zhang, J. Pan, R. Shi, H. Liu, Y. Lyu, X. Han, Y. Li, Y. Yang, Z. Xu, Y. Sui, E. Luo, Y. Zhang, S. Wei, *Biomaterials* **2018**, *163*, 25-42.

[119] Y. Kusumastuti, Y. Shibasaki, S. Hirohara, M. Kobayashi, K. Terada, T. Ando, M. Tanihara, *J Tissue Eng Regen Med* **2017**, *11*, 869-876.

[120] H. Liu, C. Wang, C. Li, Y. Qin, Z. Wang, F. Yang, Z. Li, J. Wang, *RSC Advances* **2018**, *8*, 7533-7549.

[121] C. M. Murphy, F. J. O'Brien , D. G. Little, A. Schindeler, *European Cells and Materials* **2013,** *26.* 120-132.

[122] T. Jiang, E. J. Carbone, K. W. H. Lo, C. T. Laurencin, *Progress in Polymer Science* **2015**, *46*, 1-24.

[123] K. R. Stevens, C. E. Murry, *Cell Stem Cell* **2018**, *22*, 294-297.

[124] S. P. Pasca, *Nature* **2018**, *553*, 437-445.

[125] M. P. Lutolf, J. A. Hubbell, *Nat Biotechnol* **2005**, *23*, 47-55.

[126] B.L. Seala, T.C. Oterob, A. Panitcha, *Materials Science and Engineering* **2001**, *34*, 147-230.

[127] M. K. Nguyen, O. Jeon, M. D. Krebs, D. Schapira, E. Alsberg, *Biomaterials* **2014**, *35*, 6278-6286.

[128] D. Thomas, T. O'Brien, A. Pandit, *Adv Mater* **2018**, *30*, 1703948.

[129] M. Okamoto, B. John, *Progress in Polymer Science* **2013**, *38*, 1487-1503.

[130] Z. Pan, J. Ding, *Interface Focus* **2012**, *2*, 366-377.

[131] Z. Li, B. H. Tan, *Mater Sci Eng C Mater Biol Appl* **2014**, *45*, 620-634.

[132] M. Boffito, P. Sirianni, A. M. Di Rienzo, V. Chiono, *J Biomed Mater Res A* **2015**, *103*, 1276-1290.

[133] B. L. Ekerdt, C. M. Fuentes, Y. G. Lei, M, M. Adil, A, Ramasubramanian, R, A. Segalman, D,V. Schaffer, *Adv. Healthcare Mater.* **2018**, *7*, 1800225.

[134] R. A. Stile, W.R. Burghardt, K. E. Healy, *Macromolecules* **1999,** *32*, 7370-7379.

[135] Q. Wei, T. Becherer, S. Angioletti-Uberti, J. Dzubiella, C. Wischke, A. T. Neffe, A. Lendlein, M. Ballauff, R. Haag, *Angew Chem Int Ed Engl* **2014**, *53*, 8004-8031.

[136] M. Calderon, M. A. Quadir, S. K. Sharma, R. Haag, *Adv Mater* **2010**, *22*, 190-218.

[137] M. C. Lukowiak, S. Wettmarshausen, G. Hidde, P. Landsberger, V. Boenke, K. Rodenacker, U. Braun, J. F. Friedrich, A. A. Gorbushina, R. Haag, *Polymer Chemistry* **2015**, *6*, 1350-1359.

[138] D. Wilms, S.E. STIRIBA, H. FREY, *Accounts of chemical research* **2010,** 43, 129-141.

[139] D. Steinhilber, S. Seiffert, J. A. Heyman, F. Paulus, D. A. Weitz, R. Haag, *Biomaterials* **2011**, *32*, 1311-1316.

[140] M. Wyszogrodzka, R. Haag, *Biomacromolecules* **2009**, *10*, 1043-1054.

[141] X. Zhang, S. Malhotra, M. Molina, R. Haag, *Chem Soc Rev* **2015**, *44*, 1948-1973.

[142] S. J. Bryant, K. A. Davis-Arehart, N. Luo, R. K. Shoemaker, J. A. Arthur, K. S.

Anseth, *Macromolecules* **2004**, *37*, 6726-6733.
[143] J. C. Bray and E. W. Merrillj.LJ. Biomed. Mater. Res. 1973, 7, 431-443.
[144] P. J. Martens, S. J. Bryant, K. S. Anseth, *Biomacromolecules* **2003**, *4*, 283-292.
[145] Y. H. An, D. Webb, A. Gutowska, V. A. Mironov, R. J. Friedman, *Anat Rec* **2001**, *263*, 336-341;
[146] A. Au, J. Ha, A. Polotsky, K. Krzyminski, A. Gutowska, D. S. Hungerford, C. G. Frondoza, *Thermo-reversible gelling polymers* **2003**, 1310-1319.
[147] L. Lu, S. J. Peter , M. D. Lyman, H. Lai, S. M. Leite, J. A. Tamada, S. Uyama, J. P. Vacanti, Robert Langer, A. G. Mikos, *Biomaterials* **2000**, *21*, 1837-1845.
[148] N. M. Vacanti, H. Cheng, P. S. Hill, J. D. Guerreiro, T. T. Dang, M. Ma, S. Watson, N. S. Hwang, R. Langer, D. G. Anderson, *Biomacromolecules* **2012**, *13*, 3031-3038;
[149] J. Zhu, *Biomaterials* **2010**, *31*, 4639-4656;
[150] J. M. Coburn, M. Gibson, S. Monagle, Z. Patterson, J. H. Elisseeff, *Proc Natl Acad Sci U S A* **2012**, *109*, 10012-10017.
[151] X. Liu, J. M. Holzwarth, P. X. Ma, *Macromol Biosci* **2012**, *12*, 911-919.
[152] F. Rossi, M. van Griensven, *Tissue Eng Part A* **2014**, *20*, 2043-2051.
[153] M. R. Hynd, J. N. Turner, W. Shain, *J Biomater Sci Polym Ed* **2007**, *18*, 1223-1244.
[154] R. Jin, L. S. Teixeira, P. J. Dijkstra, C. A. van Blitterswijk, M. Karperien, J. Feijen, *Biomaterials* **2010**, *31*, 3103-3113.
[155] C. G. Williams, A. N. Malik, T. K. Kim, P. N. Manson, J. H. Elisseeff, *Biomaterials* **2005**, *26*, 1211-1218.
[156] C. Hiemstra, L. J. van der Aa, Z. Y. Zhong, P. J. Dijkstra, J. Feijen, *Macromolecules* **2007**, *40*, 1165-1173.
[157] J. Patterson, J. A. Hubbell, *Biomaterials* **2010**, *31*, 7836-7845.
[158] J. T. Connelly, A. J. Garcia, M. E. Levenston, *Biomaterials* **2007**, *28*, 1071-1083.
[159] J. J. Roberts, S. J. Bryant, *Biomaterials* **2013**, *34*, 9969-9979.
[160] B. V. Sridhar, J. L. Brock, J. S. Silver, J. L. Leight, M. A. Randolph, K. S. Anseth, *Adv Healthc Mater* **2015**, *4*, 702-713.
[161] N. J. Agard, J. A. Prescher, C.R. Bertozzi, *JACS* **2004**, *126*, 15046-15047.
[162] Y. Jiang, J. Chen, C. Deng, E. J. Suuronen, Z. Zhong, *Biomaterials* **2014**, *35*, 4969-4985.
[163] J. Dommerholt, S. Schmidt, R. Temming, L. J. Hendriks, F. P. Rutjes, J. C. van Hest, D. J. Lefeber, P. Friedl, F. L. van Delft, *Angew Chem Int Ed Engl* **2010**, *49*, 9422-9425.
[164] C. P. Ramil, Q. Lin, *Chem Commun (Camb)* **2013**, *49*, 11007-11022.
[165] C. A. DeForest, K. S. Anseth, *Nat Chem* **2011**, *3*, 925-931.
[166] O. Altintas, C. Barner-Kowollik, *Macromol Rapid Commun* **2012**, *33*, 958-971.
[167] R. J. Thibault, P. J. Hotchkiss, M.Gray, V. M. Rotello, *JACS* **2003,** *125*, 11249-11252.
[168] D. C. Sherrington, K. A. Taskinen, *Chemical Society Reviews* **2001**, *30*, 83-93.
[169] X. Chen, E. Ruckenstein, *Reversible Covalently bonded linear polymers* **2000**, 1662-1672.

[170] E. Abe, S. J. Pennycook, A. P. Tsai, *Nature* **2003**, *421*, 347-350.
[171] B. Trappmann, C. S. Chen, *Curr Opin Biotechnol* **2013**, *24*, 948-953.
[172] L. Wang, Y. Li, G. Huang, X. Zhang, B. Pingguan-Murphy, B. Gao, T. J. Lu, F. Xu, *Crit Rev Biotechnol* **2016**, *36*, 553-565.
[173] S. Khetan, J. A. Burdick, *Biomaterials* **2010**, *31*, 8228-8234.
[174] P. M. Kharkar, K. L. Kiick, A. M. Kloxin, *Chem Soc Rev* **2013**, *42*, 7335-7372.
[175] C. Zhang, N. Sangaj, Y. Hwang, A. Phadke, C. W. Chang, S. Varghese, *Acta Biomater* **2011**, *7*, 3362-3369.
[176] G. D. Nicodemus, S. J. Bryant, *Tissue Eng Part B Rev* **2008**, *14*, 149-165.
[177] M. Scudellari, *Nature* **2016**, *534*, 310-312.
[178] K. E. Toyoshima, M. Ogawa, T. Tsuji, *Nat Protoc* **2019**, *14*, 1323-1338.
[179] R. Haag, A. Sunder, J.-F. o. Stumbé, *J Am Chem Soc* **2000**, *122*, 2954.
[180] E. M. Sletten, C. R. Bertozzi, *Angew. Chem. Int. Ed.* **2009**, *48*, 6974.
[181] J. C. Jewett, C. R. Bertozzi, *Chem. Soc. Rev.* **2010**, *39*,1272.
[182] C. Simon, C. Lion, C. Spriet, F. B. Cresp, S. Hawkins, C. Biot, *Angew. Chem. Int. Ed.* **2018**, *57*, 16665.
[183] S. F. van Dongen, P. Maiuri, E. Marie, C. Tribet, M. Piel, *Adv. Mater.* **2013**, *25*, 1687.
[184] K. Zhang, H. Gao, R. Deng, J. Li, Angew. Chem. Int. Ed. 2019, *58*, 2.
[185] International Stem Cell Initiative, *Nat Commun* **2018**, 9, 1925.R. Haag, A. Sunder, J.-F. o. Stumbé, *J Am Chem Soc* **2000**, *122*, 2954.
[186] Y. S. Hwang, B. G. Chung, D. Ortmann, N. Hattori, H. C. Moeller, A. Khademhosseini, *Proc. Natl. Acad. Sci. USA* **2009**, *106*, 16978.
[187] H. Lin, Q. Li, Y. Lei, *Biofabrication* **2017**, *9*, 025007.
[188] C. L. Bauwens, R. Peerani, S. Niebruegge, K. A. Woodhouse, E. Kumacheva, M. Husain, P. W. Zandstra, *Stem cells* **2008**, *26*, 2300.
[189] M. Tewary, N. Shakiba, P. W. Zandstra, *Nat Rev Genet* **2018**, *19*, 595.
[190] R. L. Carpenedo,C.Y. Sargent, T.C. Mcdevitt, *Stem cells* **2007**, *25*, 2224.
[191] J. Silva, J. Nichols, T. W. Theunissen, G. Guo, A. L. van Oosten, O. Barrandon, J. Wray, S. Yamanaka, I. Chambers, A. Smith, *Cell* **2009**, *138*, 722.
[192] S. Dommerholt, R. Schmidt, L. Temming, J. A. Hendriks, P. J. Floris, T. Rutjes, C.M.Jan van Hest, D. J. Lefeber, P. Friedl, F. L. Delft. *Angew. Chem. Int. Ed.* **2010**, *49*, 9422-9425.
[193] F. Stijn M. Dongen, *Adv. Mater* **2013**, *25*, 1687-1691.
[194] R. Haubner, R. Gratias, B. Diefenbach, S. L. Goodman, A. Jonczyk, H. Kessler, *J. Am. Chem. Soc*, **1996**, *118*, 7461-7472.
[195] S. B, Anderson, C. Lin, D. V. Kuntzler, K. S. Anseth, *Biomaterials* **2011**,*32*, 3564-3574.
[196] C. Holtze, A. C. Rowat, J. J. Agrest, J. B. Hutchison, F. E. Angil, C. H. J. Schmitz, S. K¨ oster, H. Duan, K. J. Humphry, R. A. Scanga, J. S. Johnson, D. Pisignano and D. A. Weitz, *Lab Chip* **2008**, *8*, 1632-1639.
[197] J. C. McDonald, D. C. Duffy, J. R. Anderson, D. T. Chiu, H. Wu, O. J. A. Schueller, G.M. Whitesides, *Electrophoresis* **2000**, *21*, 27-40.
[198] G. Pettinato, X. Wen, N. Zhang, *Scientific reports* **2014**, 4, 7402.

[199] S. M. Dang, R. Perlingeiro, M. Kyba, G. Q. Daley, P. W. Zandstra, *Biotec. Bioen* **2002**, *78*, 442-453.
[200] J. Koh, D. R. Griffin, M. M. Archang, A. C. Feng, T. Horn, M. Margolis, D. Zalazar, T. Segura, P. O. Scumpia, D. Di Carlo, *Small* **2019**, e1903147.
[201] P. Zhou, B. Yin, R. Zhang, Z. Xu, Y. Liu, Y. Yan, X. Zhang, S. Zhang, Y. Li, H. Liu, Y. A. Yuan, S. Wei, *Colloids Surf B Biointerfaces* **2018**, *171*, 451-460.
[202] I. Lilge, H. Schonherr, *Angew Chem Int Ed Engl* **2016**, *55*, 13114-13117.
[203] T. Scholzen, J. Gerdes, *Journal of cellular physiology* **2000**, *182*, 311-322.
[204] J. Tu, G. Tian, H. H. Cheung, W. Wei, T. L. Lee, *Stem Cell Res Ther* **2018**, *9*, 71.
[205] Y. Zhou, H. Mao, B. Joddar, N. Umeki, Y. Sako, K.-I. Wada, C. Nishioka, E. Takahashi, Y. Wang, Y. Ito, *Scientific Reports* **2015**, *5*, 11386.
[206] I. C. Yasa, A. F. Tabak, O. Yasa, H. Ceylan, M. Sitti, *Advanced Functional Materials* **2019**, *29*, 1808992.
[207] K. H. Vining, A. Stafford, D. J. Mooney, *Biomaterials* **2019**, *188*, 187-197.
[208] S. Talebian, M. Mehrali, N. Taebnia, C. P. Pennisi, F. B. Kadumudi, J. Foroughi, M. Hasany, M. Nikkhah, M. Akbari, G. Orive, A. Dolatshahi - Pirouz, *Advanced Science* **2019**, *6*, 1801664.
[209] J. Wu, P. Li, C. Dong, H. Jiang, X. Bin, X. Gao, M. Qin, W. Wang, C. Bin, Y. Cao, *Nat Commun* **2018**, *9*, 620.
[210] J. Zhang, H. Yang, B. E. Abali, M. Li, Y. Xia, R. Haag, Small **2019**, *15*, e1901920.
[211] H. G. Schild, Prog. Polym. Sci **1992**, *17*, 163-249.
[212] T. Sun, G. Qing, Adv Mater **2011**, *23*, H57-77.
[213] J. Zhang, C. Cheng, J. L. Cuellar-Camacho, M. Li, Y. Xia, W. Li, R. Haag, Advanced Functional Materials **2018**, *28*, 1804773.
[214] M. Jaspers, S. L. Vaessen, P. van Schayik, D. Voerman, A. E. Rowan, P. H. J. Kouwer, Nature Communications **2017**, *8*, 15478.
[215] B. Trappmann, J. E. Gautrot, J. T. Connelly, D. G. Strange, Y. Li, M. L. Oyen, M. A. Cohen Stuart, H. Boehm, B. Li, V. Vogel, J. P. Spatz, F. M. Watt, W. T. Huck, Nat Mater **2012**, *11*, 642-649.
[216] S. B. Anderson, C. C. Lin, D. V. Kuntzler, K. S. Anseth, Biomaterials 2011, 32, 3564-3574.
[217] T. E. Brown, I. A. Marozas, K. S. Anseth, Adv Mater **2017**, *29*, 1605001.
[218] J. Lai, L. Abune, N. Zhao, Y. Wang, Angew Chem Int Ed 2019, 58, 2820-2825.
[219] A. Alexander, Ajazuddin, J. Khan, S. Saraf, S. Saraf, *Eur J Pharm Biopharm* **2014**, *88*, 575-585.

Chapter 9. Appendix

9.1. Characterization of dPG-DIC, PEG-PCL-N_3, and dPG-RGD

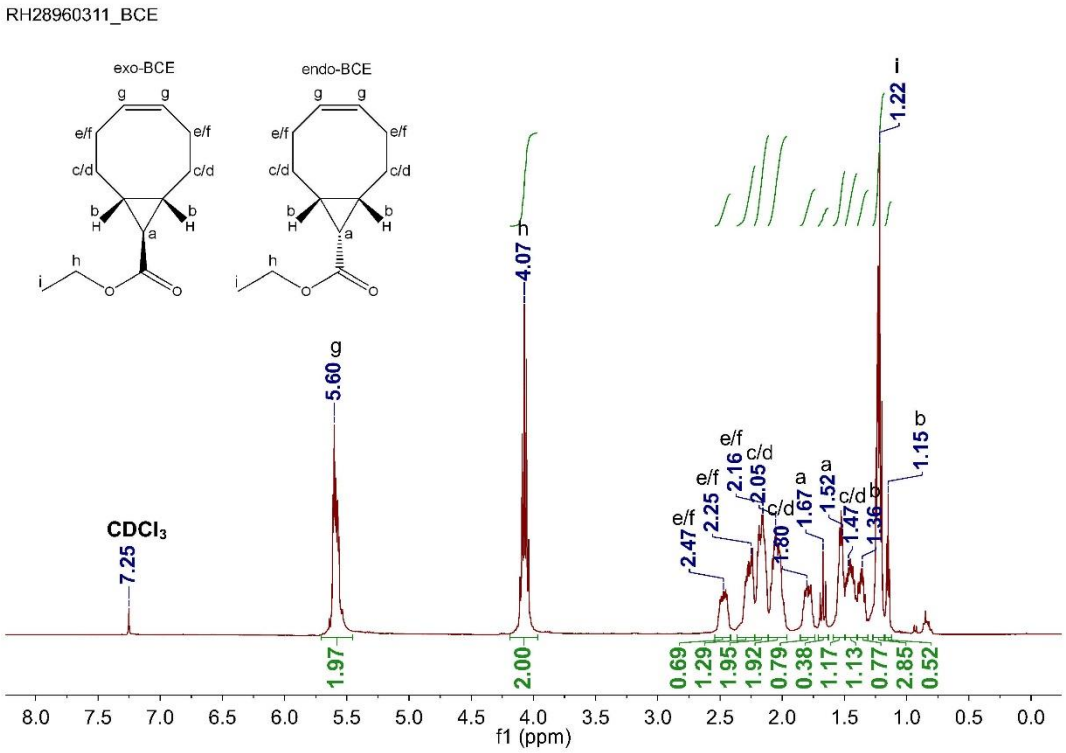

Figure S1. ^{1}H NMR of BCE.

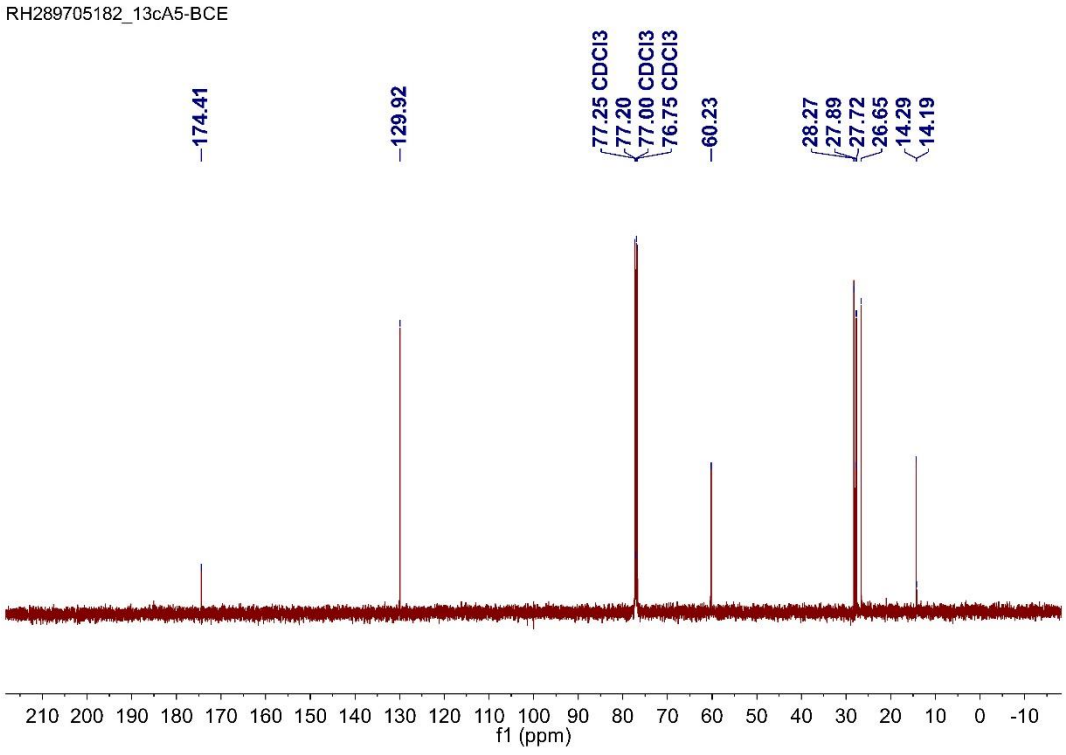

Figure S2. ^{13}C NMR of BCE.

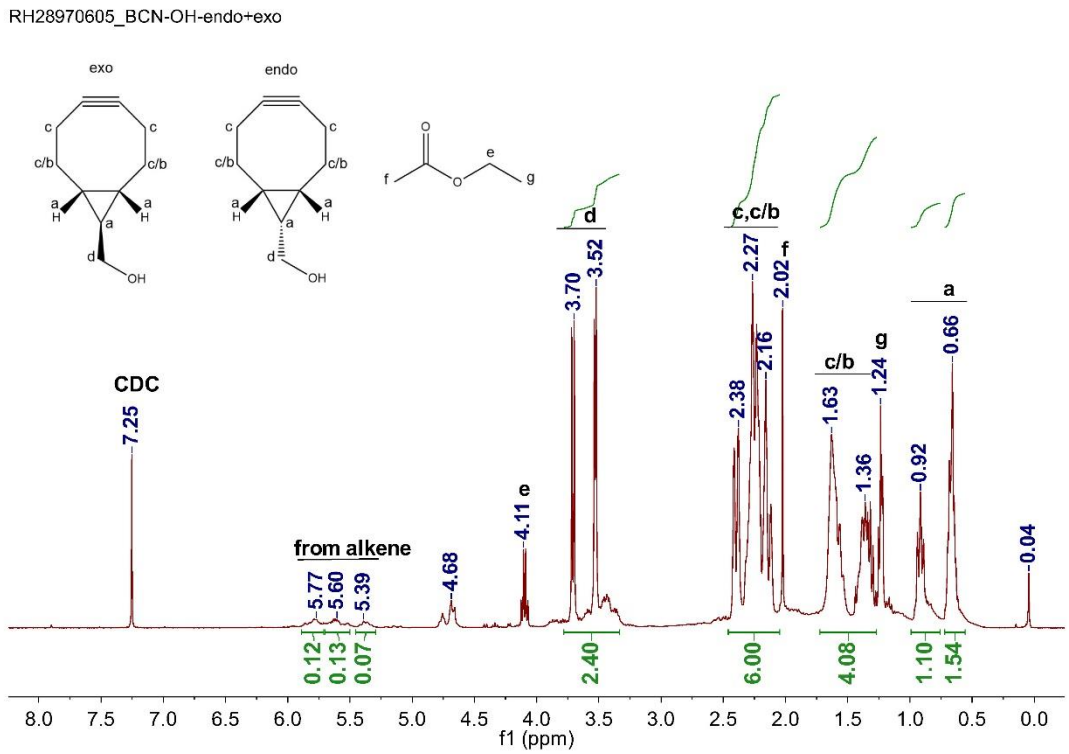

Figure S3. ^{1}H NMR of BCN-OH

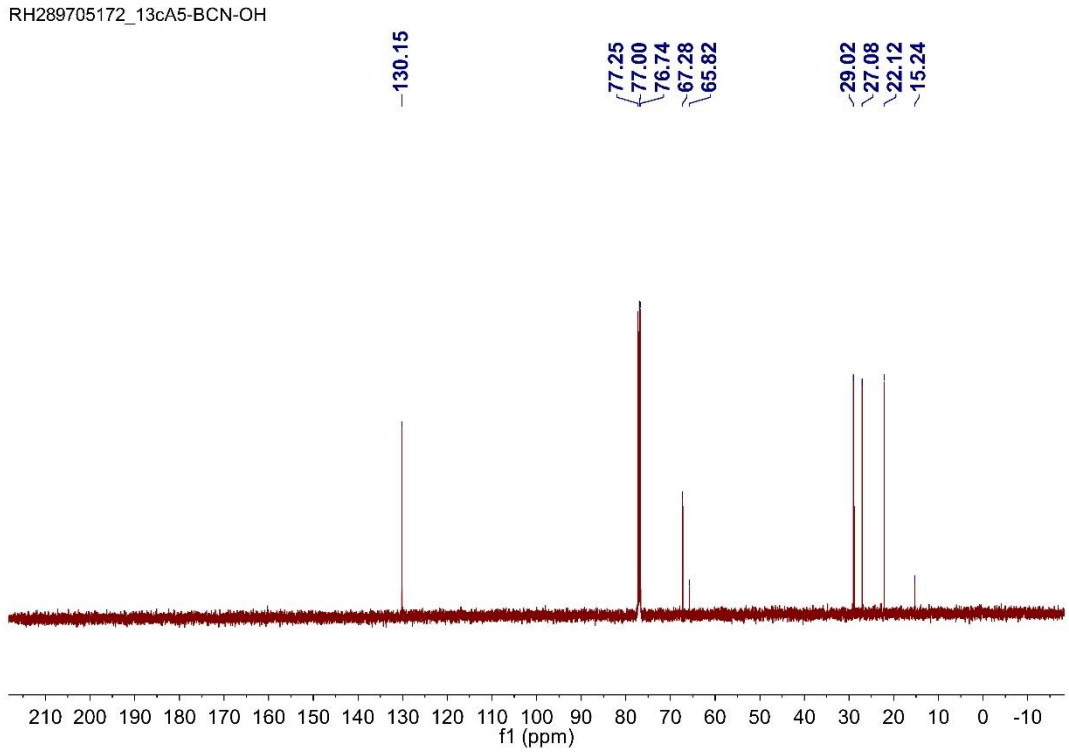

Figure S4. ^{13}C NMR of BCN-OH.

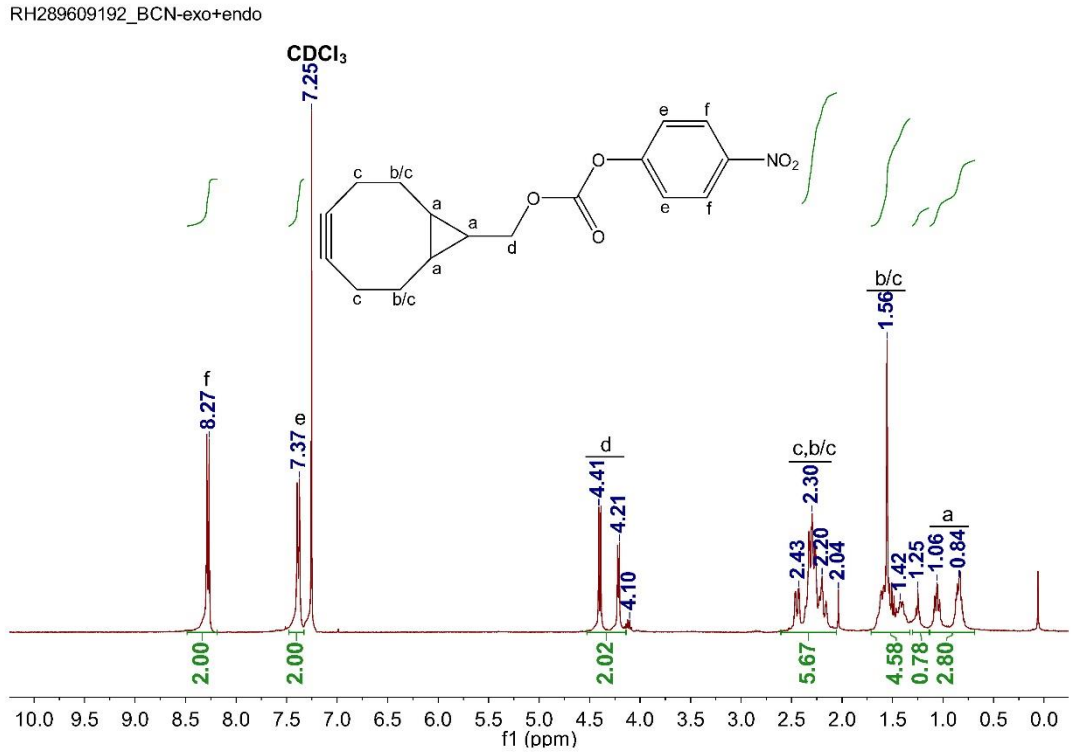

Figure S5. ^{1}H NMR of BCN.

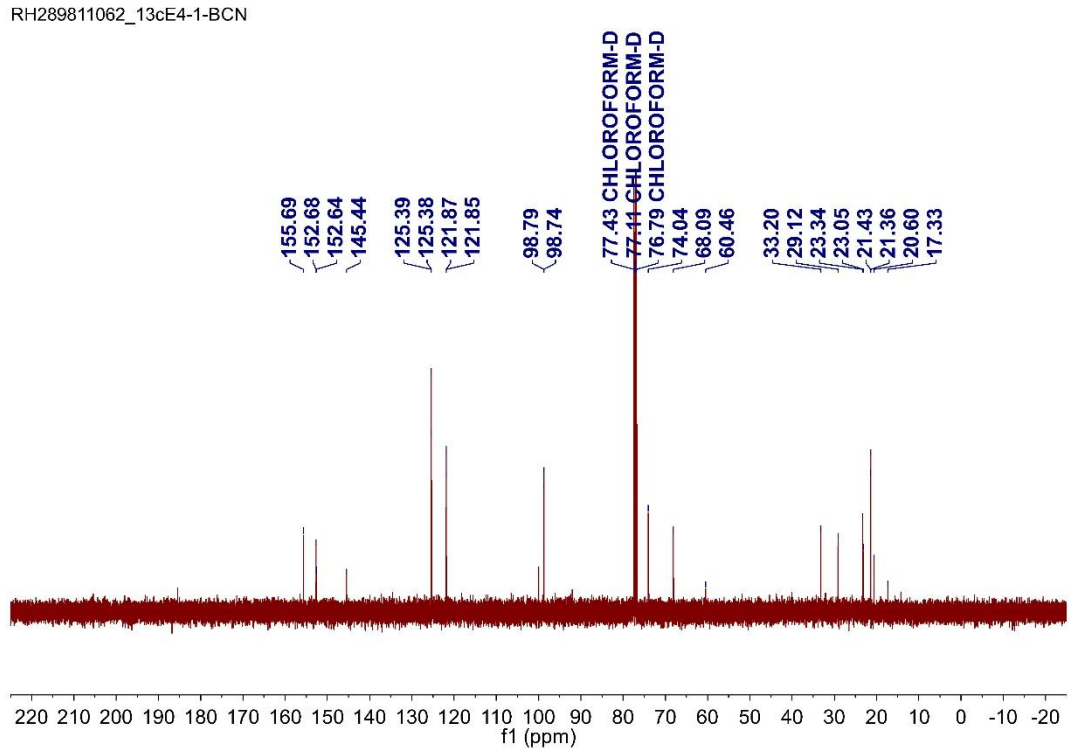

Figure S6. ^{13}C NMR of BCN.

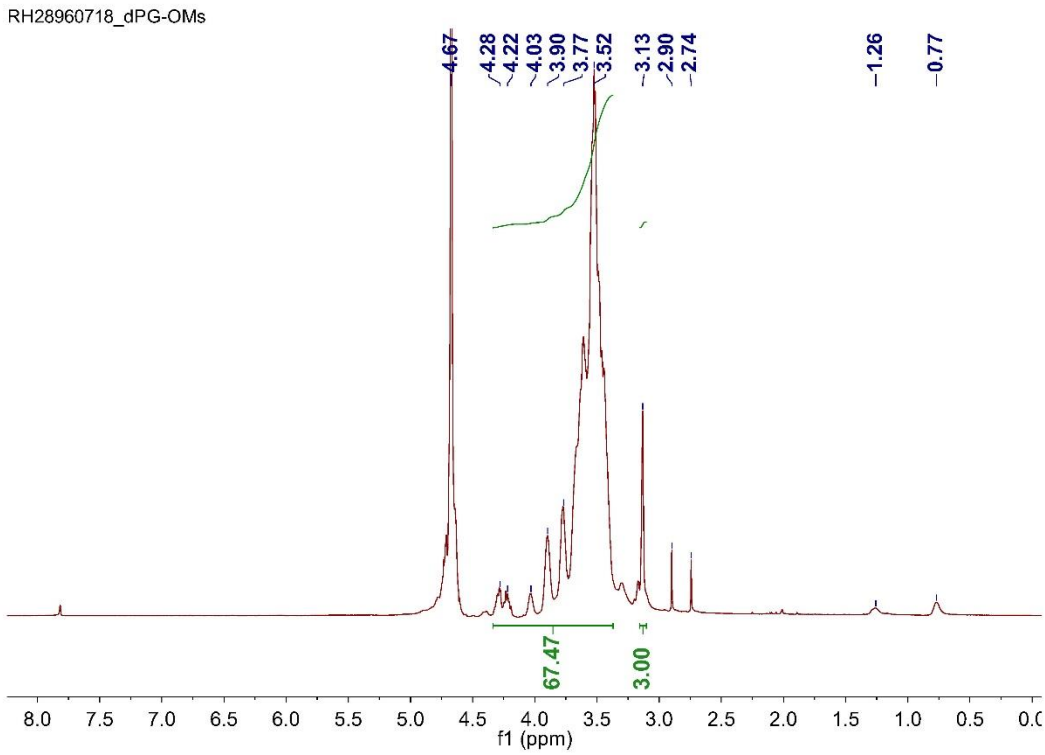

Figure S7. ^{1}H NMR of dPG-OMs.

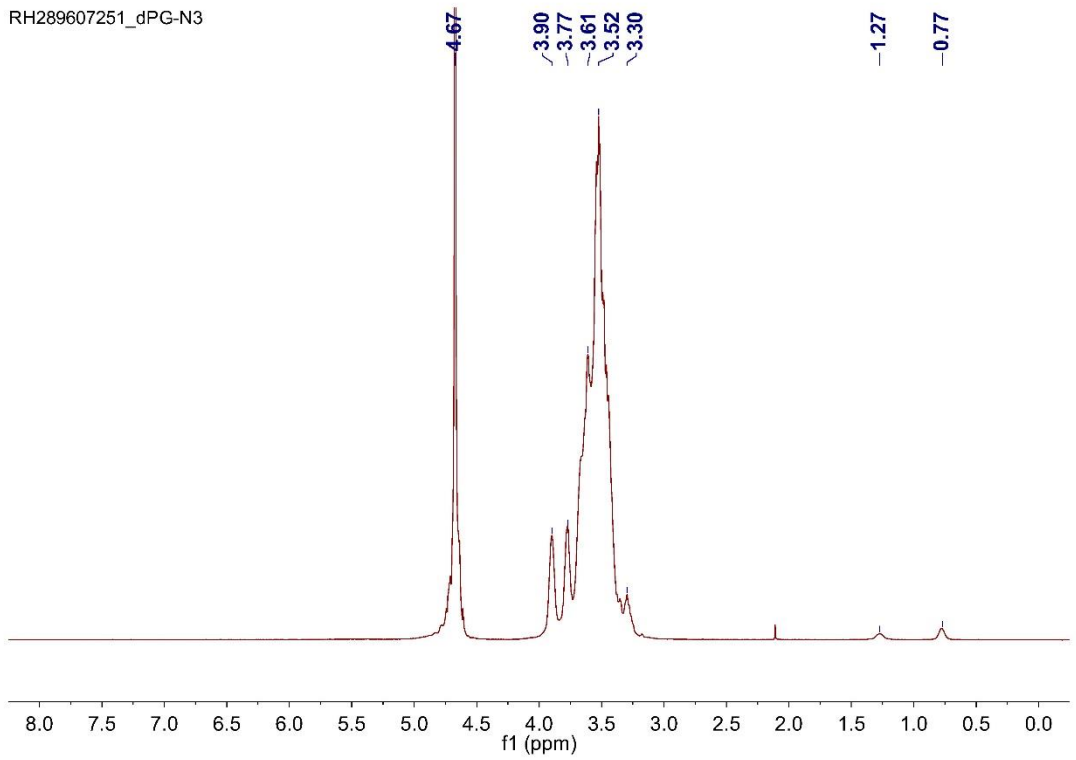

Figure S8. ^{1}H NMR of dPG-N_3.

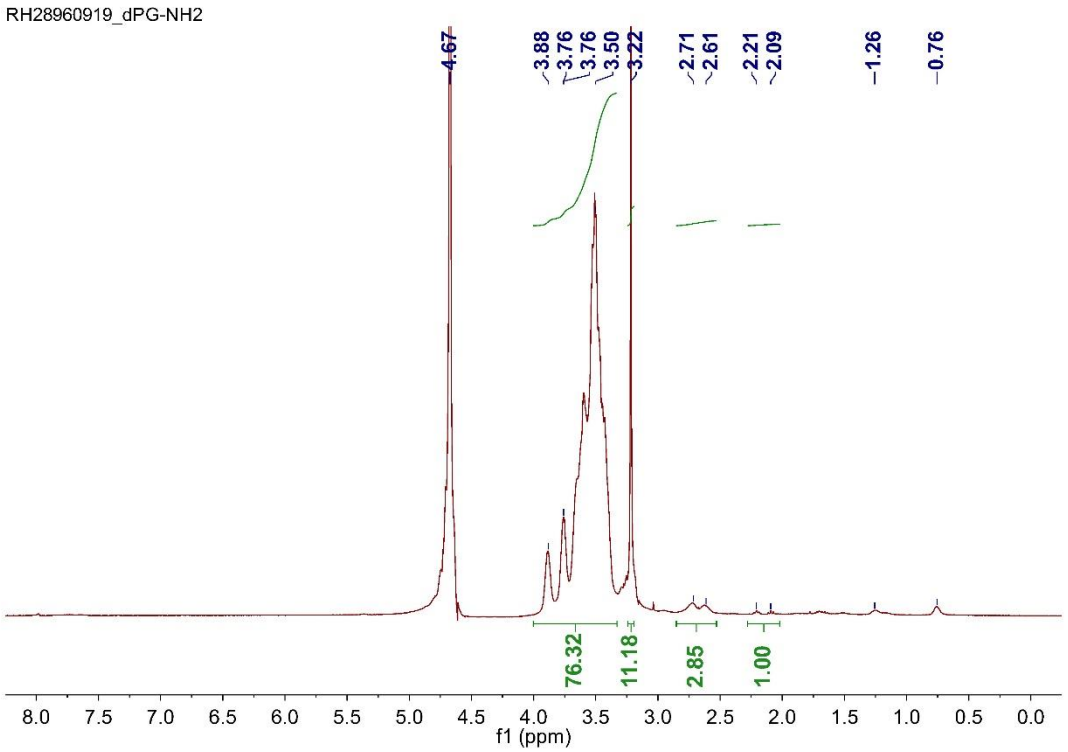

Figure S9. ^{1}H NMR of dPG-NH_2.

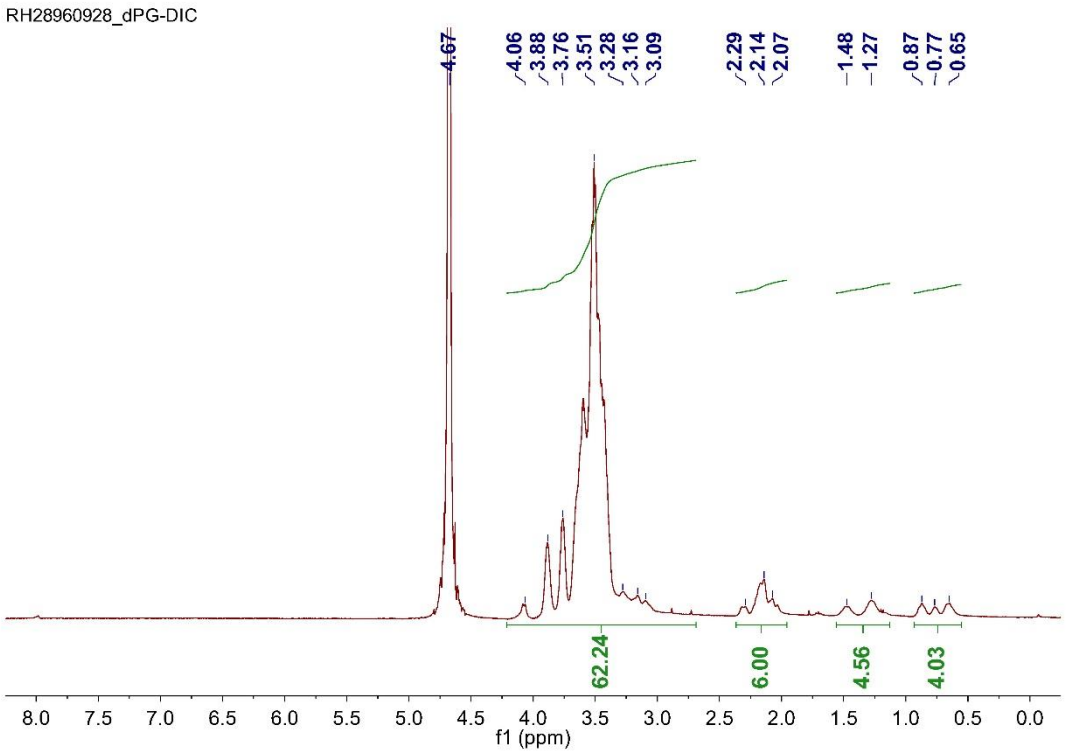

Figure S10. ^{1}H NMR of dPG-DIC.

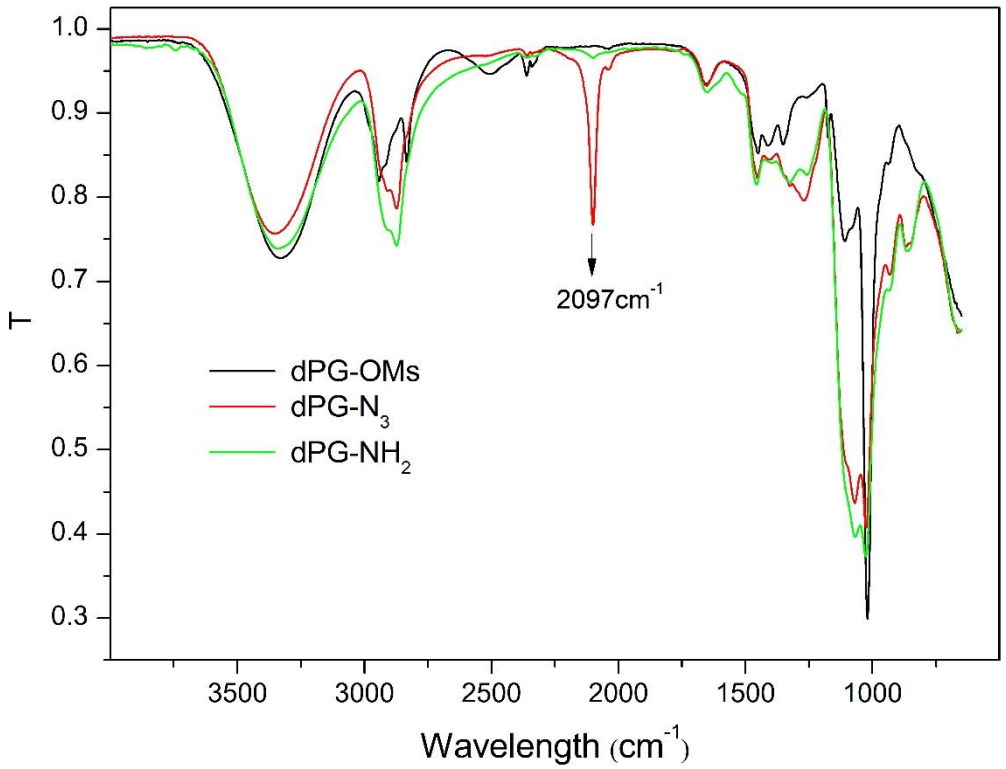

Figure S11. IR of dPG-OMs, dPG-N_3, dPG-NH_2.

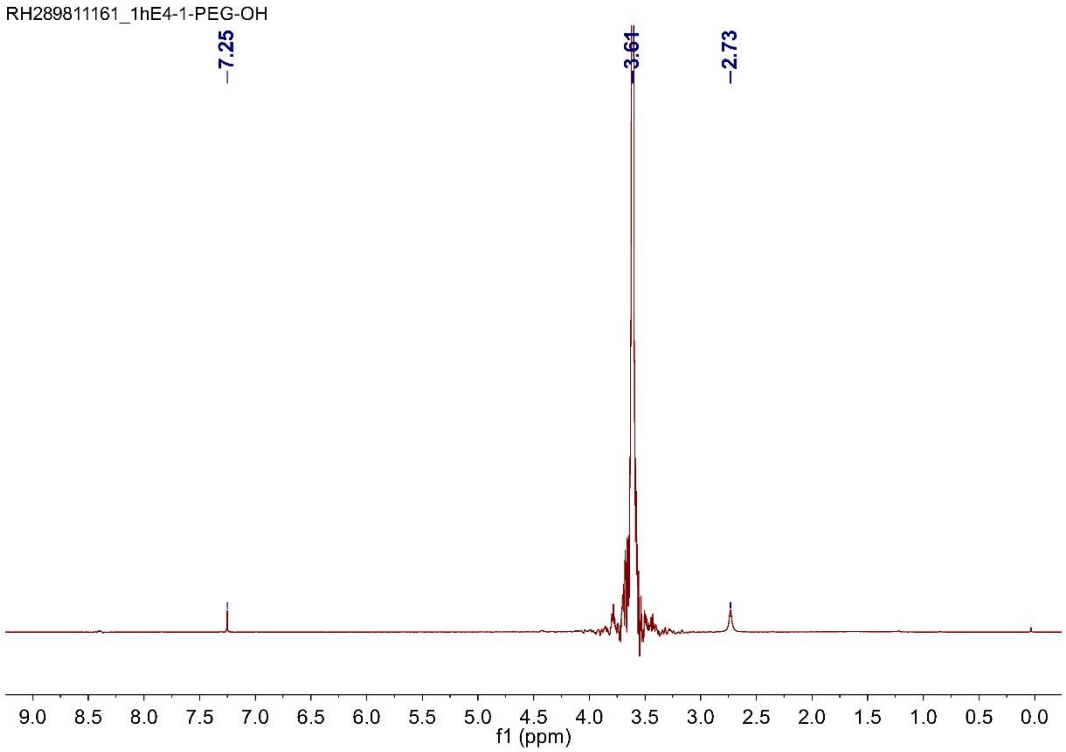

Figure S12. ^{1}H NMR of PEG-OH.

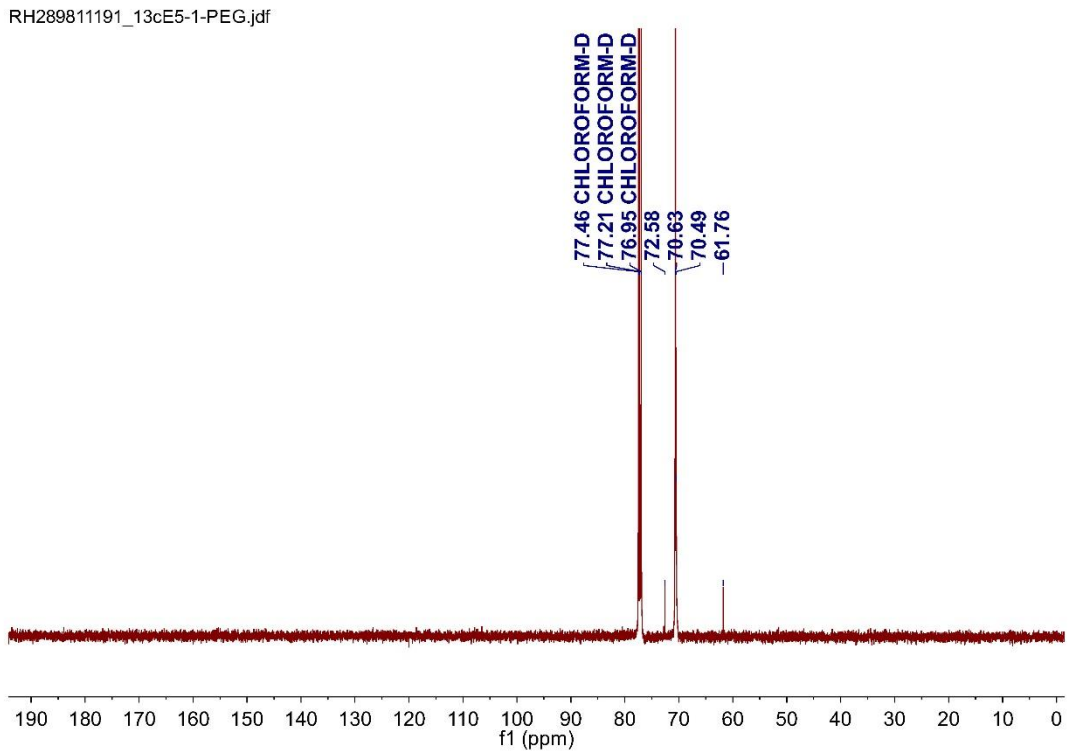

Figure S13. ^{13}C NMR of PEG-OH.

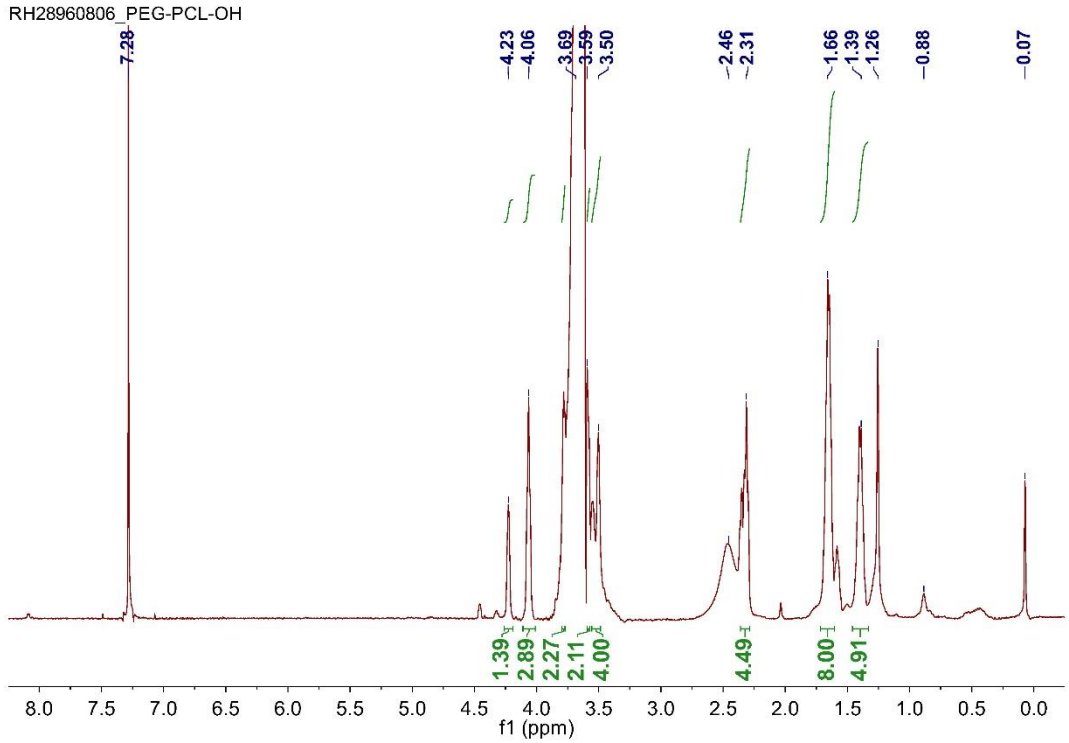

Figure S14. ^{1}H NMR of PEG-PCL-OH.

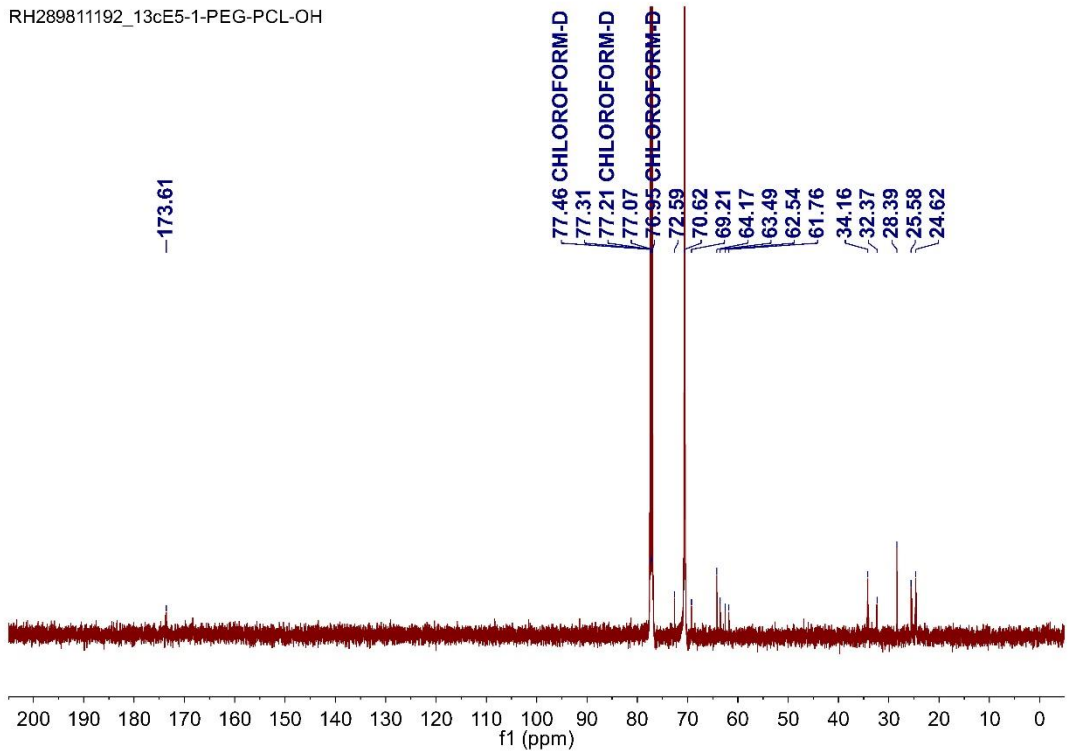

Figure S15. ^{13}C NMR of PEG-PCL-OH.

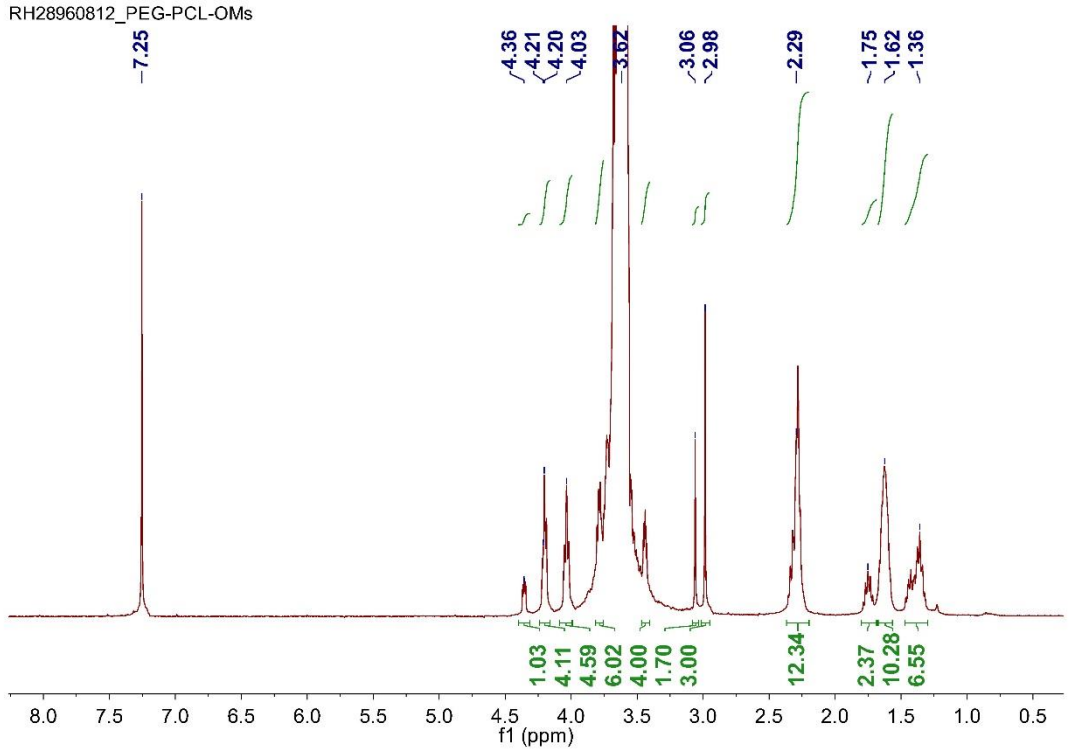

Figure S16. ^{1}H NMR of PEG-PCL-OMs.

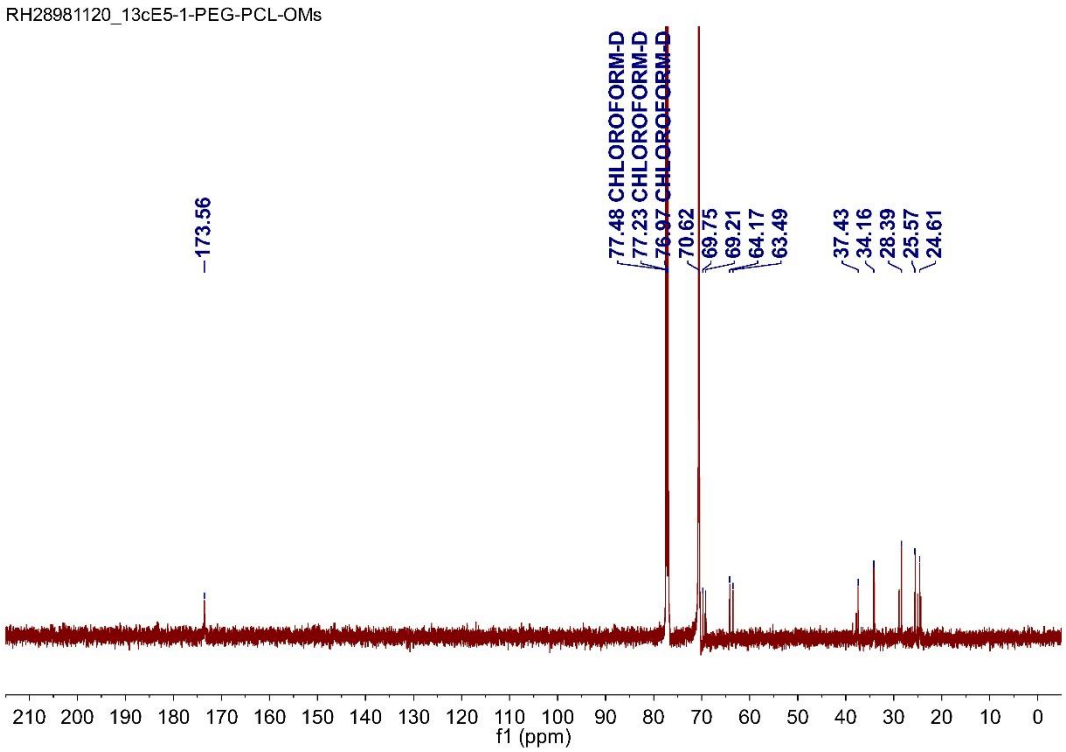

Figure S17. ^{13}C NMR of PEG-PCL-OMs.

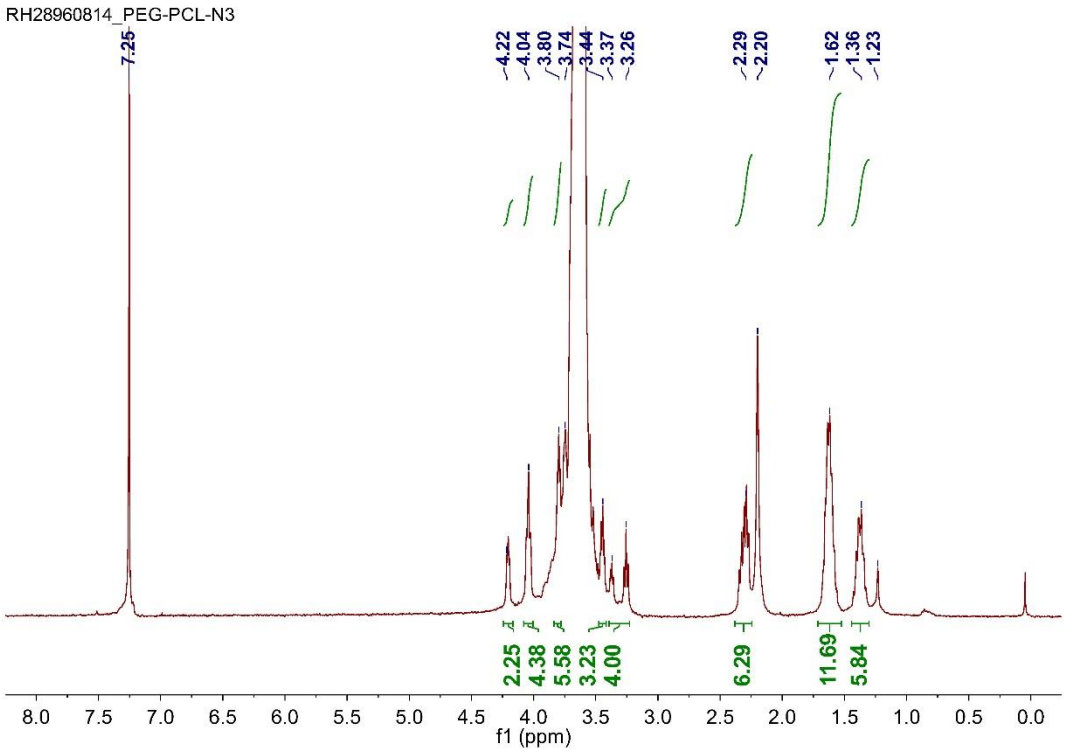

Figure S18. ^{1}H NMR of PEG-PCL-N_3.

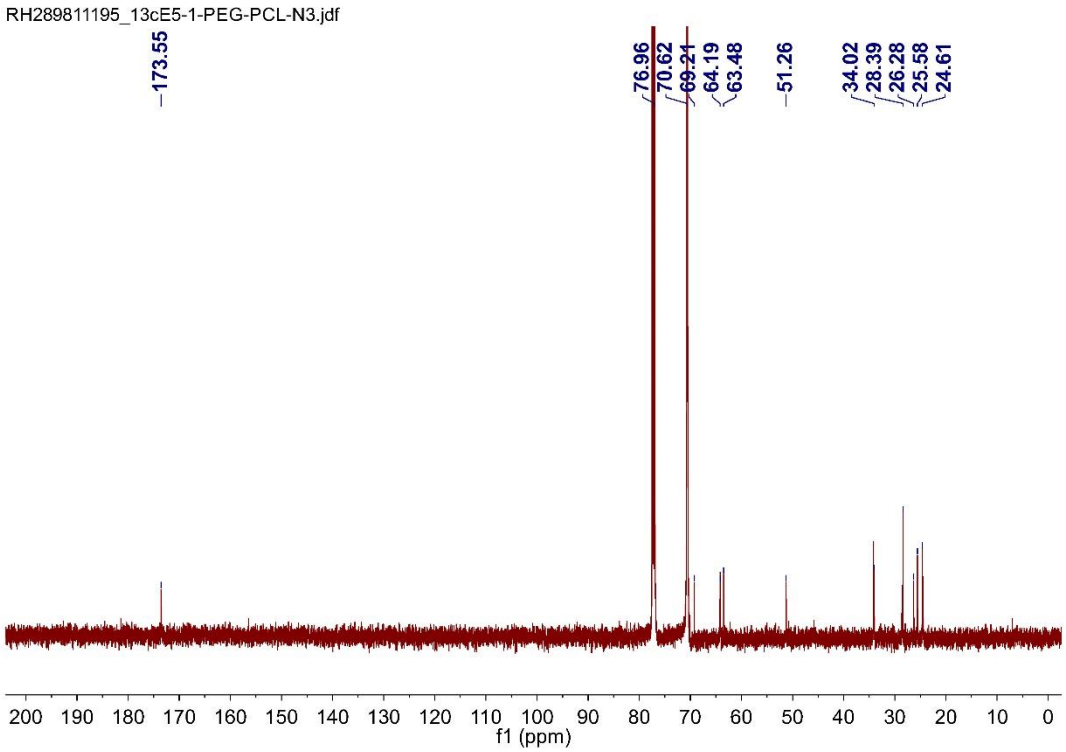

Figure S19. ^{13}C NMR of PEG-PCL-N_3.

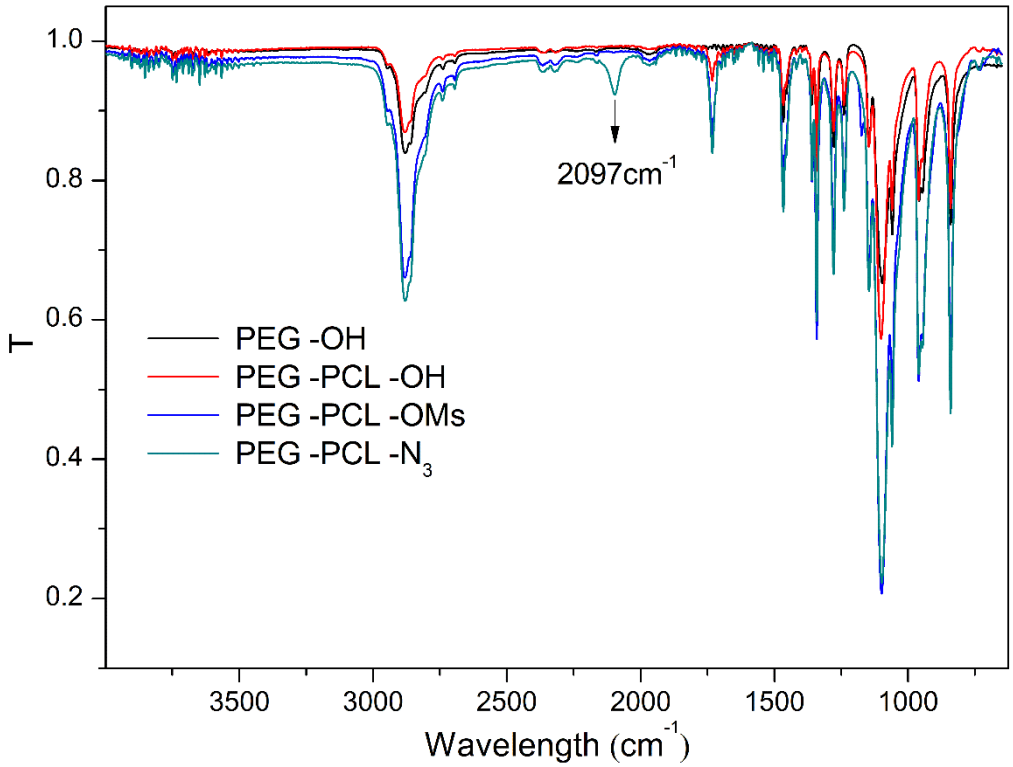

Figure S20. IR of PEG-OH, PEG-PCL-OH, PEG-PCL-OMs, PEG-PCL-N_3.

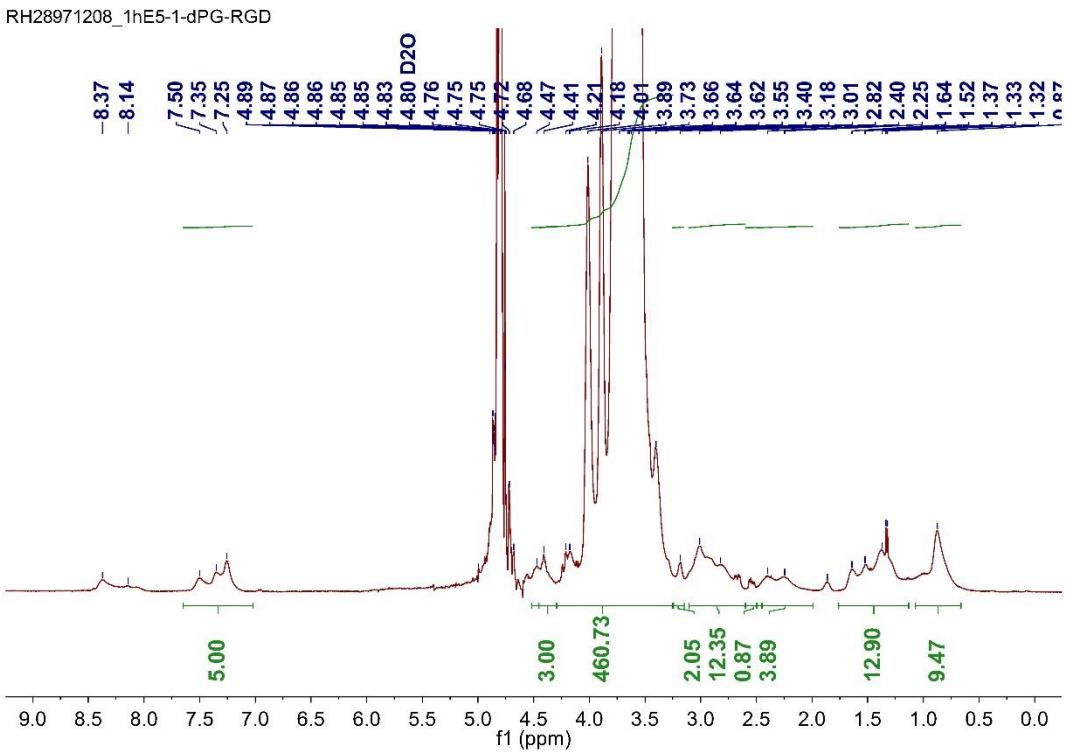

Figure S21. ^{1}H NMR of dPG-RGD.

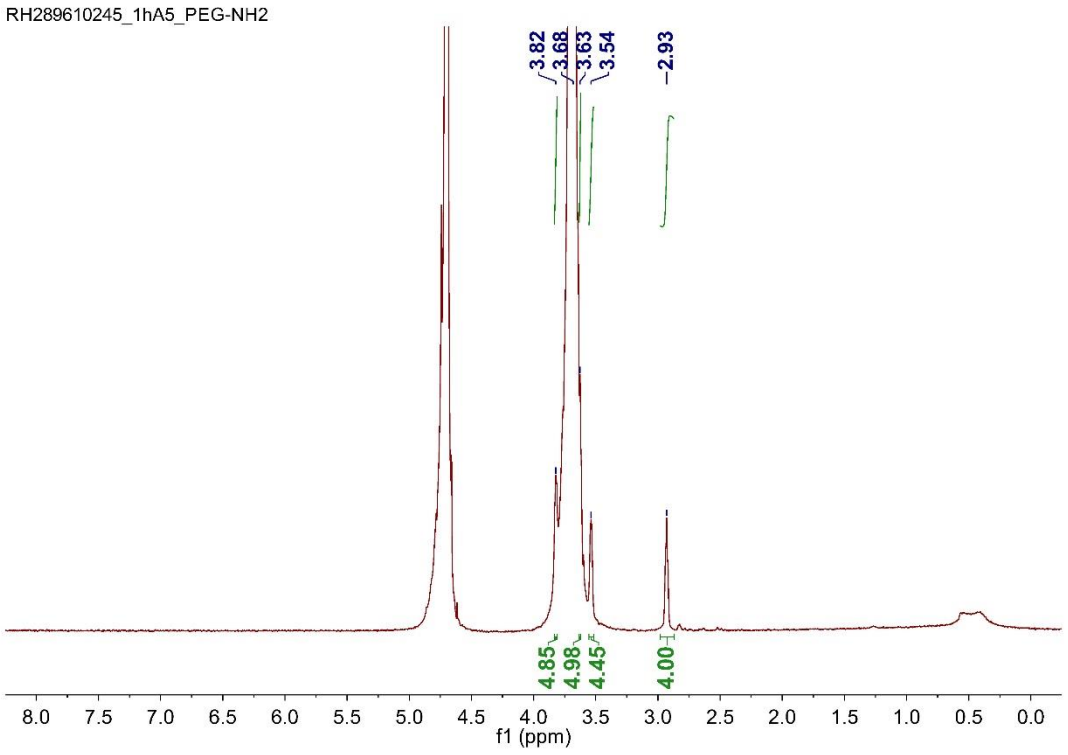

Figure S22. ^{1}H NMR of PEG-NH_2.

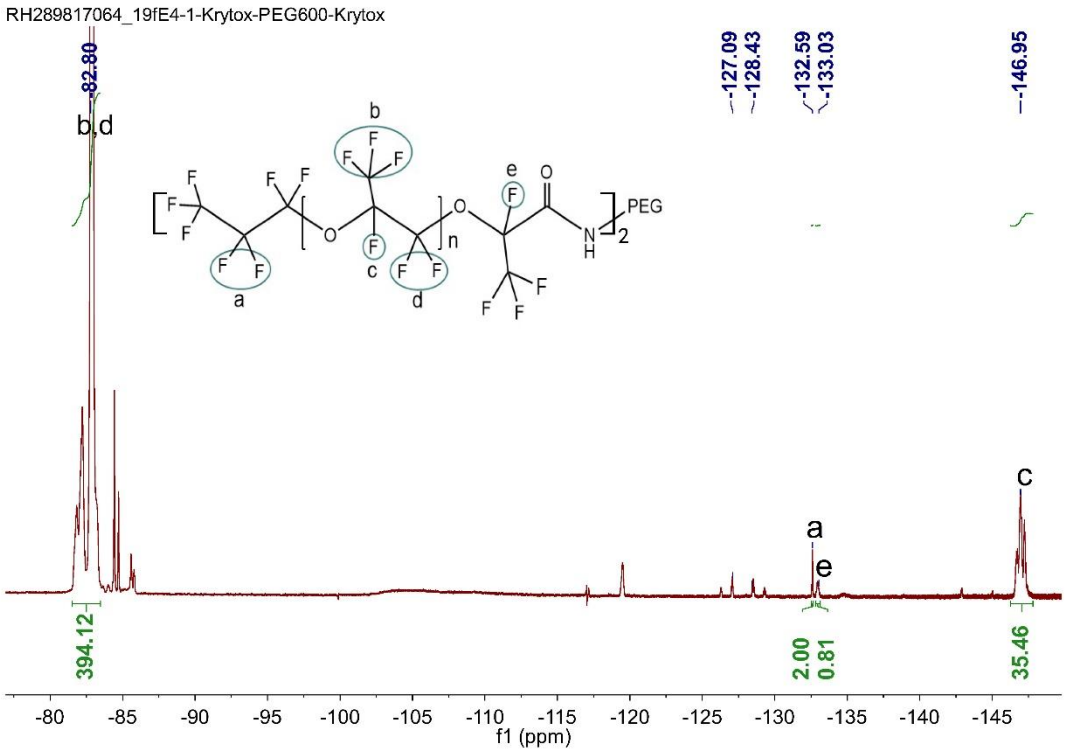

Figure S23. ^{19}F NMR of krytox-PEG-krytox.

8.2. GPC test

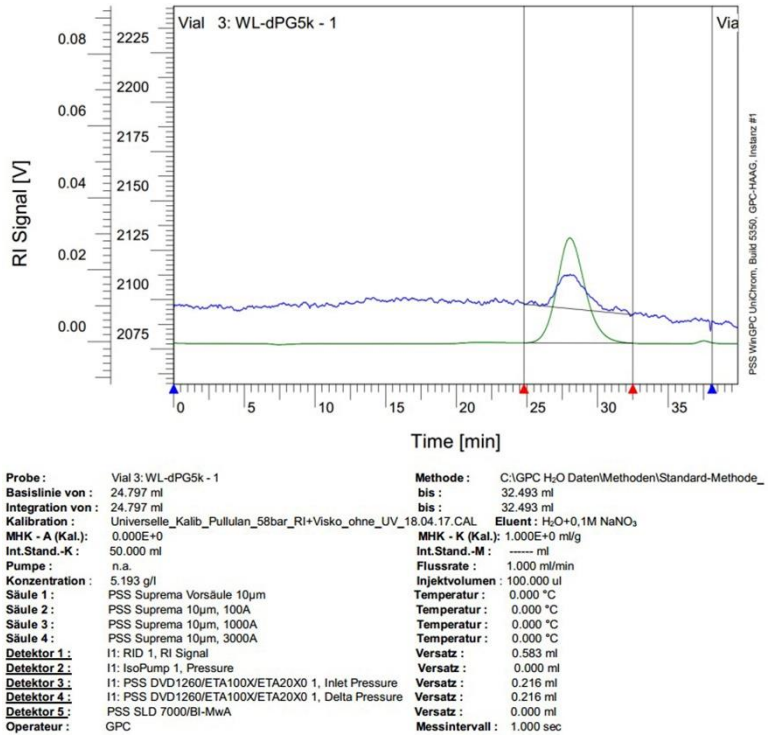

Figure S24. RI signal of the dPG for GPC test.

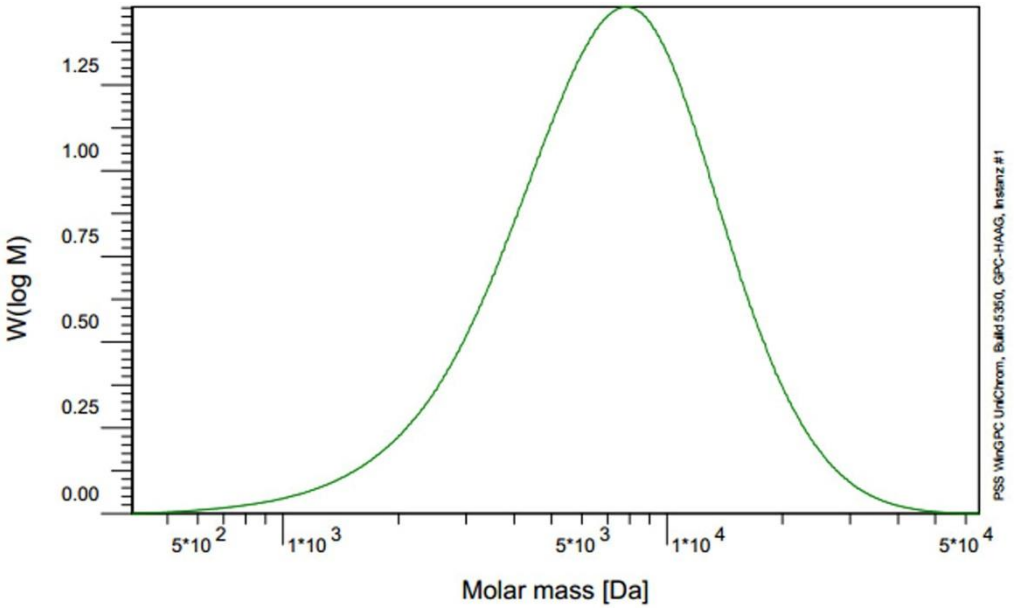

Mn: 5.4852 e3 g/mol
Mw:8.5514 e3 g/mol
D: 1.5590

Figure S25. GPC test for dPG.

9.2 Manuscripts

(1) Chemically Defined Stem Cell Microniche Engineering for iPSCs' 3D Culture and Expansion

(2) Advanced controlled-releasable iPSCs' 3D artificial niches based on dendritic polyglycerol and poly(N-isopropylacrylamide)-co-polyethylene glycol polymers via physical-chemical-co-gelation strategy

9.3 Curriculum-Vitae

Wanjun Liang
Gender: Male
Nationality: China
E-mail：liangwj829@gmail.com
Handy: +4917647399599

Education

Ph.D. (09/ 2015 – 12/2019)	PhD study (Chemistry) Free university of Berlin (Germany)
M.Sc. (09/ 2012 – 07/2015)	Master sdudy (Chemistry and biosensor) Southwest University (China)
B. Sc. (09/.2007 – 07/2011)	Bachelor study (Chemistry) Jinan university (China)

Declaration

Here, I certify that the work presnsnted in this thesis has not previously been submitted for a degree nor has been submitted as part of requirements for a degree except as fully acknowledged within the text.

I also certify that the thesis has been written by myself. Any help that I have got in the research work and the preparation of the thesis itself has been acknowledged. In addition, I certify that all information sources and literature used are indicated in the thesis.

Date and signature